University of California
Santa Cruz

Structural and biochemical characterization of B-Myb as a cell-cycle regulator

A dissertation submitted in partial satisfaction
of the requirements for the degree of

DOCTOR OF PHILOSOPHY

in

Chemistry

by

Tilini U. Wijeratne

June 2023

The dissertation of Tilini U. Wijeratne
is approved:

Dr. Seth M. Rubin
Advisor

Dr. Carrie L. Partch
Chair

Dr. Rohinton T. Kamakaka

Peter F. Biehl
Vice Provost and Dean of Graduate Studies

Table of Contents **Page**

List of Figures

Chapter 1 **Page**

Chapter 2

Chapter 3

Chapter 6

Abstract

Structural and biochemical characterization of B-Myb

as a cell-cycle regulator

Tilini U. Wijeratne

The B-Myb oncogene is overexpressed and increasingly considered a biomarker for several human cancers. B-Myb is vital in activating G_2/M phase genes in the cell cycle. B-Myb forms the activating Myb-MuvB (MMB) complex to overcome the suppression of cell-cycle dependent genes caused by the MuvB-containing DREAM complex during quiescence. B-Myb interacts with the MuvB protein complex at cell-cycle gene promoters; however, the mechanism by which B-Myb activates the G_2/M phase genes still needs to be fully understood. This study focuses on understanding the molecular mechanisms through which B-Myb and oncogenic kinases regulate G_2/M phase gene activation through phosphorylation and interactions with nucleosomes and co-activators.

Acknowledgments:

I want to thank my parents (Wijeratne and Gunaratne), my sister, and my loving husband, Ruwan Gunaratne, for their unconditional love and support for me. I want to thank my graduate advisor/ mentor, Dr. Seth Rubin, for allowing me to finish my graduate research in his lab, write journal papers, help me submit my F31 fellowship, and give me multiple opportunities to present my research in conferences. Seth also helped me learn how to think as a scientist, to find good questions, and to assess feasibility when answering them. I would also like to thank Dr. Carrie Partch, Dr. Michael Stone, and my thesis committee member Dr. Rohinton Kamakaka for their valuable insights and guidance toward my career success. I would also like to thank my graduate advisor Karen Meece for providing me with all the resources to achieve my graduation milestones and being an unofficial therapist. I thank my mentor Dr. Keelan Guiley for his support and guidance. I want to thank my lab mates from Rubin, Partch, Stone, and Millhauser labs, both past and present, for being incredible friends and making my graduate school experience so wonderful. I would also like to thank my cohort, Dr. John Philpott, Ray Harold, Dr. Alie Smart, Kenna Sarka, and Angela Amorello, for the excellent support network and for being my friends through all the ups and downs during graduate school. I thank my science teachers at Mahamaya Girls' College, Kandy; Mrs. Rajika Edirisinghe and Upamalika Dissanayake who first taught me advanced chemistry and inspired me to pursue research

in chemistry. I want to thank my undergraduate mentors, Dr. Paul Weers and Dr. Vasanthy Narayanaswami, who gave me my first impressions of biochemistry research. They were remarkable mentors and genuinely cared for all their students who worked hard to achieve their life goals. Finally, I want to thank my professors from Antelope Valley College, Dr. Athanasia Cholvin, Dr. Zia Nisani, Dr. Rae Agahari, Prof. John Vento, Dr. Sherri Zhu, and Dr. Matthew Jaffe, for their unconditional love, encouragement, and support and not letting me feel alone when my family was thousands of miles away.

Chapter 1: Cell-cycle transcription factors regulate proper completion of cell division

1.1: Introduction

1.1.1 *Myb family of transcription factors and oncogenesis*

Organismal growth and differentiation in cells go through a process known as the cell cycle. Proper regulation of the cell cycle is needed for any organism for the survival of its species. Cell-cycle transcription factors play a crucial role in regulating the proper timing of cell-cycle dependent gene expression, which carefully controls the completion of each cell-cycle phase. Aberrant division of cells in multicellular organisms disrupts the normal physiology of the organism by causing cancerous tumors. The Myb family of transcription factors is a long-studied set of oncogenic proteins that regulate cell division and differentiation. Myb proteins were initially discovered as avian myelomas and lymphomas caused by a retrovirus called avian myeloblastosis virus. The viral oncogene of avian myeloblastosis virus *v-Myb* is a product of retroviral insertion mutation and recombination to cellular gene *MYB* or the protein c-Myb (Ganter S. and Lipsick JS. 1999). V-Myb protein is truncated from the N-terminus and C-terminus compared to the cellular counterpart c-Myb. It also contains eleven point mutations spanning from the N-terminus to the C-terminus. These point mutations are critical to inducing transformation.

in monoblasts (Lipsick JS. 2010). Other studies have shown that the truncations in the c-Myb protein, especially the N-terminus truncation, can cause efficient transformation of myelomonocytic cells in culture (Lipsick JS. 1996). The *v-Myb* oncogenes fused to *v-ets* oncogene from E26 retrovirus induces avian erythroblastosis. This chimeric protein has retroviral Gag protein fused in the N-terminus and Ets-1 protein fused to the C-terminus of the cellular c-Myb containing the eleven point mutations making it the oncoprotein v-Ets (Westin, E. H. et al. 1982). Overexpression of c-Myb is found in several cancers, including acute myeloid leukemia (AML), non-Hodgkin lymphoma, colorectal cancer, and breast cancer (Okada, M. et al. 1982), (Torelli, G. et al. 1987), (Thompson, MA. 1997), (Li, Y. et al. 2016). Oncogenesis of c-Myb can be generated in three ways; fusion with viral genes, overexpression, and c-Myb protein interacting with mutated enhancer sequences (Mansour, M. R. et al. 2017). For example, mutations in *TAL1* enhancer causing a similarity to the c-Myb binding motif cause overexpression of TAL1 oncoprotein, causing acute lymphoblastic leukemia (ALL).

v-Myb and c-Myb proteins share a highly conserved DNA binding domain (DBD). This characteristic domain became the defining factor for classifying Myb transcription factors. In vertebrates, there are two other Myb transcription

factors named A-Myb (*MYBL1)* and B-Myb (*MYBL2)* that share more than 95% sequence similarity in the DBD and recognize the DNA sequence [CT]AAC[N]G (Ogata, K. et al. 1992), (Carr MD et al. 1996), (Cicirò Y and Sala A. 2021). However, they differ in their biological roles shown through different tissue expression patterns. Unlike c-Myb, A-Myb is expressed in the central nervous system, germinal B-lymphocytes, mammary ductal epithelium, and the testis (Toscani, A. et al. 1997), (Mettus, R. V. et al. 1994). A-Myb alterations in cancer are caused by chromosomal rearrangements, such as low-grade gliomas, pediatric CNS neoplasm, and adenoid cystic carcinoma are few examples (Qaddoumi, I. et al. 2017) (Armstrong, G. T. et al. 2011). However, gene expression patterns and patient outcomes are similar between *MYB* and *MYBL1* translocations showing that the oncogenic potential of the proteins is interchangeable between c-Myb and A-Myb (Brayer et al. 2016).

B-Myb alterations in cancer are much more complex because it is expressed ubiquitously in all proliferating cells. Unlike *MYB* (c-Myb) and *MYBL1* (A-Myb)*, MYBL2* (B-Myb) is not unknown to have chromosomal translocation causing oncogenesis in cells. B-Myb is important for proliferating and differentiating cells supported by the lethal phenotype seen in *MYBL2* knockout mice (Lorvellec, M. et al. 2010) (Tanaka, Y et al. 1999). Even though B-Myb shares the highly conserved DNA binding domain with

the other Myb family members, its distinct role in cancer and essential role in proliferation and survival may come from being an integral component in the cell-cycle master regulator MMB complex [**M**uvB (synMuv genes, class B), B-MYB] (Iness et al. 2019). B-Myb association with MuvB makes a complex that activates the expression of many genes needed for completing the cell cycle. Of all three Myb family members, B-Myb (MYBL2) has the highest homology to the only Myb protein found in invertebrates essential to control their cell cycle (Davidson, C. J. et al. 2013). B-Myb transcription is regulated by activating E2Fs in the early G_1 phase of the cell cycle and is required to express cyclin-dependent kinases (Lam, E. W. & Watson, R. J. 1993). However, c-Myb is also known to regulate the expression of critical cell-cycle regulators like Cyclin D1 and Cyclin B1. However, it has yet to be discovered how the Myb family of transcription factors evolved to have multiple means of driving oncogenesis in tissue-specific and ubiquitous cells.

The prominent role of B-Myb in differentiating and proliferating cells is reflected by its deregulation in several cancers. Overexpression of the MYBL2 gene is considered a biomarker for poor prognosis in osteosarcoma, breast cancer, esophageal cancer, and multiple myeloma (Bayley R. et al. 2020), (Musa J. et al. 2017), (Qin H., 2019), (Sun C. et al. 2019). Overexpression of *MYBL2* contributes to evading apoptosis in human hepatocarcinogenesis and directly regulates an anti-apoptotic gene apolipoprotein-J (Calvisi DF. Et al.

2011), (Frau M. et al. 2011) (Cervellera M. et al. 2000). B-Myb knockout mice show embryonic lethality and poor inner cell mass formation, showing that *MYBL2* is essential for all proliferating cells and their limitless replicative potential (Tanaka et al., 1999). Therefore, in recent years, B-Myb has become an attractive target for understanding mechanistic details of oncogenic TFs for cancer therapeutics.

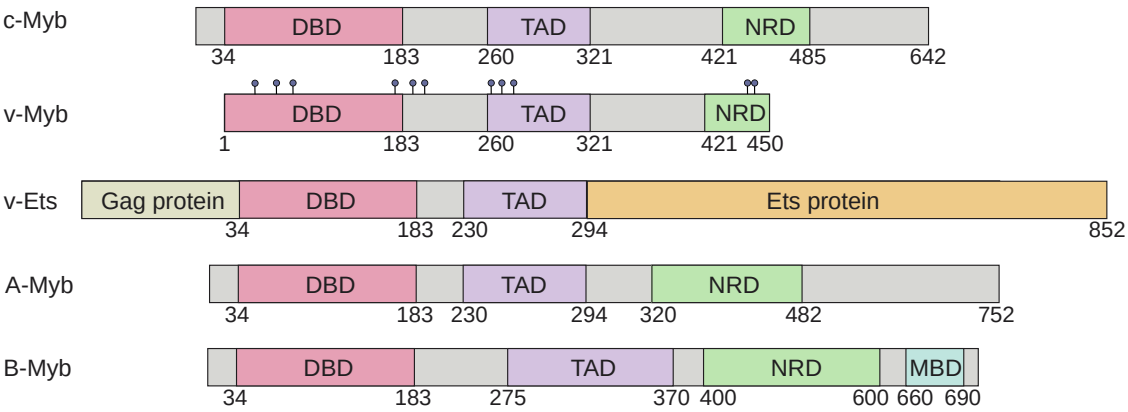

Figure 1.1 Myb family of transcription factors and viral variants. Myb DNA binding domain (DBD), transactivation domain (TAD), and negative regulatory domain (NRD) are conserved domains among Myb family members, although their boundaries vary to some extent. V-Myb has eleven mutations and truncations from both termini, making the viral version of c-Myb oncogenic. Fusions of Gag protein and Ets proteins to the c-Myb DBD and TAD make the v-Ets oncoprotein. A-Myb and B-Myb are two homologs of c-Myb in eukaryotic cells. B-Myb has a different domain in the C-terminus, which is called MuvB binding domain (MBD) and interacts with the MuvB complex.

1.1.2 *Variations of Myb proteins in the cell-cycle*

The cell cycle comprises four phases that regulate the duplication of DNA, the number of organelles, and cell size to complete one cell to produce two daughter cells. The cells that are not actively dividing are retained in the quiescence stage called G_0. Cells enter the cell cycle when they decide to divide however will have until proper cues are received in the form of chemical signals known as mitogens or growth factors (Lloyd AC. 2013). This gap phase is called G_1. In this phase, the cell is sensitive to its environment and waits for enough physical space for growth (Conlon, IJ et al. 2001). If there is a limitation for such growth factors, the cell temporarily goes to the G_0 phase. The S phase is when the DNA is duplicated in the cell. Once the cell enters the S phase, the cell is committed to complete cell division (Matthews HK et al. 2022). The G_2 phase follows the S phase when the cell forms the necessary organelles and places them correctly in the cell where they are needed to complete mitosis. The final phase of the cell cycle is mitosis. During mitosis, massive structural changes occur to the enclosure's integrity to form two daughter cells. The duplicated and condensed DNA is carefully divided, and the cell walls for the daughter cells are formed (Foley, E. A. & Kapoor, T. M. 2013).

Even though c-Myb is expressed and essential for the proliferation and differentiation of hematopoietic cells, its involvement in the cell cycle is seen

through interaction and regulated by the cycling-dependent kinase 4/6 (CDK 4/6) and Cyclin D1, which are essential kinases for regulating the G_1/S transition (Ganter B. et al. 1998). The complex formation between c-Myb and CDK 4/6 is necessary for activating c-Myb and regulating human T cells' S phase (Lei W. et al. 2005). Additionally, chromatin immunoprecipitation assay shows that c-Myb regulates the Cyclin B1 gene expression by directly binding to its promoter CCNB2 (Nakata, Y. et al., 2007). This experiment was done in K562 cells, a myelogenous leukemia cell line. However, in HCT116 cells (human colorectal carcinoma cell line) in which B-Myb is expressed as a mitotic activator, c-Myb can partially rescue the B-Myb knockout phenotype (Nakata, Y. et al., 2007). This result shows that c-Myb and B-Myb can be interchangeable as cell-cycle regulators. It still needs to be discovered how c-Myb is localized to the CCNB2 promoter.

CDK2-Cyclin A/E complexes phosphorylate both A-Myb and B-Myb to relieve the repression caused by the Negative regulatory domain (**Figure 1.1)** (Ziebold U. and Klempnauer KH. 1997). However, it is yet to be discovered if A-Myb regulates cell-cycle genes. B-Myb also has a similar phosphorylation pattern by CDK2-Cyclin A; however, its implication on cell cycle regulation is also limited. It is known that the hyperphosphorylated form of B-Myb is present in the S phase of the cell cycle right before it is targeted for proteasomal-mediated degradation (Musa J. et al. 2017). However, whether

B-Myb phosphorylation is necessary for cell-cycle regulation is unknown. It is yet to be studied if it is needed for B-Myb to interact with MuvB and to get recruited to the cell cycle-dependent promoters, which contain a conserved motif called cell cycle homology region (CHR). B-Myb regulation through phosphorylation for activation of Myb-specific promoters is discussed in detail in **Chapter 2**.

1.1.3 *B-Myb as a G_2/M gene activator*

B-Myb regulation of cell-cycle dependent genes through interacting with the MuvB protein complex at the cell-cycle dependent promoters are well characterized. In mammalian cells, the master coordinator for the cell-cycle dependent genes is the MuvB complex which occupies the cell-cycle dependent promoters called CHR (cell cycle homology region) in the genome (Müller GA et al. 2014). MuvB forms the DREAM complex with Rb-like proteins and repressive E2Fs to repress the genes needed for mitosis. It also forms the activating complex MMB (**M**yb-**M**uv**B**) with B-Myb and FoxM1 to activate genes required for mitosis (Sadasivam S. and De Caprio JA. 2013) (Knight AS. 2009). When MuvB proteins are knocked down using siRNA, B-Myb localization to CHR promoters is markedly reduced in the S-phase (Sadasivam S. and De Caprio JA. 2013). It is also shown that overexpression of B-Myb can disrupt the formation of the MuvB complex at the CHR promoters by sequestering LIN9 from assembling the MuvB complex at those

promoters (Iness AN. et al. 2019). Chromatin immunoprecipitation assays show that B-Myb is recruited to CHR promoters through binding to the MuvB complex during S-phase (Sadasivam S. and De Caprio JA. 2013).

During S-phase, B-Myb interacts with the MuvB complex through its MuvB binding domain (MBD) (**Figure 1.1**). The MuvB proteins, LIN9 and LIN52, form the binding surface for B-Myb MBD. The LIN9-LIN52 critical surface is conserved across various B-Myb species, even in C. elegans, in which no B-Myb ortholog is present (Vorster et al. 2020). Although the B-Myb MBD is roughly conserved across the Myb family members, only B-Myb interacts with LIN9 and LIN52 with high affinity (Guiley KZ. et al. 2018). It is shown in the Drosophila model that the MBD is necessary and sufficient to interact with LIN9-LIN52, localize B-Myb to the CHR promoters and regulate cell-cycle genes in vivo (Andrejka L et al. 2011). However, this has not been tested in mammalian cells. Therefore, it will be interesting to understand the mechanism of how c-Myb would rescue the B-Myb knockdown phenotype in mammalian cells without having a conserved MBD.

The most convincing results supporting that B-Myb acts as a G_2/M gene activator are that B-Myb knockdown phenotype in mammalian cells leads to poor formation of mitotic spindle fibers, polyploidy, abnormal cytokinesis and G_2/M arrest (Yamauchi, T. et al. 2008), (Tarasov, K.V. et al. 2008), (Werwein E. et al. 2019). B-Myb interacts with the cell-cycle kinase Plk1 in the G_2/M

phase to phosphorylate B-Myb at the TAD region (**Figure 1.1**). Mutating these residues to alanine in mammalian cells also results in mitotic arrest and downregulation of genes needed to complete mitosis (Werwein E. et al. 2019). It is also known that during the late S-phase, the MMB complex also interacts with the FoxM1 transcription factor, which is a crucial G_2/M phase driver (Sadasivam S. and De Caprio JA. 2013). FoxM1 also gets highly phosphorylated and regulated by Plk1 during the G_2/M phase (Marceau AH. et al. 2019). In summary, B-Myb regulates the activation of G_2/M phase genes through localization to the CHR promoters by interacting with MuvB proteins LIN9 and LIN52. B-Myb's function as a cell-cycle regulator extends beyond the G_2/M phase as it continues to interact with other G_2/M phases transcription factors like FoxM1, clathrin, and filamin to assist further activation of genes needed to complete mitosis (Sadasivam S. et al. 2012), (Yamauchi, T. et al. 2008).

1.1.4 *Myb-like domains and DNA/ nucleosome binding*

The B-Myb DNA binding domain (DBD) is the classical Myb-like domain which consists of three tandem repeats (R1, R2, and R3) of antiparallel helices arranged in a helix-turn-helix motif (HTH) (Ogata K. et al. 1994), (Tahirov, T. H. et al. 2001). Each repeat has a bulky tryptophan 18-19 amino acids apart, making a hydrophobic core (Ogata K. et al. 1994). The B-Myb DBD is highly conserved across its family members and species and

recognizes the same DNA sequence [CT]AAC[*N*]G (Lipsick JS. 1996), (Ganter B. et al. 1999), (Rosinski, J.A. and Atchley W.R. 1998) as shown in **Figure 1.2.A**. This sequence was first discovered through the v-Myb oncoprotein and has been named the Myb-recognition motif (MRE) or the Myb-binding site (MBS) (Biedenkapp H. et al. 1988) (Mizuguchi G. et al. 1990). This motif was found in the transcriptional start site of the E26 viral gene *mim-1* and the SV40 enhancer (Ness SA. et al. 1989) (Nakagoshi H. et al. 1990).

However, there are three point mutations in the DBD R2, namely, I91, L106, and V117, which make v-Myb acquire oncogenic potential compared to other Myb family members. The DNA binding properties do not seem to be affected by the L106 and V117, which suggests that other protein-protein interactions may be essential to drive oncogenesis facilitated by these point mutations (Introna M. et al. 1990). The v-Myb DBD only has helices in the R2R3 motif. The truncated R1 is insufficient to form a Myb repeat on its own. A similar pattern of DNA binding is seen in other Myb family members, where only R2R3 is enough to interact with DNA. It is seen that only the R2 repeat contributes to the specific interactions with the canonical DNA, while the R3 repeat contributes to both particular and non-specific binding to DNA (Oehler T. et al., 1990). The recognition from the R2R3 is also known to be divided

between R2 and R3. R3 recognizes the first part of MBS ([CT]AAC), and the second part ([*N*]G) is recognized by R2 (Gabrieson OS. et al. 1991).

Even though vertebrate Myb family proteins are highly conserved, some differences account for how the Myb DBDs interact with the canonical DNA sequence. The experiments done with the c-Myb DBD using electrophoretic mobility shift assays show a five-fold reduction in affinity to the canonical DNA when R1 is present. Therefore, similar to v-Myb, the minimum DNA binding region for c-Myb is R2R3 (Ording E. et al. 1994). Another similarity between v-Myb and c-Myb is that the R3 repeat contributes the recognizing the specific sequence while R2 has non-specific interactions. However, R1 increases the alpha-helical content when bound to the canonical DNA sequence, which is not seen with just the R2R3 motif (Ebneth A. et al. 1994). This evidence suggests that the R3 repeat is essential in the initial anchoring of the molecule to the DNA sequence, followed by R2 and R1 unspecific interactions, which contribute to the structural stabilization of the complex formed with DNA without affecting the overall affinity. In contrast to c-Myb, B-Myb has a higher affinity to DNA with all three repeats (Jamin N. et al. 1993) (McIntosh PB. et al. 1998). The solution structures of c-Myb and B-Myb R2R3 have minor differences. The B-Myb third turn in R2 is less structured and seems to have multiple conformations in solution compared to c-Myb. Even though the proteins have 96% similarity, the differences in the NMR models

are accounted for overlapping signals (Carr. MD. et al. 1996). Alphafold prediction tool shows with very high confidence that the structure of R1 repeat has three tandem repeats with a similar hydrophobic core when unbound to DNA (**Figure 1.2.B**) (https://alphafold.ebi.ac.uk/ entry/P10244).

The structure of c-Myb DBD bound to DNA shows that residues N174, K173, and K119 in the R2 and R3 helices are essential to make specific interactions with the DNA (Tanikawa, J. et al. 1993) **(Figure 1.2.C**). The N174A mutation in B-Myb also shows reduced binding to the MBS sequence, suggesting that B-Myb similarly interacts with c-Myb (Werwein E. et al. 2012). NMR solution structure comparing R1R2R3 and R2R3 shows that chemical shift perturbations in R1 are unchanged upon adding to DNA (Ogata K. et al. 1994). It also shows how R2 and R3 come closer together to insert themselves into the major groove of the DNA, thus bringing R2 and R3 closer together compared to the DNA unbound version (**Figure 1.2.C and 1.2.D**). Biochemical and in vivo characterization of A-, B-, and c-Myb shows that A-Myb and c-Myb form a more stable complex with MBS than B-Myb (Bergholtz S. et al. 2001). This is demonstrated by comparing the dissociation rate with MBS DNA when titrating non-specific DNA. However, the biological reason for this difference is still unknown. It is possible that the less structured R2 in B-Myb is contributing to forming a weaker interaction with the DNA, and it needs R1 to create a more stable

complex (**Figure 1.2.E**). However, B-Myb may recognize a more specific DNA sequence than MBS, and having R2 as a weakly structured helix can avoid unspecific binding to DNA.

The most conserved elements of the Myb DBDs in the acidic patch in each repeat (**Figure 1.2.A**). This EEED element is highly conserved across the Myb family and species. The fact that it is facing away from the DNA binding groove suggests it is essential in making protein-protein interactions (**Figure 1.2.C**). These acidic patches are also conserved in proteins with Myb-like domains, such as TRF2 and RAP1 (Hanaoka S. et al. 2005) (Konig P. et al. 1996). These acidic patches show you reduced c-Myb activity towards the *mim-1* promoter in a Luciferase promoter assay. Particularly the acidic patch mutant EEED to EAAA in the R3 repeat show reduced DBD interaction with DNA, possibly due to disrupted protein stability by not forming the salt bridge. Additionally, it was shown that acidic patch mutation of the R3 repeat in c-Myb was essential to interact with the H4 and H2A tails of nucleosomes (Ko ER. et al. 2007). However, the effect of the acidic patches on A-Myb and B-Myb activity or DNA/nucleosome binding needs to be studied and is a focus here.

One function of Myb DBDs interacting with nucleosomes might be acquiring a secondary transcription regulation layer through chromatin-modifying proteins. Myb family proteins are known to interact with chromatin-

modifying histone acetyltransferase CBP/p300 to regulate MBS promoters (Dai P. et al. 1996), (Oelgeschläger M. et al. 1996), (Facchinetti V. et al. 1997). It has been shown that c-Myb is a pioneer transcription factor that facilitates the acetylation of histone tails at the promoters. Remarkably, this function is fulfilled by the c-Myb DBD residue D152 residue (Fuglerud BM. et al. 2018). It is also shown that c-Myb p300 interaction is important in myeloid leukemogenesis and continues the proliferation of leukemia cells (Pattabiraman DR. et al. 2014). All three Myb family members interact through the transactivation domain (TAD) (Figure 1.1). The transactivation domain is not conserved across the Myb family members, which supports the evidence showing how all three family members have different binding sites in CPB/p300. c-Myb interacts with both TAZ1 and KIX domains of CBP/p300, and B-Myb only interacts with the TAZ2 domain, while A-Myb interacting domain is not yet characterized (Dyson HJ and Wright PE. 2016) (Oka O. et al. 2012). The regulation of activity towards MBS promoters by CBP/p300 interaction has been studied in detail using Luciferase promoter assays for B-Myb however, whether this interaction is necessary to activate cell-cycle dependent genes is still unknown. More information regarding the B-Myb-p300 interaction will be discussed in **Chapter 4.**

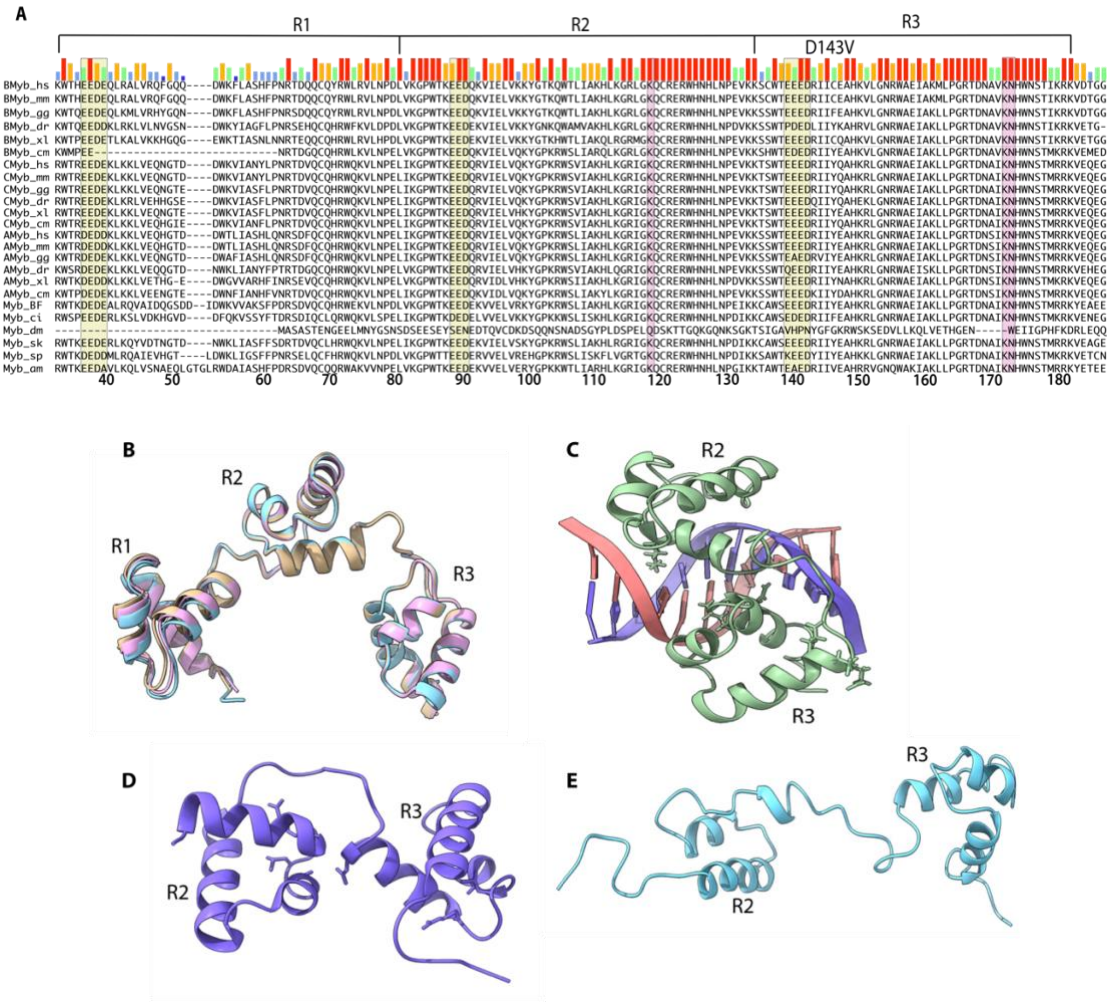

Figure 1.2 Myb DNA binding domains. Myb family of transcription factors share 96% sequence similarity; however, there are differences in secondary structure and how the domains interact with DNA. **A.** Sequence alignment of DBD of Myb family members and their orthologs. Conserved acidic patches in each repeat are highlighted in yellow. The residues important for c-Myb DNA binding are highlighted in pink. **B.** Alphafold prediction tool models of A-Myb, B-Myb, and c-Myb DBD structures aligned using Pymol software show that when DBD is not bound to DNA, the structures look similar. In pink is A-Myb, in blue is B-Myb, and in tan is c-Myb DBD. **C.** c-Myb DNA binding domain NMR solution structure shows K119, K173, and N174 residues in the stick facing the DNA major groove. The acidic patch EEED in the R3 repeat is shown in a stick-facing solvent. **D.** c-Myb DBD R2R3 NMR solution structure unbound to DNA. **E.** B-Myb DBD R2R3 NMR solution structure when unbound to DNA.

1.1.5 *Conclusions*

The Myb family of transcription factors is an essential set of oncogenic drivers in many cancers. Currently, B-Myb is emerging as a biomarker for breast cancer; however, limited knowledge exists about how B-Myb is regulated and activates cell-cycle-dependent genes. Even though B-Myb has been studied along with Myb family members for over 35 years, the molecular mechanisms of B-Myb regulation in the cell cycle are still unknown. In this thesis, I share my research understanding the molecular details of B-Myb and its associated proteins. In **Chapter 2,** I describe a possible mechanism of B-Myb autoregulation through its negative regulatory domain and phosphorylation. In **Chapter 3,** I describe the structural details of B-Myb interaction with nucleosomes. In **Chapter 4,** I describe the biochemical characterization of B-Myb interaction in the TAZ2 domain of p300. In **Chapter 5,** I explain how mitotic kinase Aurora regulates its activity by interacting with Bora, and understanding molecular details of B-Myb and Aurora kinase as oncogenic drivers will further the knowledge that could be possibly used as cancer therapeutics.

Chapter 2: B-Myb association with DNA is mediated by its negative regulatory domain and Cdk phosphorylation. (Published: Wijeratne T. et al. 2022)

2.1 Introduction

The Myb family of transcription factors (TFs) are present in a range of species from slime mold to higher eukaryotes and have high conservation in their (DBD) (Bergholtz S. et al. 2001), (Carr. MD. et al. 1996), (Graf T. 1992). TFs with evolutionary conserved DBDs recognize a common DNA sequence; however, they often diverge in their distinct functions through different intra- and inter-molecular interactions (Nitta K.R. et al. 2015). Vertebrate Myb family members A-Myb, B-Myb, and c-Myb share more than 70% amino sequence homology in their DBDs, which recognize the Myb-binding site (MBS) DNA sequence (C/TAACNG) (Lipsick JS. 1996), (Biedenkapp H. et al. 1988), (Ogata, K. et al. 1992), (Oh IH. and Reddy EP. 1999). All the Myb family members regulate transcription of genes important for cell differentiation and proliferation, but they differ in their tissue-specific expression. A-Myb (encoded by MYBL1) is mainly expressed in cells of the developing central nervous system, sperm cells, and breast tissue, while c-Myb (MYB) is expressed specifically in immature hematopoietic stem cells (Mucenski ML. et al. 1991), (Toscani A. et al. 1997). In contrast, B-Myb (MYBL2), which is the most ancient of the paralogs, is ubiquitously expressed in all proliferating cells (Sala A. 2005). The prominent role of B-Myb in both differentiating and proliferating cells is reflected by its deregulation in several cancers. Overexpression of the MYBL2 gene is considered a biomarker for poor prognosis in osteosarcoma, breast cancer, esophageal cancer, and multiple

myeloma (Bayley R. et al. 2020), (Musa J. et al. 2017), (Qin H., 2019), (Sun C. et al. 2019). Therefore, in recent years, B-Myb has become an attractive target to understand mechanistic details of oncogenic TFs for cancer therapeutics.

The B-Myb domain architecture is similar to A-Myb and c-Myb. B-Myb contains a DBD, a negative regulatory domain (NRD) toward the C-terminus, and a transactivation domain (TAD) (**Figure 2.1.A**). In all three Myb proteins, C-terminal protein truncations that remove the NRD trigger activation of Myb-dependent reporter promoters (Dubendorff JW. et al. 1992), (Lane S. et al. 1997), (Takahashi T. et al. 1995). Recurrent chromosomal translocations involving the genes MYB and MYBL1 produce NRD truncated versions of the respective proteins c-Myb and A-Myb that are sufficient to induce leukemias in mice (Brayer et al. 2016) (Gonda TJ. Et al. 1998). These truncated proteins more resemble the viral oncoprotein v-Myb, which shares the same DBD as all the Myb proteins and has a TAD but lacks a potent C-terminal NRD (Lipsick JS. and Wang DM. 1999). In contrast, c-terminal truncations of B-Myb are not reported to have oncogenic properties. However, the B-Myb C-terminus contains the MuvB-binding domain (MBD), which binds the MuvB complex to assemble Myb-MuvB (MMB) (Andrejka L. et al. 2011), (Guiley KZ. et al. 2018), (Sadasivam S. and De Caprio JA. 2013). The MMB complex activates cell-cycle–dependent genes that contain a CHR sequence (cell-

cycle genes homology region) in their promoter in a manner that is both B-Myb and MuvB dependent (Sadasivam S. et al. 2012). Thus, B-Myb functions as a site-specific TF that activates MBS genes and as a coactivator of CHR genes when present in the MMB complex. This latter function is unique among Myb family members.

The mechanisms by which the NRD affects the transactivation potential of B-Myb are also not yet fully understood. Several studies show that autoinhibition of B-Myb by the NRD is relieved when B-Myb is phosphorylated by the cell-cycle regulatory kinase Cdk2-CyclinA (Cdk2-CycA), which results in the activation of MBS-dependent promoters (Lane S. et al. 1997), (Petrovas C. 2003), (Ziebold U. and Klempnauer KH. 1997). The NRD of Myb proteins contains several highly conserved Cdk consensus sites (S/TP) (**Figure 2.1.A** and **2.2**), including a TPTPFK motif (amino acids 518–523 in B-Myb). This region is a direct target of Cdk-mediated phosphorylation in cell-based studies and shows a positive correlation with activation (Bessa M. et al. 2001) (Tashiro S. et al. 1995). Cdk-dependent phosphorylation of B-Myb also primes for binding of Polo-like kinase 1 (Plk1), and subsequent phosphorylation by Plk1 in the TAD also promotes B-Myb activity (Werwein E. et al. 2019). Although evidence suggests that NRD phosphorylation releases an inhibited state of B-Myb to significantly transactivate MBS-dependent promoter reporters, two studies did not find that Cdk2-CycA alters B-Myb

interactions with DNA (Johnson TK. et al. 1999), (Werwein E. et al. 2020). However, evidence of enhanced DNA binding upon truncation of the NRD in A-Myb and c-Myb has been reported (Dubendorff JW. et al. 1992), (Takahashi T. et al. 1995). A recent study showed that the B-Myb DBD undergoes an intramolecular interaction with the NRD. Cdk-mediated phosphorylation at a specific site (S577) disrupted the interaction; however, it was not conclusive if the NRD–DBD interaction affected the ability of B-Myb to bind DNA and if phosphorylation regulated the NRD-DBD association (Werwein E. et al. 2020). B-Myb phosphorylation is not only required for MBS-dependent transactivation, but it is also important for G_2/M cell cycle–dependent gene activation. B-Myb is extensively phosphorylated by Cdk2-CycA during S phase of the cell cycle coinciding with its peak in expression (Sadasivam S. et al. 2012), (Werwein E. et al. 2019). On the other hand, other studies conclude that extensive phosphorylation of B-Myb is essential for its ubiquitination and proteasomal mediated degradation (Charrasse S. et al. 2000). Thus, despite these various studies, it remains unclear how phosphorylation of B-Myb overcomes negative regulation by the NRD to activate B-Myb. In part, disparate models have arisen because of the challenges of interpreting cell-based assays to draw conclusions about direct molecular interactions and the effects of phosphorylation on specific interactions.

In this chapter I show a study of B-Myb autoregulation that focuses on biophysical assays using purified proteins. We used recombinant expression, which provided us with a minimal system to control phosphorylation, and we quantified interactions by measuring dissociation constants. We found that the B-Myb NRD binds the DBD with a low micromolar affinity, and the interaction is sufficient to inhibit B-Myb binding to MBS DNA. We identified amino acids that are critical for NRD-DBD association and observed that Cdk2-CycA–mediated phosphorylation of T515, T518, and T520 disrupts the NRD–DBD interaction to enhance binding to an MBS DNA sequence probe. We also show that specific mutations that disrupt the NRD–DBD interaction increase B-Myb–dependent activation of an MBS luciferase reporter. Our findings reveal a structural mechanism for B-Myb autoregulation of site-specific gene activation and how repression is relieved by Cdk phosphorylation.

2.2 Results

2.2.1 *Phosphorylated B-Myb binds to DNA tighter than unphosphorylated B-Myb*

In order to determine the effects of B-Myb phosphorylation on its association with DNA, we used fluorescence polarization (FP) assays to measure binding affinities using recombinant, purified proteins. Considering that both Cdk2-CycA and Plk1 sites are present throughout the NRD and TAD

regions, respectively (**Figure 2.1.A**) (Bessa M. et al. 2001), (Werwein E. et al. 2019), (Johnson TK. et al. 1999), we sequentially phosphorylated purified, full-length B-Myb. We phosphorylated first with Cdk2-CycA and then with Plk1, and we verified phosphorylation with a mobility shift on a PhosTag gel (**Figure 2.3.A and B**). We then assayed DNA binding of phosphorylated and unphosphorylated protein to a fluorescently labeled DNA probe containing the MBS sequence. The resulting single-site protein-DNA binding curve for the phosphorylated B-Myb showed a dissociation constant KD = 3 ± 1 μM (**Figure 2.1.B**). The unphosphorylated B-Myb showed weak (Kd > 10 μM), potentially nonspecific, binding to the probe.

2.2.2 *Phosphorylation of the NRD regulates DBD binding to DNA*

We found that the affinity of phosphorylated B-Myb for the MBS probe was similar to the affinity of the DBD alone (B-Myb34–183, KD = 1.0 ± 0.1 μM) and to the affinity of a construct in which the NRD was deleted (B-Myb34–370, KD = 1.0 ± 0.1 μM) (**Figure 2.3.C**). In contrast, a C-terminal truncation of the MBD that leaves the NRD intact (B-Myb34–600) bound with similar weak affinity as unphosphorylated full-length B-Myb (**Figure 2.1.C**). The observation that binding of the construct containing the DBD-TAD-NRD domains is greatly reduced compared to both the DBD and DBD-TAD only constructs demonstrates that the NRD inhibits DBD binding to the MBS probe. These results and the fact that there are no Cdk sites in the DBD

support a model in which the DBD–DNA interaction is inhibited by the NRD in the context of unphosphorylated B-Myb and that this inhibition is relieved upon Cdk2-CycA–mediated phosphorylation of the NRD. To test this model, we phosphorylated B-Myb with Cdk2-CycA only and found a similar affinity as phosphorylating with both kinases. In contrast, phosphorylation with only Plk1 had no effect on the binding compared to unphosphorylated B-Myb (**Figure 2.1.D and Figure 2.3.B**).

To further test the role of the NRD in inhibiting DBD-DNA binding and the role of NRD phosphorylation, we performed FP assays, titrating DBD into DNA in the presence of unphosphorylated and Cdk2-phosphorylated NRD 440–600 (verified by mass spectrometry, Figure 2.2.C). As shown in **Figure 2.1.E**, when added in trans, 30 μM unphosphorylated NRD reduced DBD binding to the MBS probe (KD = 16 ± 3 μM). In contrast, when 30 μM phosphorylated NRD was added in trans, there was little effect of the NRD on the affinity of the DBD for the MBS probe (KD = 1.0 ± 0.1 μM). The addition of Plk1-phosphorylated TAD in trans also did not influence DBD binding to the MBS probe (**Figure 2.1.F and 2.3.D**). These data further support the model that Cdk phosphorylation of NRD 440–600 and not Plk1 phosphorylation of sites in the TAD increases the affinity of DNA binding through release of autoinhibition.

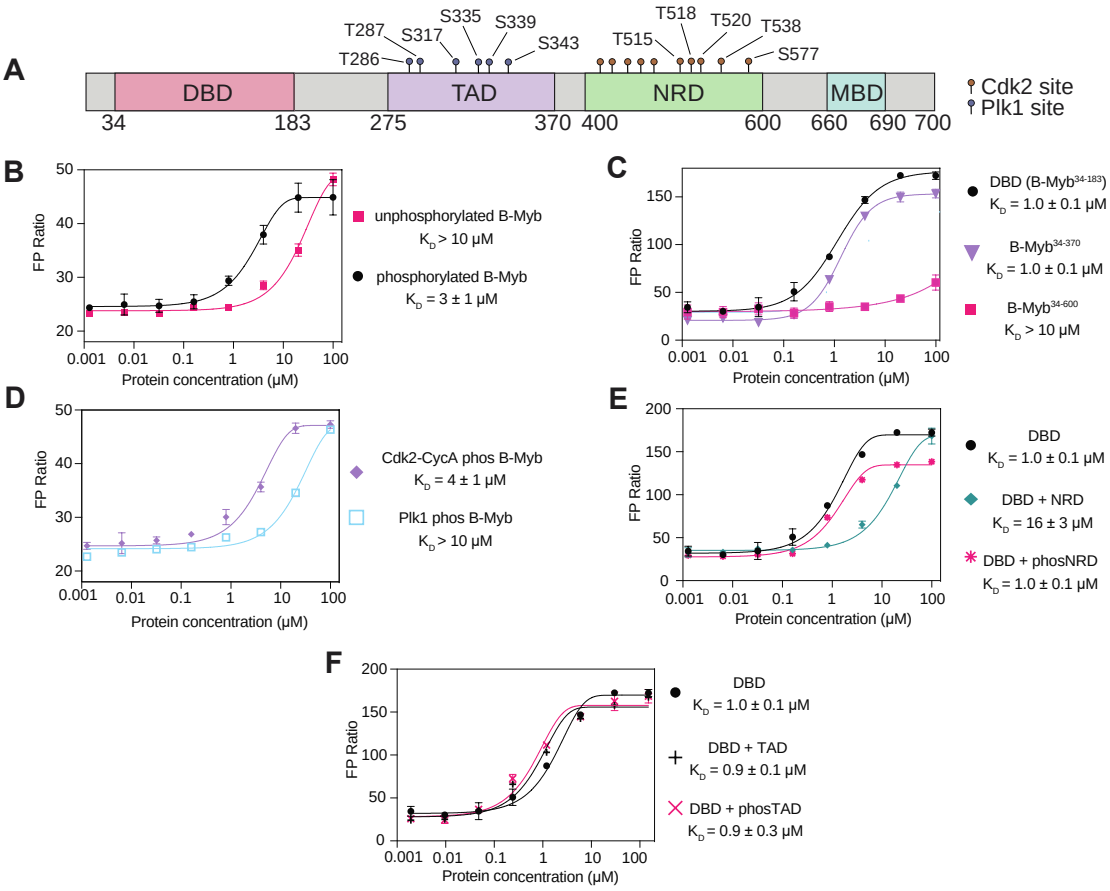

Figure 2.1 Phosphorylation by Cdk2-CycA enhances B-Myb binding to MBS DNA. A. a schematic presenting the boundaries of the DBD (DNA-binding domain), TAD (transactivation domain), NRD (negative regulatory domain), and MBD (MuvB- binding domain). Previously identified Cdk2 and Plk1 sites are indicated. **B**. fluorescence polarization (FP) assay of B-Myb binding to a TAMRA-labeled MBS probe. The measurements compare unphosphorylated B-Myb to B-Myb that was sequentially phosphorylated by Cdk2-CyclinA and Plk1. **C**. Same FP assay used to measure binding affinities of C-terminal truncations of B-Myb to the MBS probe. **D**. same FP assay used to measure probe affinity of B-Myb phosphorylated only by Cdk2-Cyclin A or Plk1 .BE. FP assay of DBD binding to MBS probe as in panel (C) but also performed by using DBD incubated with 30 μM NRD or phosNRD. **F.** as in panel (E) but using DBD incubated with 30 μM TAD or phosTAD, MBS, Myb-binding site.

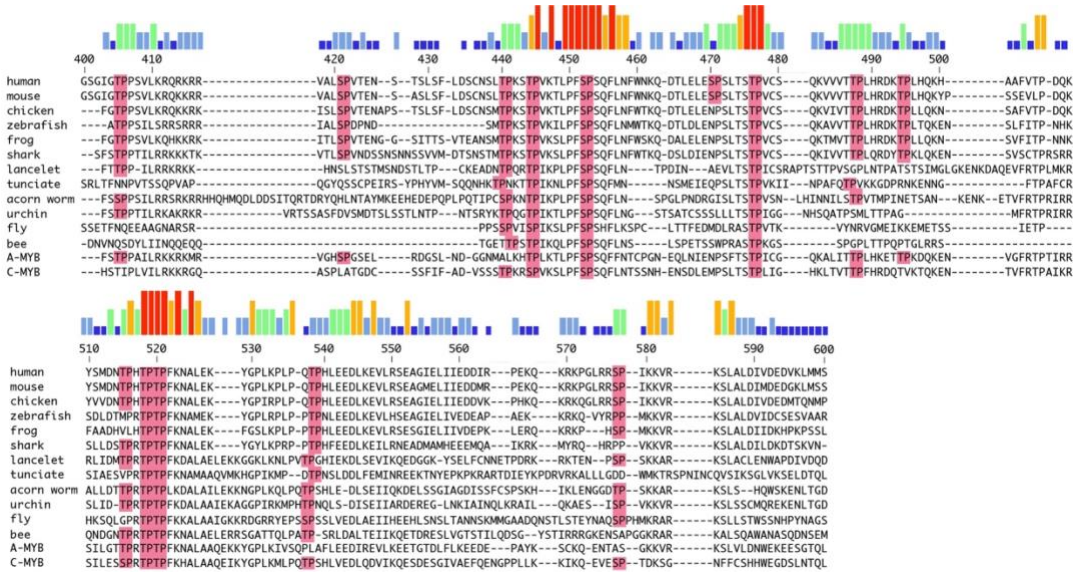

Figure 2.2. Sequence alignment of the B-Myb NRD. Sequences for B-Myb orthologs are shown along with the sequences of human A-Myb and c-Myb. Minimal Cdk sites consensus sites (S/TP) are highlighted in pink.

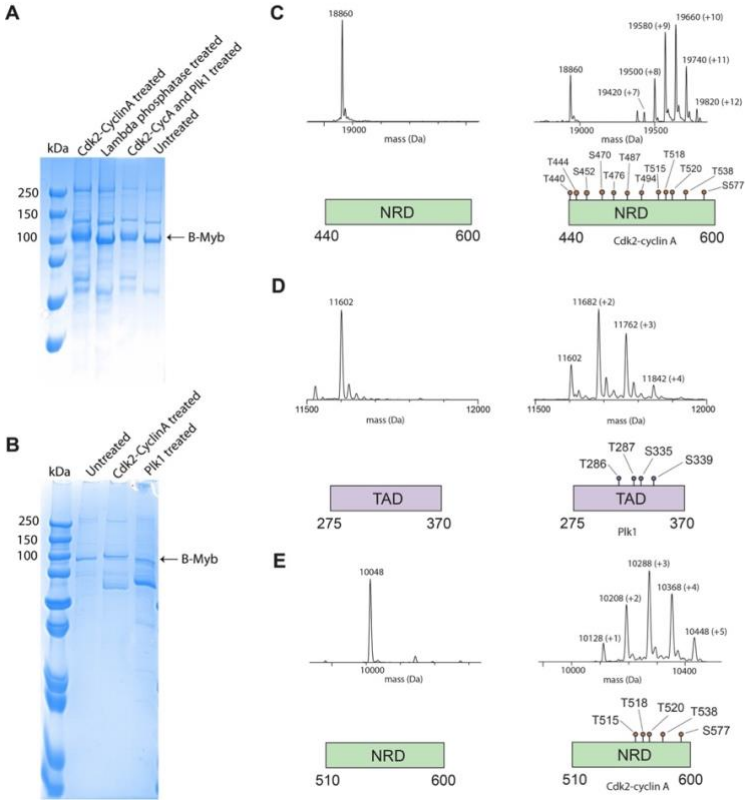

Figure 2.3. Confirmation of recombinant protein phosphorylation. A, B. PhosTag gels following purification of full-length B-Myb expressed in Sf9 cells and treatment with the indicated enzyme(s). The B-Myb band appears with similar mobility in the phosphatase treated and untreated samples, suggesting that untreated purified protein is not extensively phosphorylated. Phosphorylation with Cdk2-CycA produces a noticeable shift, whereas the shift with Plk1 treatment is not detectable when using Plk1 alone or together with Cdk2-CycA. However, we are confident in the activity of our Plk1 enzyme preparation considering our mass spectrometry results detecting TAD phosphorylation in panel D. **C.** B-Myb $NRD^{440-600}$ unphosphorylated (left) and phosphorylated (right) by Cdk2-Cyc A detected by mass spectrometry. In this construct there are 3 strong Cdk consensus sites ({S/T}Px{K/R}) at T444, T520 and S577 and 9 other weak consensus sites ({S/T}P). Peaks are labeled with the final mass and the number of phosphoryl groups added in parenthesis (+80 Da). **D.** B-Myb TAD unphosphorylated (left) and phosphorylated (right) by Plk1. This construct contains 4 Plk1 consensus sites ({D/N/E/Q}xSΦ) as depicted in the schematic diagram. **E.** B-Myb $NRD^{510-600}$ unphosphorylated (left) and phosphorylated (right) by Cdk2-Cyc A detected by mass spectrometry.

2.2.3 *Direct association of the NRD with the DBD*

We next probed the presence of intramolecular interactions within B-Myb that may drive the observed autoinhibition of DNA binding. We mixed separately purified domains and detected interdomain association by isothermal titration calorimetry (ITC). We observed no detectable binding of the TAD or MBD to an NRD construct that contains amino acids 440 to 600 (NRD 440–600, **Figure 2.4.A and B**). In contrast, we detected association of the DBD and NRD 440–600 and measured an affinity of K_D = 4.5 ± 0.5 μM (**Figure 2.4.C**). To map a more minimal NRD, we used sequence conservation to divide the NRD into two halves (**Figure 2.2**). We observed that the C-terminal half (amino acids 510–600, B-Myb 510–-600) binds the DBD with a similar affinity of KD = 4.9 ± 0.2 μM (**Figure 2.4.D**), and we did not observe association of the N-terminal half (B-Myb 440–510, **Figure 2.4.E**).

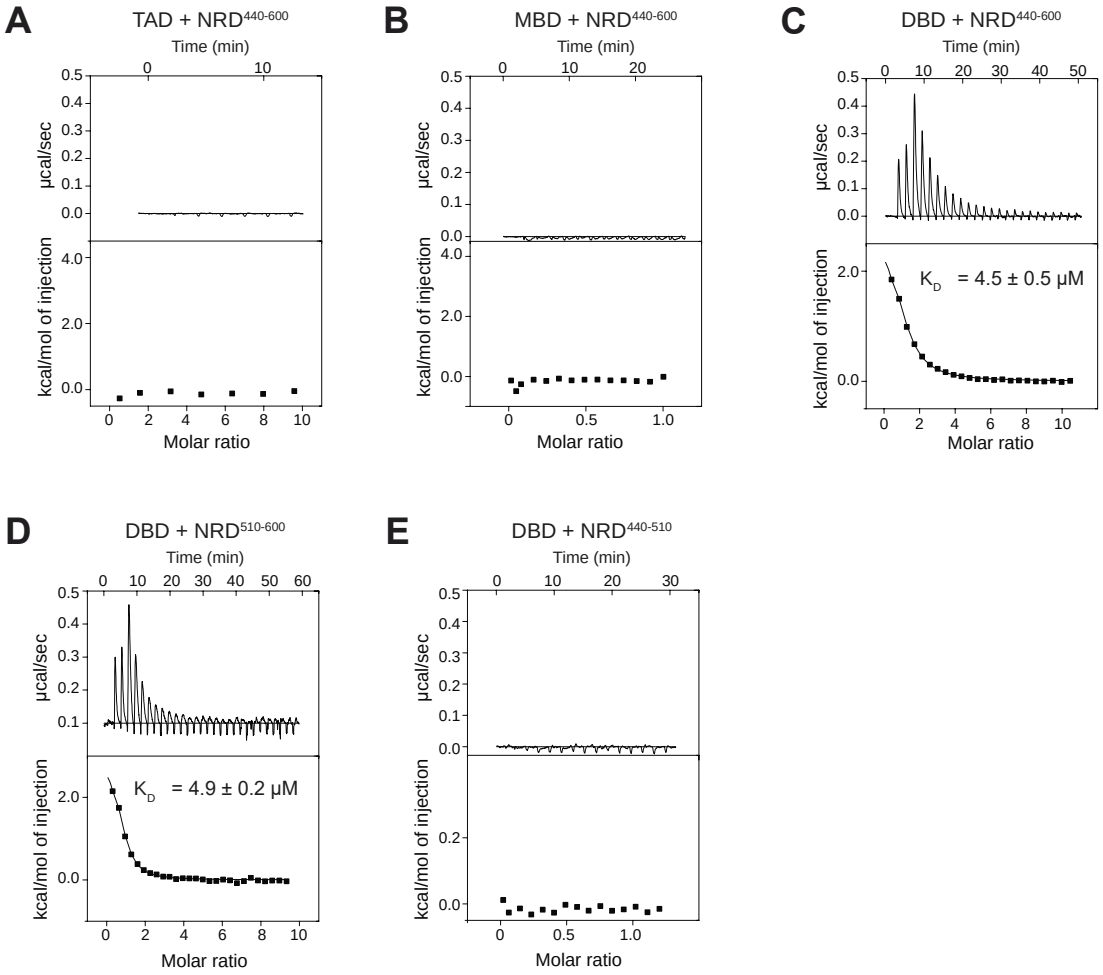

Figure 2.4. **B-Myb NRD510–600 directly binds DBD**. **A**, isothermal titration calorimetry (ITC) binding measurement between NRD440–600and TAD. **B**. ITC binding measurement between NRD440–600and MBD. **C**. ITC-binding measurement between NRD440–600and DBD. **D**. ITC-binding measurement between NRD 510–600 and DBD. **E**. ITC-binding measurement of NRD440–510and DBD. DBD, DNA-binding domain; MBD, MuvB-binding domain; TAD, transactivation domain.

2.2.4 *NMR spectroscopy mapping of the amino acids mediating the B-Myb DBD–NRD interaction*

We next used NMR to further probe the NRD510–600–DBD interaction. The minimal chemical shift dispersion of the 1H-15N HSQC spectrum of 15N-labeled B-Myb510–600 suggests that the fragment is structurally disordered (**Figure 2.5.A**). We therefore generated a 13C-15N double-labeled sample and proceeded with 13C-15N CON spectroscopy, which is well suited for studying interactions of intrinsically disordered proteins (Bastidas M. et al. 2015).

The two-dimensional CON spectrum contains crosspeaks at the chemical shifts of the backbone carbonyl carbon and amide nitrogen and is typically better dispersed than the 1H-15N HSQC spectrum. To observe the NRD-DBD association, we added isotopically unlabeled DBD to 13C-15N-labeled NRD and monitored the chemical shift perturbations in a two-dimensional CON spectrum. A number of cross-peaks showed changes in both intensity and position, which is consistent with the binding we observed by ITC (**Figure 2.5.B**). The most pronounced perturbations appear as loss of intensity, which reflects peak broadening from either intermediate exchange or from the NRD510–600 forming a larger molecular weight complex when bound by the unlabeled DBD.

We assigned the CON spectrum using standard backbone correlation experiments, and these assignments enabled identification of amino acid sequences in the NRD510–600 that are potentially critical for DBD binding (**Figure 2.5.C** and **D**). Plots of peak intensity loss (**Figure 2.5.D**) and chemical shift change (**Figure 2.6**) upon addition of DBD to the NRD 510–600 sample show that perturbations occurred at regions throughout NRD 510–600. We were particularly interested in the perturbations that clustered around residues 514 to 526 and 542 to 547 (**Figure 2.5.D** and **2.2**). These clusters of residues show broadening, and the sequences are relatively well conserved. In addition, the sequence between 538 and 565 has helical propensity, and analysis suggests a hydrophobic surface containing several leucines that are conserved in B-Myb orthologs (**Figure 2.7**). We surmised that if formed upon binding, such a helix would be a good candidate for facilitating interdomain interactions. To determine whether these regions are important for NRD-DBD association, we made two sets of alanine mutations in the most conserved residues found in these regions; we mutated together L541, E542, E543, D544 (NRD LEED) and together L541, L545, and L549 (NRD LLL). We expressed and purified the mutant NRD510–600 constructs and tested binding to DBD using ITC. We found that these NRD mutant domains do not bind to DBD (**Figure 2.5.E and F**). We note that mutations in the NRD do not markedly perturb the overall NMR spectrum, suggesting that the ensemble of

disordered NRD conformations remains intact (**Figure 2.8**). Together, these mutagenesis and NMR data support the conclusion that residues within 540 to 550 make critical contacts with the DBD.

There are five consensus Cdk2-CycA phosphorylation sites in NRD510–600 (T515, T518, T520, T538, and S577), and all of these phosphosites except T538 have been validated by two-dimensional tryptic peptide mapping and point mutagenesis (Lane S. et al. 1997), (Johnson TK. et al. 1999), (Sala A. et al. 1997), (Saville M.K. and Watson R.J. 1998). In our NMR spectra, we were unable to assign all the phosphorylation sites due to repetitive amino acid sequences, but we successfully assigned S577 and T518 (**Figure 2.5.D**). We observed a substantial change in intensity for the peak corresponding to T518 and for peaks corresponding to nearby residues (N514, T515, H517, T518) when DBD was added (**Figure 2.5.C** and **D**). In contrast, we observed minimal perturbations for the S577 peak and peaks corresponding to the residues around S577, which were reported to disrupt the NRD–DBD interaction when deleted (Werwein et al. 2019). To test the role of these phosphorylation sites in the NRD–DBD interaction, we created three C-terminal NRD 510–600 fragments with different phosphosites mutated to alanine (NRDS577A, NRD T538A, and NRD TTT, which contains T515A, T518A, T520A). We used these mutated and not phosphorylated NRDs in ITC experiments to detect binding affinities with DBD. We found that both

NRD S577A and NRD T538A bound to DBD with KD = 3.2 ± 0.2 μM and KD = 6.5 ± 0.2 μM, respectively (**Figure 2.5.G and H**). However, NRD TTT showed no detectable binding, indicating that these threonines, when unphosphorylated, are important to interact with DBD (**Figure 2.5.I**).

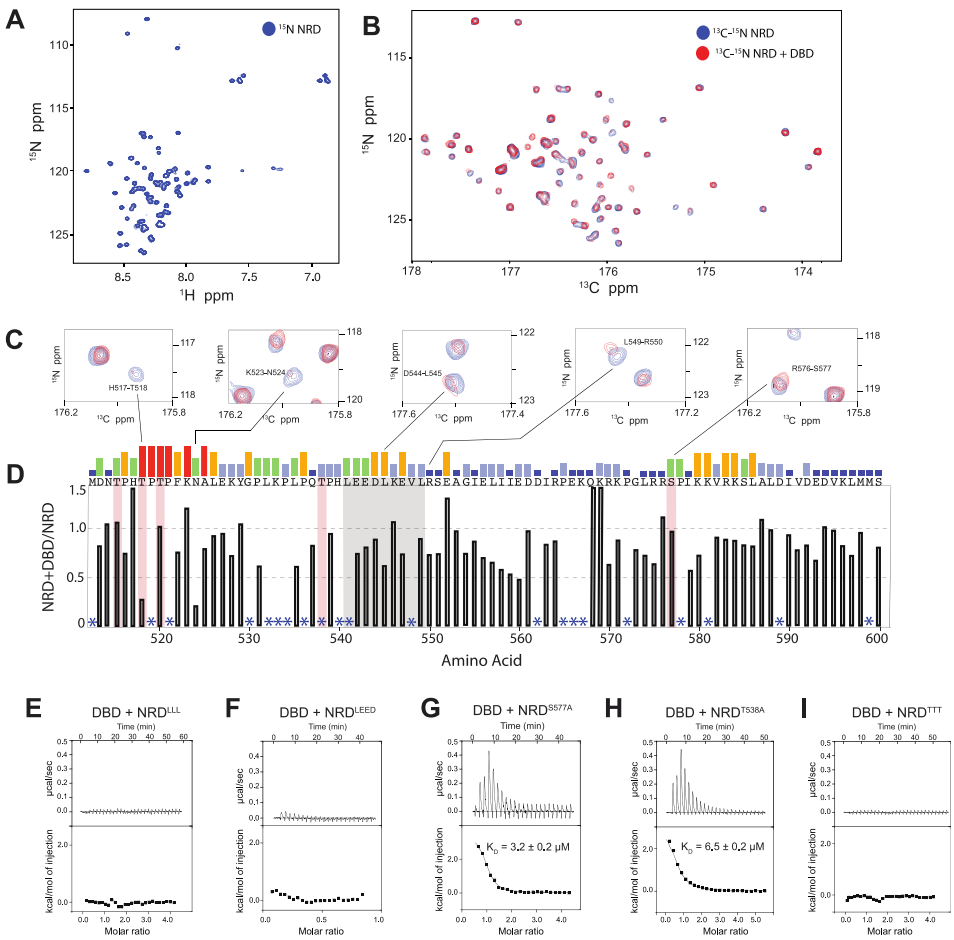

Figure 2.5. NMR spectroscopy maps potential NRD residues that interact with DBD. **A**.1H-15N HSQC spectrum of labeled NRD510–600at 300µM. **B**.13C-15NCON spectra of labeled NRD510–600at 300µM alone (blue) and with 600µM unlabeled DBD (red). **C**. close-up views of exemplary assigned peaks in the13C-15N CON spectra showing significant peak broadening. **D**. relative intensity of each amino acid plotted as the ratio of the intensity of NRD alone to the intensity of NRD + DBD. Asterisks mark amino acids that could not be assigned. Residues marked in red are Cdk consensus phosphorylation sites. Relative sequence conservation through Myb family members is displayed by the height of the bars above the primary sequence at the top of the graph. The sequence highlighted in gray corresponds to a region of high conservation and is the focus of our following mutagenesis studies. See **Figure 2.2** for the full NRD sequence alignment and **Figure 2.6** for analysis of chemical shift perturbations. **E–I**. ITC-binding measurements of DBD to mutant NRD510–600constructs. LLL refers to L541, L545, and L549, LEED refers to L541, E542, E543, D544, and TTT refers to T515A, T518A, T520A. DBD, DNA-binding domain; ITC, isothermal titration calorimetry; NRD, negative regulatory domain.

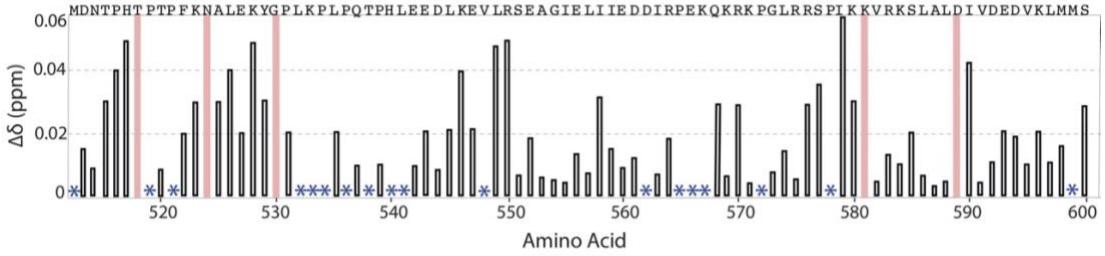

Figure 2.6. Chemical shift perturbation plot of NRD-DBD association. Chemical shift change ($\Delta\delta$) of the corresponding peak for each amino acid in the ^{13}C-^{15}N CON spectrum. The change compares the labeled NRD alone to the labeled NRD plus unlabeled DBD. $\Delta\delta$ is calculated using $\Delta\delta = \sqrt{((0.3\Delta N)^2 + \Delta C^2)}$, where ΔN and ΔC are the shift differences in each dimension and the 0.3 normalizes to the different nuclear gyromagnetic ratios. Overall, the perturbations are modest compared to the observed loss in peak intensities shown in Fig. 3D, although regions near the T515/T518/T520 phosphorylation sites and conserved L541/L545/L549 residues show relatively larger changes that is consistent with the peak intensity analysis.

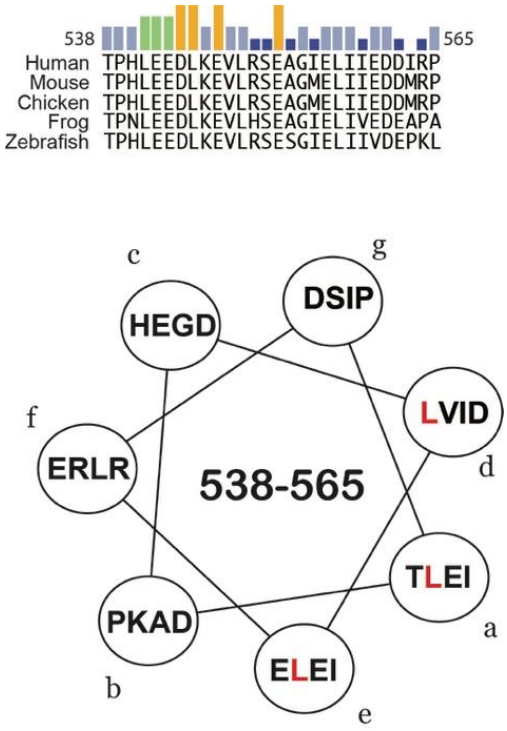

Figure 2.7. Rational for probing the L541/L545/L549 NRD mutant. (Top) Sequences for five B-Myb orthologs. The bars on top of the sequence reflect conservation from the larger sequence alignment shown in **Figure 2.2**. (Bottom) Helical wheel projection beginning with T538 in the “a” position. The projection suggests that this sequence has the potential to form an amphipathic helix with the three leucines (colored in red) positioned along one face.

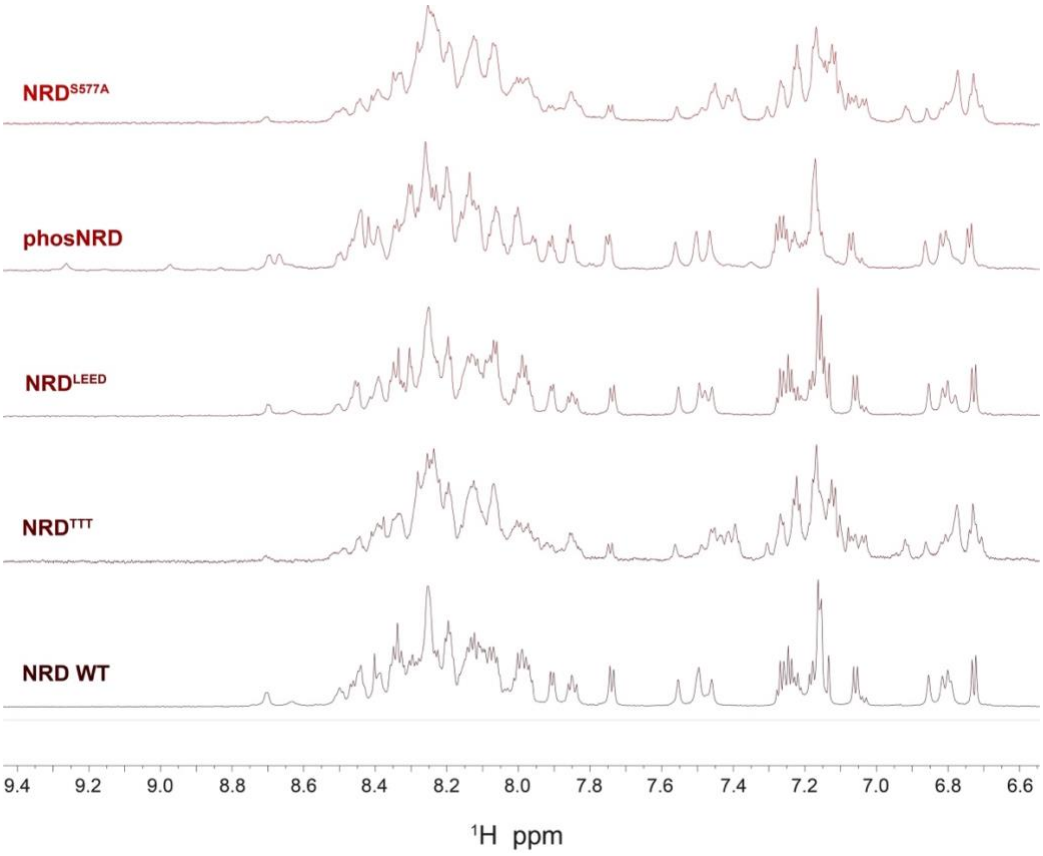

Figure 2.8. ^{1}H-NMR spectra of B-Myb NRD domains. 1D ^{1}H-NMR spectra were acquired for the indicated NRD construct at 300 μM: unphosphorylated WT (NRD WT), phosphorylated WT (phosNRD), S577A phosphorylation site mutant (NRD^{S577A}), L541A/E542A/E543A/D544A mutant (NRD^{LEED}), and T515A/T518A/T520A phosphorylation site mutant (NRD^{TTT}). The spectra show several chemical shift changes for select peaks from site specific phosphorylation or mutagenesis; for example, the downfield shifts of several amide protons in the phosNRD spectrum from sidechain phosphorylation are observable. However, there are no gross overall differences in the spectra, and the limited but similar chemical shift dispersion is consistent will all the constructs adopting similar distributions of disordered conformations.

2.2.5 *Phosphorylation of Cdk consensus sites in the conserved region of the NRD modulates the NRD–DBD interaction to regulate DNA binding.*

We next tested to what extent phosphorylation of Cdk sites in NRD 510–600 influences NRD binding to the DBD and the inhibition of DBD-DNA binding. We phosphorylated purified NRD 510–600 constructs with Cdk2-CycA and tested NRD-DBD affinities using ITC (**Figure 2.9**). We verified phosphorylation of the WT NRD 510–600 (B-Myb 510–600) on five sites with electrospray mass spectrometry (**Figure 2.3.E**). We observed no detectable binding toward DBD when WT NRD was phosphorylated (**Figure 2.9.A**). Similarly, we observed that phosphorylated NRD S577A and NRD T538A did not bind to DBD, indicating that phosphorylation of those specific sites is not required and that phosphorylation of T515A, T518A, T520A is sufficient to disrupt the interaction (**Figure 2.9.B** and **C**). Phosphorylation of NRD TTT also resulted in no binding to DBD (**Figure 2.9.D**), although we had already established that these threonine residues are critical for the association when the protein is unphosphorylated (**Figure 2.5.I**).

We performed the FP-binding assay with fluorescently labeled MBS probe and added the various WT and phosphorylation-site mutant NRD 510–600 constructs in trans (**Figure 2.9.E** and **F**). As previously shown in **Figure 2.1.F**, the DBD alone binds to the MBS probe with KD of 1.1 ± 0.1 μM and when NRD is added in trans to DBD, the affinity decreases to a KD of 16 ± 3 μM.

We found that, when unphosphorylated, the mutants NRD S577A and NRD T538A still inhibited DBD binding to the MBS probe. When NRD TTT was added in trans, DBD-binding affinity to the MBS probe was more weakly inhibited, consistent with our observation that T515, T518, and T520 are important for the interaction between the NRD and DBD that inhibits DBD binding to DNA (**Figure 2.5.E**). Phosphorylation of the NRD S577A and NRD T538A constructs with Cdk2-CycA abrogated their inhibitory effect on DNA binding, but phosphorylation of NRD TTT resulted in DNA-binding inhibition similar to the unphosphorylated mutant (**Figure 2.5.F**). Together, these FP and ITC results are consistent with a model in which phosphorylation of T515, T518, T520 modulates the association of the NRD with the DBD in a manner that can regulate DNA-binding affinity. Considering that neither mutation of the threonine phosphorylation sites nor phosphorylation of the WT NRD results in widespread changes to NMR spectra that would suggest overall structural changes (**Figure 2.8**), we favor the interpretation that these threonine residues make specific contacts with the DBD that are broken upon mutation or phosphorylation.

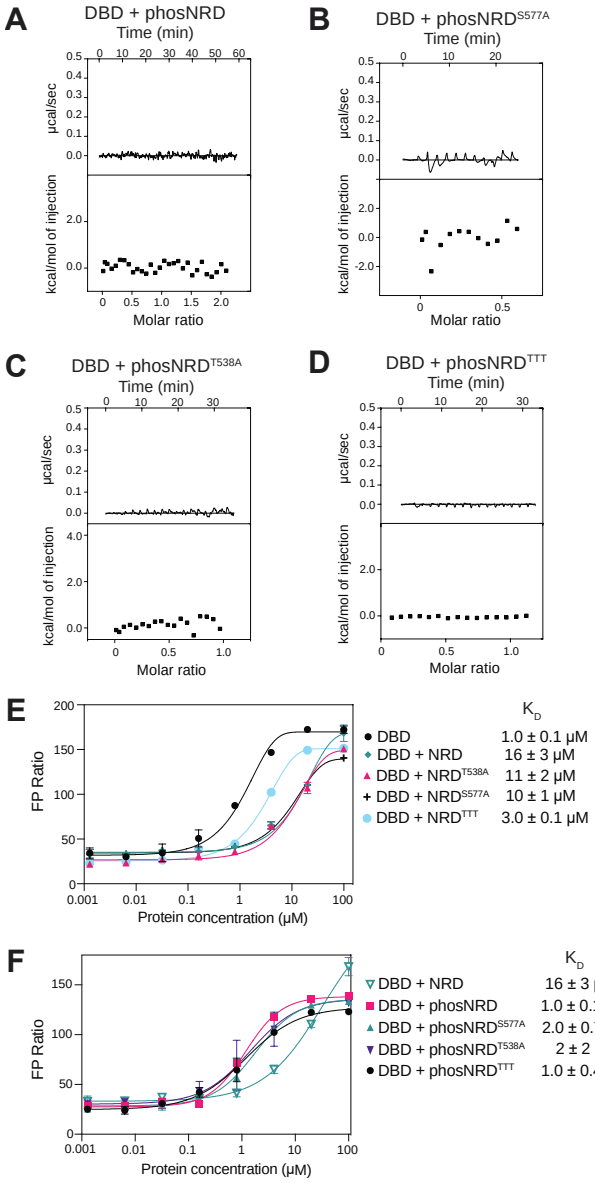

Figure 2.9. Phosphorylated NRD does not interact with DBD allowing DBD to interact with MBS DNA. A–D, ITC measurements of DBD binding to the indicated NRD construct after phosphorylation by Cdk2-CyclinA. Phosphorylation of NRD was confirmed through electrospray mass spectrometry shown in **Figure 2.2. E** and **F**, FP assay measurements of DBD binding to the TAMRA-labeled MBS probe incubated with the indicated NRD construct at 30µM. DBD, DNA-binding domain; FP, florescence polarization; ITC, isothermal titration calorimetry; MBS, Myb-binding site; NRD, negative regulatory domain.

2.2.6 *Disruption of the NRD–DBD interaction increases the transactivation potential of B-Myb*

To probe the functional significance of the NRD–DBD interaction in B-Myb–mediated transcriptional activation, we performed luciferase reporter assays in HCT116 cells (**Figure 2.10**). Plasmids encoding WT and mutant B-Myb were transfected along with the pGL4.10 luciferase reporter plasmid containing an artificial promoter with three MBS consensus sequences. Such constructs have already been utilized to detect B-Myb–dependent gene activation (Ness SA. Et al. 1989), (Seong HA. et al. 2003). As previously described, we observe a positive effect of B-Myb on the activity of the MBS promoter and a significant decrease of activation when the DBD is deleted. We tested mutation of phosphorylation sites in the NRD that we found to be important for NRD-DBD association in the NMR and ITC assays (**Figure 2.5** and **2.9**). We found that B-Myb with mutation of the three NRD Cdk site threonines (T515/T518/T520) to either alanine or glutamate showed higher activity in the luciferase assay. Considering these mutations resulted in loss of NRD-DBD association, we propose that disruption of the repressive interaction leads to the observed more efficient B-Myb transactivation. We also tested two other mutations at Cdk consensus sites in the NRD, one of which was previously shown to regulate B-Myb by modulating the repressive activity of the NRD (Werwein E. et al. 2020). However, in our assay, we found

that T538 mutation did not change B-Myb activity significantly from that of WT and that S577 mutation resulted in a subtle, albeit significant, reduction of activity.

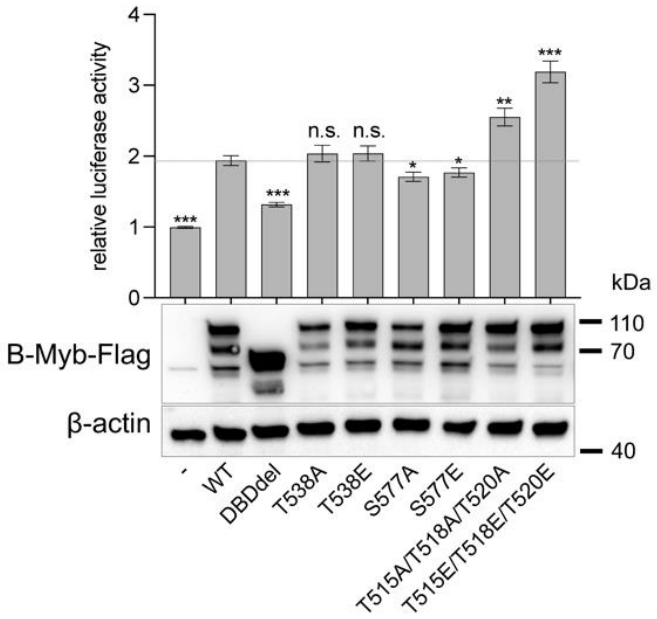

Figure 2.10. Disruption of a critical NRD-DBD interface hyperactivates B-Myb. HCT116 cells were transfected with a luciferase reporter plasmid containing three Myb-binding sites (MBSs) upstream of a minimal promoter together with plasmids expressing Flag-tagged wild-type (WT) B-Myb or the indicated mutants. DBDdel is mutant with entire DNA-binding domain deleted (amino acids 12-182). Mean values ± SD of four biological replicates are given, and significances were calculated by the Students paired t test (*p≤0.05, **p≤0.01, ***p≤0.001 compared with WT B-Myb). Expression levels of B-MYB variants in the luciferase assay samples were analyzed by SDS-PAGE/Western blot. DBD, DNA-binding domain; NRD, negative regulatory domain.

2.3 Discussion

Our data show that B-Myb binding to an MBS DNA sequence is inhibited by the intramolecular association between the DBD and the NRD region between 510 and 600 (**Figure 2.11**). This inhibited conformation is regulated by Cdk2-CycA–dependent phosphorylation of T515, T518, and T520, which disrupts the interdomain interaction between the NRD and DBD and permits stronger DNA association. Our mechanistic findings are generally consistent with a number of studies demonstrating, primarily using cell-based reporter assays, that B-Myb transactivation of MBS promoters is autoinhibited by the NRD and increased by co transfection with CycA (Lane S. et al. 1997), (Petrovas C. et al. 2003), (Ziebold U. et al. 1997) (Bessa M. et al 2001), (Sala A. et al. 1997), (Saville M.K. and Watson R.J. 1998), (Ansieau S. et al. 1997). Moreover, our biochemical data that Cdk phosphorylation specifically modulates DNA binding offers mechanistic explanation for previous observations that B-Myb phosphorylation and localization to target promoters are coincident (Sadasivam S., 2012).

We note several differences between our findings here monitoring the behavior of purified proteins and previous results from cell-based assays. For example, previous studies determined that C-terminal truncations starting from D561 cause the strongest hyperactivity of B-Myb toward a promoter containing Myb-binding sites (Lane S. et al. 1997), (Bessa M. et al. 2001). Co

transfection with Cdk2-CycA further stimulated the activity of the truncations; however, the activity of full-length B-MYB was much further increased by Cdk2-CycA overexpression (Bessa M. et al. 2001). More recently, it was reported that the B-Myb DBD interacts with a region in the NRD between 560 and 589 and Cdk-mediated phosphorylation of the residue S577 relieves this inhibition (Werwein E. et al. 2020). In contrast, our NMR and mutagenesis data from biochemical and reporter assays implicate sequences in the NRD that are N-terminal to D561 as those making primary contact with and regulating the DBD, including sequences around the T515, T518, and T520 phosphorylation sites and the amino acid stretch from L541 to L549 (**Figure 2.5**). Our studies did not find S577 to be involved in regulating the NRD-DBD association or S577E to have a positive effect on MBS promoter activity. Rather, we found the more conserved T515/T518/T520 as important phosphorylation sites that regulate MBS-dependent activity. In contrast, other studies using reporter-based cell assays found that point mutations of T518/T518/T520 inhibit MBS transactivation (Ziebold U. et al. 1997), (Johnson TK. et al. 1999), (Bartsch O. et al. 19990) however, it should be noted that other phosphorylation sites were mutated in addition to these sites and may function through independent mechanisms. As an overarching explanation to differences between previous studies and our results, which specifically focus on DNA binding, we speculate that other protein interactions

or additional posttranslational modifications also account for the importance of the NRD and its phosphorylation for B-Myb activity and regulation.

Our results demonstrate how intrinsically disordered regions (IDRs) in TFs can regulate TF interactions and how this regulation can be modulated through posttranslational modifications. Other examples of IDRs specifically influencing TF binding to DNA include p53, PU1, ETS1, and TFB2M (Sun X. et al. 2021), (Basu U. et al. 2020), (Pufall MA. 2005), (Xhani S. et al. 2020). Like B-Myb, other proteins that control the cell cycle are typically phosphorylated at multiple sites in their IDRs by Cdks (Fu Z. et al. 2008), (Marceau AH. et al. 2019), (Rubin SM. 2013), (Xu M. et al. 1994). Multisite Cdk phosphorylation of TFs like B-Myb and their regulators modulates unique functions through significant changes in structure and interdomain interactions. For example, multisite phosphorylation of the retinoblastoma protein (Rb) promotes ordered structure and induces interdomain interactions that compete with binding to E2F transcription factors (Rubin SM. 2013). In contrast, phosphorylation of the mitotic transcription factor FoxM1 by Cdk2-CycA and Plk1 induces an order to disorder transition (Marceau AH. et al. 2019). FoxM1 phosphorylation switches the protein conformation from an inactive to an active state by inhibiting intramolecular interactions. Our observation that B-Myb inhibition via the interdomain NRD-DBD association is released upon Cdk phosphorylation aligns with this common theme of

regulation in cell-cycle transcription factors through control of interdomain interactions and structural transitions that promote or reduce structural disorder.

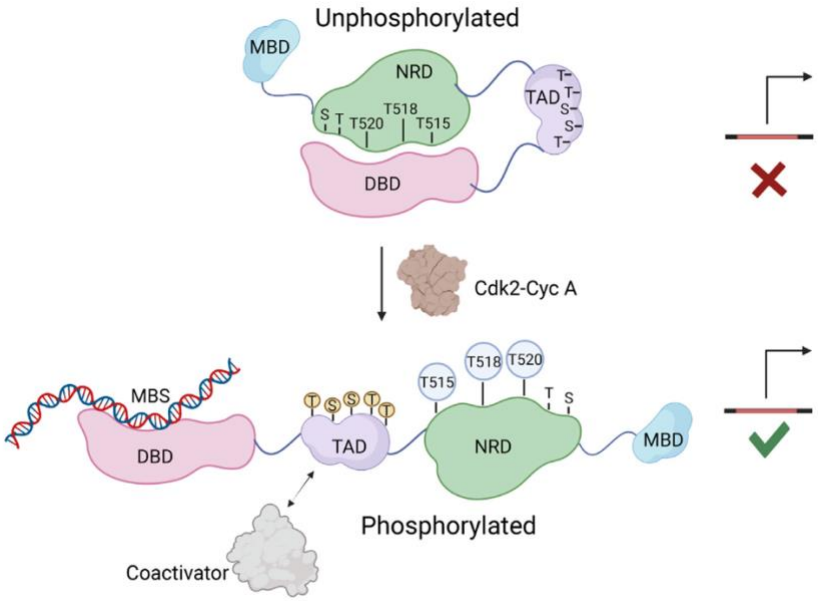

Figure 2.11. Structural model for B-Myb autoinhibition and activation upon Cdk2 phosphorylation. Autoinhibition results from an interdomain association of the NRD and DBD. Cdk2 phosphorylation inhibits this association, releasing the DBD for promoter association. In the canonical model for B-Myb activation, TAD association with coactivators stimulates gene expression. DBD, DNA-binding domain; NRD, negative regulatory domain; TAD, transactivation domain.

2.4 Materials and Methods

2.4.1 *Recombinant protein expression and purification*

The human B-Myb full-length protein and B-Myb34–600 constructs were expressed in Sf9 cells with a cleavable N-terminal Strep tag using the FastBac expression system. Cells were harvested and lysed in a buffer containing 300 mM NaCl, 50 mM Tris, 1 mM DTT, 10% Glycerol v/v, Sigma Protease Inhibitor (P8340), and 1 mM PMSF (pH 8.0). Protein was purified with StrepTactin Sepharose High Performance resin (Cytiva) equilibrated in lysis buffer. The lysed cells were clarified by centrifugation at 19,000 rpm for 45 min at 4 °C. The cleared lysate was incubated with resin for 1 h at 4 °C, and the resin was washed with a buffer containing 300 mM NaCl, 50 mM Tris, 1 mM DTT, and 10% glycerol v/v (pH 8.0). The protein was then eluted in 300 mM NaCl, 50 mM Tris, 5 mM desthiobiotin, 10% glycerol v/v, and 1 mM DTT (pH 8.0). Protein was dialyzed into storage buffer (200 mM NaCl, 50 mM Tris, 1 mM BME, and 10% glycerol v/v (pH 8.0)) and stored at −80 °C.

The human B-Myb–truncated constructs (DBD, TAD, NRD, B-Myb34–370) were expressed in *Escherichia coli* from an engineered pGEX plasmid with an N-terminal GST tag and a TEV protease cleavage site. Proteins were expressed overnight by inducing with 1 mM IPTG at 19 °C. All proteins were lysed in a buffer containing 200 mM NaCl, 40 mm Tris, 5 mM DTT, and 1 mM PMSF (pH 8.0). The lysed cells were clarified by centrifugation at 19,000 rpm

for 45 min at 4 °C. Protein lysates were allowed to bind to equilibrated Glutathione Sepharose resin (Cytiva) for 30 min and washed to remove unspecific proteins. The proteins were eluted with a buffer containing 200 mM NaCl, 40 mM Tris, 5 mM DTT, and 10 mM reduced L-Glutathione (pH 8.0). Eluted proteins were further purified using Q-sepharose and cleaved with TEV protease at 4 °C overnight. Proteins were then passed through Glutathione Sepharose resin to remove the free GST and concentrated to run through Superdex-75 (GE Healthcare) into 200 mM NaCl, 25 mM Tris, and 1 mM DTT (pH 8.0). Cdk2-CycA and Plk1 kinase domains were expressed and purified as previously described (Marceau AH. et al. 2019).

To generate phosphorylated protein reagents, kinase reactions were performed similar to as previously described (Marceau AH. et al. 2019). B-Myb protein constructs following final purification were incubated with 10 mM ATP, 50 mM MgCl2, and 20% by mass of either Cdk2-CycA, Plk1 kinase domain, or both Plk1 and Cdk2-CycA, overnight at 4 °C. The kinase reaction was concentrated and run over Superdex-75 (GE Healthcare) to remove kinases and ATP, and phosphorylation of the proteins was confirmed by electrospray mass spectrometry using a Sciex X500B QTOF system.

2.4.2 *Fluorescence Polarization assay*

Dissociation constants for direct binding between DBD and MBS DNA sequence were determined by titrating increasing amounts of DBD into 20 nM

of TAMRA dye-labeled MBS DNA probe. The duplex DNA probe was synthesized by Integrated DNA Technologies and had the following sequence: 5′-GCATTATAACGGTCTTTTAGCGCCTGG/36-TAMSp/-3′. For DBD + NRD assays, DBD and NRD were incubated for 30 min on ice before titrating the labeled MBS probe in a buffer containing 150 mM NaCl, 25 mM Tris, 1 mM DTT, and 0.1% Tween20 (pH 8). FP measurements were acquired on a PerkinElmer EnVision 2103 Multilabel plate reader with excitation at 559 nm and emission at 580 nm. The dissociation constants (KD) were calculated by fitting millipolarization (mP) values of three technical replicates against concentration using a one site–binding model in GraphPad Prism 8.

2.4.3 *Calorimetry*

Dissociation constants (K_D) for DBD and NRD interactions were measured using ITC with a MicroCal VP-ITC system. All proteins were concentrated as needed and dialyzed into a buffer containing 150 mM NaCl, 20 mM Tris, and 1 mM BME (pH 8). DBD (500 μM) was titrated into NRD (50 μM) at 19 °C. The dissociation constant of NRD mutants and phosphorylated NRDs were determined similarly. K_Ds are the average fits from three technical replicates analyzed using the Origin ITC software package with the SD reported as error. All the fit stoichiometry (n) values were between 0.6 and 1.

2.4.4 *NMR Spectroscopy*

The HSQC and CON spectra for DBD and NRD interaction studies in **Figure 2.5** were collected at 25 °C on a Bruker Avance III HD 800-MHz spectrometer equipped with a cryogenically cooled probe. The sample contained 13C-15N-labeled NRD510–600 at 300 μM in a buffer containing 20 mM sodium phosphate pH 8.0, 100 mM NaCl, 1 mM DTT, and 5% (v/v) D_2O. The backbone assignment of the NRD was accomplished using standard NH-edited triple-resonance experiments [HNCO, HNCACB, CBCA(CO)NH, C(CO)NH] supplied by Varian/Agilent (Bathisdas M. et al. 2015). The NH-edited experiments were collected on a Varian/Agilent INOVA 600 MHz NMR equipped with a cryogenically cooled probe. The experiments for backbone assignments were collected at pH 6.0 (otherwise same buffer) due to favorable chemical exchange, and assignments were transferred to pH 8.0 CON spectra through pH titrating. The 1D 1H spectra were acquired using the Avance III HD 800-MHz NMR system. Samples contained 300 μM NRD in a buffer containing 50 mM sodium phosphate pH 6.0, 100 mM NaCl, 1 mM DTT, and 10% (v/v) D2O. All spectra were processed using NMRPipe and analyzed and assigned using Sparky (Delaglio F. et al. 1995), (Lee W. et al. 2105).

2.4.5 *Cell culture, luciferase assays, and Western blot*

HCT116 colon carcinoma cells were grown in Dulbecco's modified Eagle's medium (Gibco, high glucose, GlutaMAX Supplement, pyruvate)

supplemented with 10% fetal bovine serum (Corning, Regular Fetal Bovine Serum) and penicillin/streptomycin (Gibco). Cells were maintained at 37 °C and 5% CO_2.

The 3xMBS luciferase reporter construct was created by inserting a double-stranded oligonucleotide containing three copies of a high-affinity B-Myb–binding site (TAACGGTG) (1, 2, 3, 4) upstream of the herpes simplex thymidine kinase minimal promoter (5-TTATAACGGTCTTAATAACGGTCTTAATAACGGTCTTTTAGCTTCGCATATTAAGGTGACGCGTGTGGCCTCGAACACCGAGCGACCCTGCAGCGACCCGCTTAA-3; MBSs in bold, minimal TK promoter in italics) into the KpnI and NcoI sites of the pGL4.10[luc2] vector (Promega). The ORF of human MYBL2/B-Myb isoform 1 (NM_002466.4) was cloned into pcDNA3.1+ (ThermoFisher Scientific) and fused with an N-terminal Flag tag. Point mutations were introduced following the QuikChange site-directed mutagenesis protocol, and the DBD (amino acids 12-182) was deleted following the NEB Q5 protocol.

Stimulation of the 3xMBS promoter activity was analyzed by luciferase reporter assays with extracts of transfected HCT116 cells. Thirty thousand cells per 48 wells were plated and transfected with 1 µl PEI (Polysciences, PEI 25K), 75 ng of promoter-reporter plasmids (3xMBS-pGL4.10 or pGl4.10 empty vector), 100 ng of pcDNA3.1 plasmids expressing Flag-B-Myb (WT or

mutants), and 25 ng renilla luciferase plasmid (pGL4.70). Cells were lysed 48 h after transfection, and luciferase activity was measured with the Dual-Luciferase Reporter Assay System (Promega) following the manufacturer's recommendations on an EnVision 2105 plate reader (PerkinElmer). Relative promoter activities of the 3xMBS-pGL4.10 reporter after expression of WT or mutant B-Myb were calculated by normalizing to renilla luciferase activity, and the activity of the pGL4.10 empty vector cotransfected with the respective B-MYB constructs.

Expression levels of WT and mutant B-Myb were analyzed by loading 10 µg of the remaining luciferase assay lysates onto a 10% SDS gel, followed by Western blotting. Flag-B-Myb was detected with the Anti-OctA-Probe antibody (Santa Cruz Biotech, sc-166355 HRP, dilution 1:2000), and β-actin was probed with the Direct-Blot HRP anti-β-actin antibody (BioLegend, clone W16197A, Cat. # 664804, dilution 1:10,000).

Chapter 3: Structural and biochemical characterization of B-Myb binding to nucleosomes

3.1 Introduction

In this chapter, I describe the chromatin organization in a cell and how transcription factors regulate the structure of the chromatin subunit: nucleosome. Multicellular organisms have different cell types that carry out defined functions controlled by cellular gene expression programs. These

gene expression programs depend on the genome packaging state in the nucleus. The eukaryotic genome is organized as chromatin in the nucleus and packaged as nucleosomes (Bram S and Ris H. 1971) (Olins A.L. and Olins D.E. 1974). The nucleosome core particle (NPC) is the subunit of chromatin that wraps the genomic DNA 146 base pairs at a time around a histone octamer comprised of four histone proteins, H2A, H2B, H3 and H4 (Kornberg RD. 1974) (Thomas J.O. and Kornberg R.D. 1975), (Lutter L.C et al. 1977). The histone octamer contains one H3-H4 tetramer and two H2A-H2B dimers. The linker DNA between two nucleosome core particles is occupied with the H1 histone, which facilitates the compaction of nucleosome arrays to make a 30 nm fiber of chromatin (Blank, TA. and Becker, PB. 1995). The highly negatively charged DNA with about 146 base pairs interacts with the positively charged surface at the outer edge of the histone octamer as seen through the crystal structure of a nucleosome (Luger K. et al. 1997) (**Figure 3.1.A** and **B**). The wrapping of the DNA around the histones keeps it spatially organized in the nucleus and regulates the activation of transcription sites by sterically hindering the accessibility of transcription initiation complexes interacting with the DNA (Knezetic JA and Luse DS. 1986).

There are two significant states in how nucleosomes are arranged. The static state model explains two distinct states of heterochromatin: the more compacted form of chromatin and the more loosely packed form of

euchromatin (Wang J. et al. 2016). However, recently heterochromatin has been in a more dynamic state with chromatin repressors making it inaccessible to transcription machinery; thus, such genome locations are unavailable for gene activation (Kamakaka T. 2003). In the euchromatin state, the nucleosomes are occupied with activator factors that more prominently unravel the transcription start sites for the necessary machinery to interact with promoter sites and activate genes (Fan, Y. et al. 2005). These two dynamic states of the genome are critical to maintaining the homeostasis of the genome by carefully regulating gene activation and repression. However, in the genome, nucleosomes are not arranged stochastically; instead, they are abundant and well positioned downstream of transcription start sites (TSSs) and replication origins (ORIs), and only two nucleosomes positioned in the nucleosome-free regions (NFRs) or nucleosome-depleted region (NDRs) (Kaplan N. et al. 2009). The stereotypical organization of the nucleosomes in *Saccharomyces cerevisiae* shows that a promoter region has a nucleosome-depleted area immediately upstream of TSS and is flanked on either side with nucleosomes. Nucleosomes downstream of the NDR are named …,-2, -1, and nucleosomes in the gene body are described numerically as +1, +2,... as shown in the **Figure 3.1.C** (Zang Z. and Pugh, BF. 2011), (Jansen A. and Verstrepen KJ. 2011).

It is still unclear whether there is a general pattern to how nucleosomes are arranged around transcriptionally active promoters; however, histone modifications and positioning of nucleosomes are the general features that distinguish between active and repressed promoters. The rearrangement of the promoter architecture is highly dynamic during the transitions between the heterochromatin and euchromatin, which depends upon factors like ATP-dependent remodelers, transcription factors, pioneer factors, and DNA sequence features at a given promoter (Kubik S. et al. 2015) (Zhang Y. et al. 2009). During the *Saccharomyces cerevisiae* cell cycle, the TSSs are seen to change their occupancy in a cyclic manner showing more fuzziness during the S and Mitosis phases compared to the G1 and G2 phases. This positioning change is seen in the nucleosomes downstream of NDR, i.e., the -2 and -1 nucleosomes (Denize O. et al. 2016). It is also known that some transcriptionally active genes have more disorder to how the nucleosomes downstream of NDR are positioned (Lee W. et al. 2007).

It should also be noted that not only nucleosome occupancy but general patterns on histone modifications also play a role in nucleosome organization and regulation of promoters. RNA-seq and ChIP-seq data in cancer cell lines show more significant enrichment of active histone marks (H3K4me2 and H3K27ac) during mitosis (Liu Y. et al. 2017). However, the nucleosome

architecture spanning cell-cycle-dependent promoters during the normal cell cycle in non-cancerous cells remains largely unknown.

Recently, our lab published data supporting that MuvB protein complex interacts and stabilizes the +1 nucleosome at several selected cell-cycle dependent promoters (Asthana A. et al. 2022). The MuvB protein complex is the master regulator of cell-cycle dependent genes occupying CHR promoters throughout the cell cycle (Sadasivam S. and DeCaprio JA. 2013). MuvB protein complex consists of five proteins, namely, LIN9, LIN37, LIN52, LIN54, and RBAP48). The RBAP48 is a known histone-binding protein interacting with the H3-H4 tetramer and H3 tail (Zhang W. et al. 2013). A more recent publication shows the Cryo-EM structure of MuvB associating with nucleosomes through LIN9 interacting with an acidic patch of nucleosomes (H2A-H2B) (Koliopoulos MG. et al. 2023). However, it is not known how activator proteins B-Myb and FoxM1 contribute to the nucleosome structure, possibly explaining a mechanism by which they activate the cell-cycle-dependent genes during the S phase. In this chapter, I report my finding that B-Myb DNA binding domain interacts with nucleosomes and my results characterizing this interaction's structural and functional details.

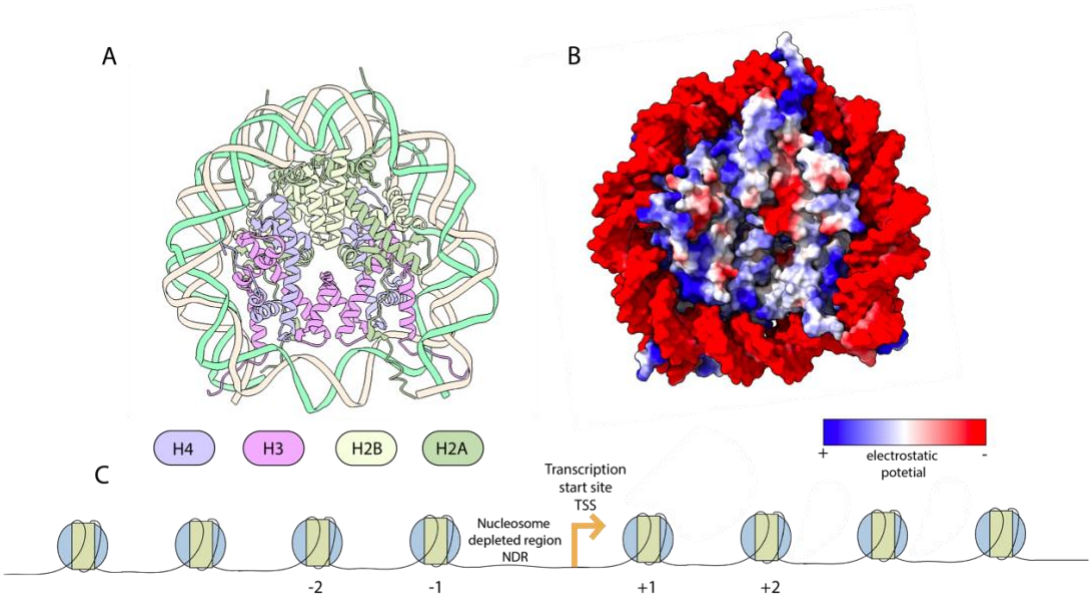

Figure 3.1. Structure of the nucleosome and nucleosome architecture in the promoter. A. 2.8 Angstrom crustal structure of nucleosome core particle reconstituted from *Xenopus laevis* histones refolded using widom 601 positioning sequence. PDB ID 1AOI. **B.** Electrostatic potential surface map showing the charge distribution of histone core and DNA. **C.** Stereotypical organization of nucleosomes in a promoter

3.2 Results

3.2.1 *Biochemical characterization of B-Myb binding to nucleosomes*

To determine whether B-Myb interacts with nucleosomes, we first reconstituted the nucleosome core particle from *Xenopus laevis* histones and the Widom 601 positioning sequence with fluorescein (Lowary PT, Widom J. 1998). We performed a fluorescence polarization (FP) assay using the fluorescein-tagged nucleosomes to determine recombinant and purified B-Myb binding efficiency. To test binding, we purified the full-length B-Myb protein and the DNA binding domain (DBD) alone from Sf9 cells and *E. coli* expression systems. We found that the B-Myb DBD interacts with nucleosomes tighter than the full-length protein (**Figure 3.2.A**). We recently investigated how the phosphorylation of B-Myb by Cdk2-cyclin A regulates the DBD, and we hypothesized that B-Myb must be phosphorylated to interact with nucleosomes. Therefore, we used the full-length protein phosphorylated with Cdk2-cyclin A. As expected, phosphorylated B-Myb was found to interact with nucleosomes with a similar affinity to DBD alone (**Figure 3.2.B**). We also note that neither phosphorylated B-Myb nor DBD bound to the free 601 DNA sequence with high affinity, although there may be a nonspecific interaction at high DNA concentration (**Figure 3.2.B**). It was proposed based on a low-resolution EM structure by Koliopoulos MG. et al. that the MuvB binding domain of B-Myb interacts with nucleosomal DNA; however, in our FP assay,

we found that only the DBD can interact with nucleosomes (**Figure 3.2.C**). We also tested DBD-nucleosome complex formation using electrophoretic mobility shift assay, and we discovered that unphosphorylated B-Myb shows the construction of the complex much later than the phosphorylated B-Myb (**Figure 3.2.D, E**).

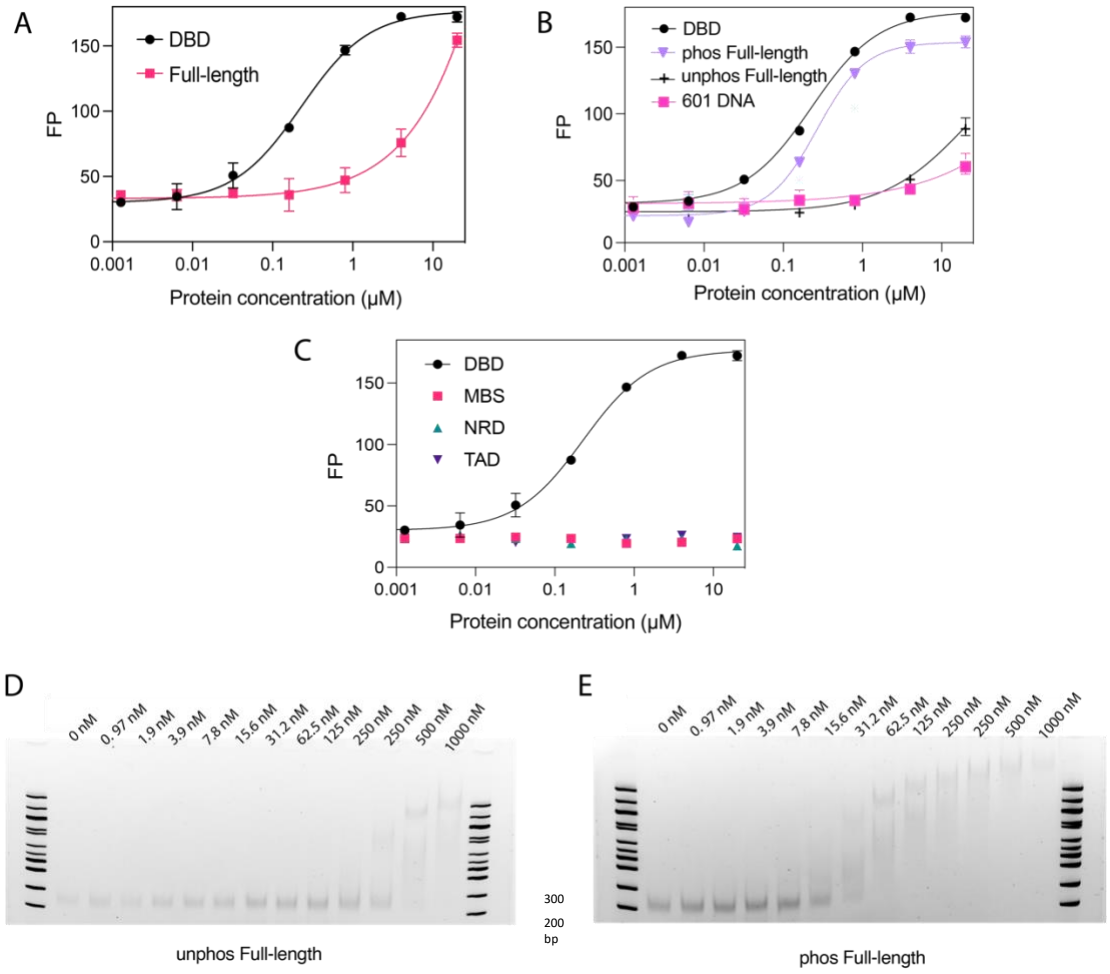

Figure 3.2. Biochemical characterization of B-Myb binding to nucleosomes. A. DBD interacts with nucleosomes with a binding affinity of 230 ± 20 nM with full-length protein binding non-specifically. **B.** Phosphorylated full-length protein interacts with nucleosomes with a 270 ± 20 nM. The phosphorylated full-length protein interacts with 601 sequences non-specifically. **C.** Only DBD shows nucleosome binding capacity, while TAD, NRD, and MBS domains do not interact with nucleosomes. **D.E.** Binding of phosphorylated and unphosphorylated B-Myb show different affinities with nucleosomes with increasing concentrations of B-Myb starting from 0 to 1000 nM.

3.2.2 *Cryo-EM structure of B-Myb DNA binding domain bound to Nucleosomes.*

To understand the structural details of how B-Myb interacts with nucleosomes, we used Cryo-EM with the DBD-nucleosome complex. We first isolated the complex using gel-filtration and used the fractions with all the components to set cryo-EM grids (**Figure 3.3.A** and **B**). We got good particle density and distribution with many orientations of the nucleosome, as seen through the micrographs and 2D classes (**Figure 3.3.C** and **D**). CryoSparc was our software tool to process the data (**Figure 3.4.A**). The overall resolution for the nucleosome was at 2.8 angstroms; however, because the electron density for the DBD is not high, we couldn't get a high resolution for the DBD. The initial refined density showed that the DBD possibly interacted with the H2A-H2B dimer and the DNA between SHL 1 and SHL 2 (**Figure 3.4.B**).

To get high-resolution details on where the DBD is binding at the DNA, we tightened the mask around the DNA, which resulted in the loss of information near the H2A-H2B dimer (**Figure 3.4.C**).

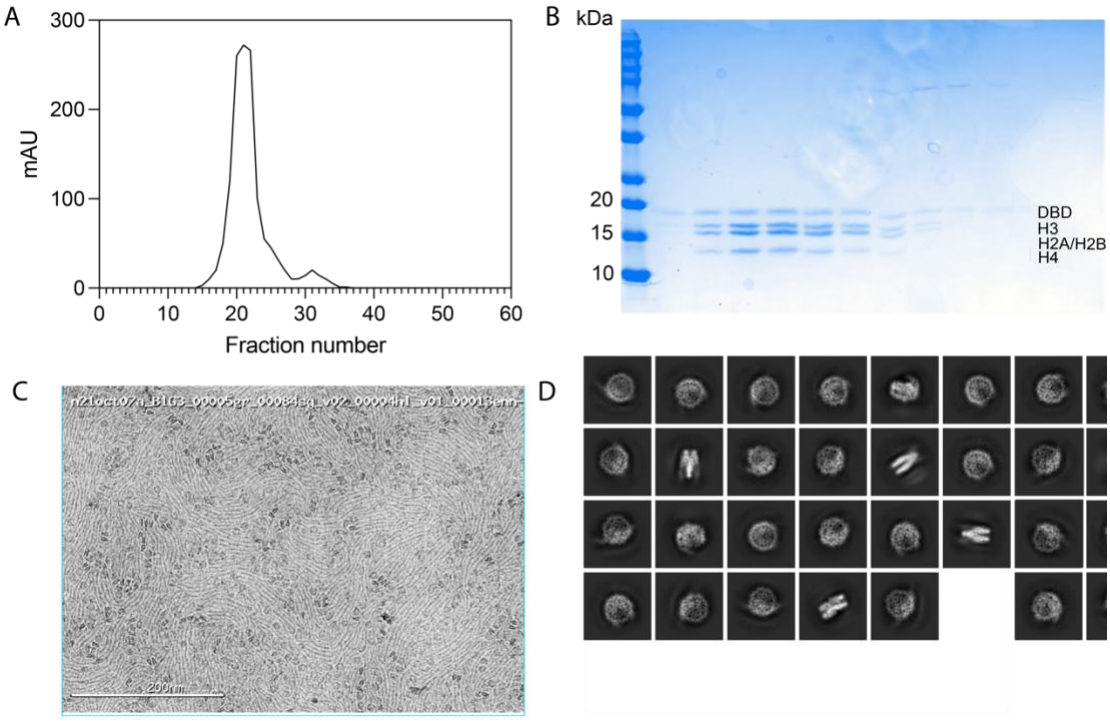

Figure 3.3. Isolation of DBD-nucleosome complex for Cryo-EM grids. A. Size exclusion chromatography of the DBD-nucleosome complex. **B.** SDS-PAGE analysis of the chromatography's peak fractions from 18-24. **C.** A Titan Krio 300KeV microscope was used to collect 22,120 movies. All movies were beam-induced motion corrected using CryoSparc. Particles were picked using a Blob picker. **D.** The best 2D classes were selected after particles picked from the blob picker tool.

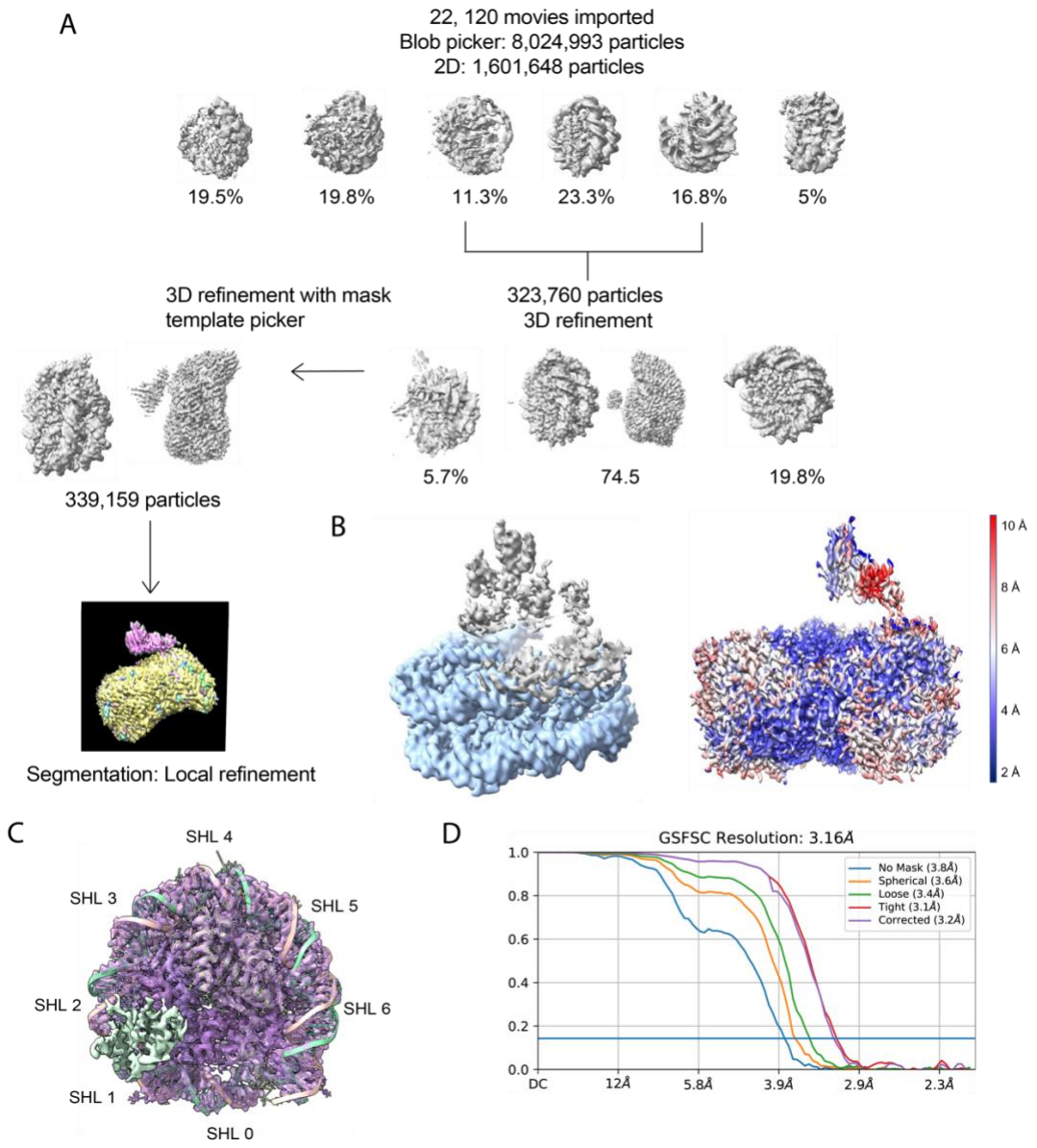

Figure 3.4. Refinement workflow of cryo-EM dataset using CryoSparc software. A. Initial 3D reconstructions were used to identify particles with good signals in all orientations. 3D refinement showed heterogeneity in the sample. 19.8% of the particles showed no DBD density in the 3D reconstruction. Particles that underwent 3D reconstruction with the DBD density were used for template picking and local refinement. **B.** Segmentation of DBD refined using *RELION 3.0* with local resolution map. **C.** Local refinement at the DNA shows DBD interacting between SHL 1 and SHL 2. Nucleosome density is aligned with the PDB 6R94. **D.** Gold-standard Fourier shell correlation curve.

Although this processing approach resulted in the loss of information near the H2A-H2B dimer, we obtained a high-resolution map for the nucleosome at 2.3 angstroms, allowing us to confirm the DNA sequence where the DBD interacts. Surprisingly, this DNA sequence is a MBS site (TAAGCG) in-between SHL +1 and SHL +2 and the GCG partial sequence right below the cryo-EM density (**Figure 3.5.A**) (Bergholtz S. et al. 2001). To test whether this partial motif is necessary for DBD to interact with the nucleosome, we mutated this motif to CGGATC and reconstituted nucleosomes with the fluorescein-tagged 601 Widom sequence and performed an FP assay. B-Myb affinity towards the nucleosomes with the MBS site mutated showed a significant reduction. However, it retained some unspecific binding, possibly due to histone interactions (**Figure 3.5.B**). From the cryo-EM model, the density appears near the solvent-exposed CGC partial MBS sequence. Thus, we wondered how the accessibility to this partial sequence embedded in the nucleosome would affect DBD binding to nucleosomes. Therefore, we changed the position of the partial MBS sequences +1, +2, and +3 base pairs upstream towards SHL +2 (**Figure 3.5.C**). We reconstituted nucleosomes with the shifted partial motifs in the fluorescently labeled Widom DNA. All three cases showed a decreased affinity when the partial MBS motif was moved from the original binding site towards the minor groove, consistent with

the MBS partial motif is not fully accessible when it's in the minor groove (**Figure 3.5.D**).

The acidic patch formed by the H2A and H2B dimer is a popular target for transcription factors that bind nucleosomes (McGinity RK. and Tran S. 2021). The cryo-EM density hovers over the H2A helix (**Figure 3.6.A**). To test whether DBD interacts with the H2A-H2B dimer, we refolded the H2A-H2B dimer and labeled H2A with fluorescein. Our FP experiment showed that DBD interacts with H2A-H2B dimer with 3.0 ± 0.4 μM affinity (**Figure 3.6.B**). We also mutated the H2A helix binders, which are the solvent-exposed residues of the H2A helix (E105A, K108A, H109A, and S112A) (**Figure 3.6.C**). All the mutations except S112A of H2A showed reduced and unspecific binding; however, not a complete loss of interactions altogether, suggesting that DBD interacts with nucleosomes through both H2A-H2B dimer and partial MBS motif; both interactions are necessary to form a stable complex (**Figure 3.6.D**).

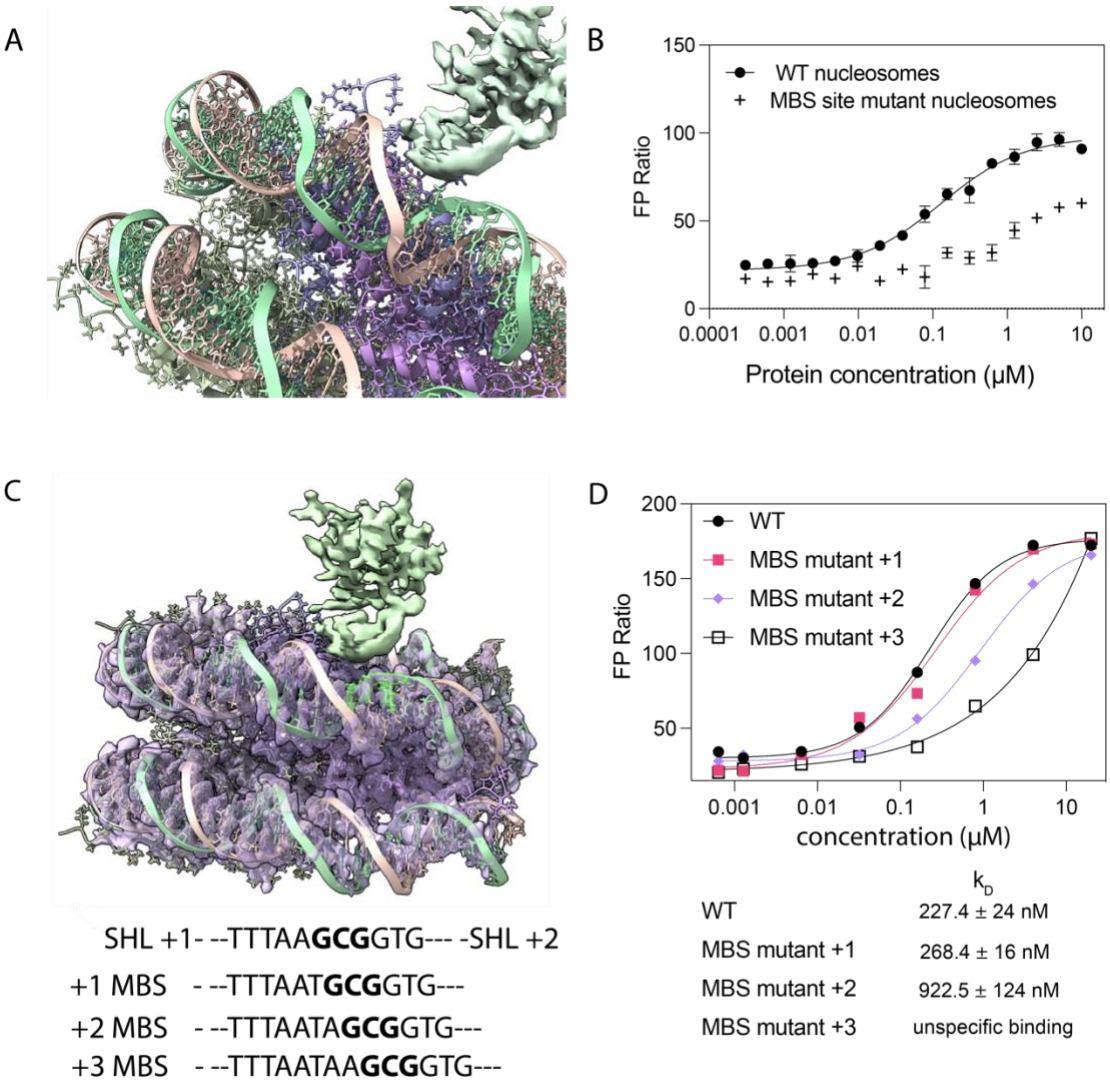

Figure 3.5. B-Myb DBD recognizes a partial MBS motif in the Widom 601 DNA. A. Density for the DBD is nestled in the major groove in-between SHL +1 and SHL +2. **B.** FP assay to determine the K_D for binding to the nucleosomes with the mutated Widom 601 sequence show weakened affinity compared to the WT nucleosomes. **C.** Partial MBS sequence GCG motif is shifted +1, +2, and +3 bases at a time towards SHL +2. **D.** Mutated Widom 601 sequences were generated by PCR using fluorescently labeled primers to be refolded into nucleosomes. FP assays were carried out by titrating DBD.

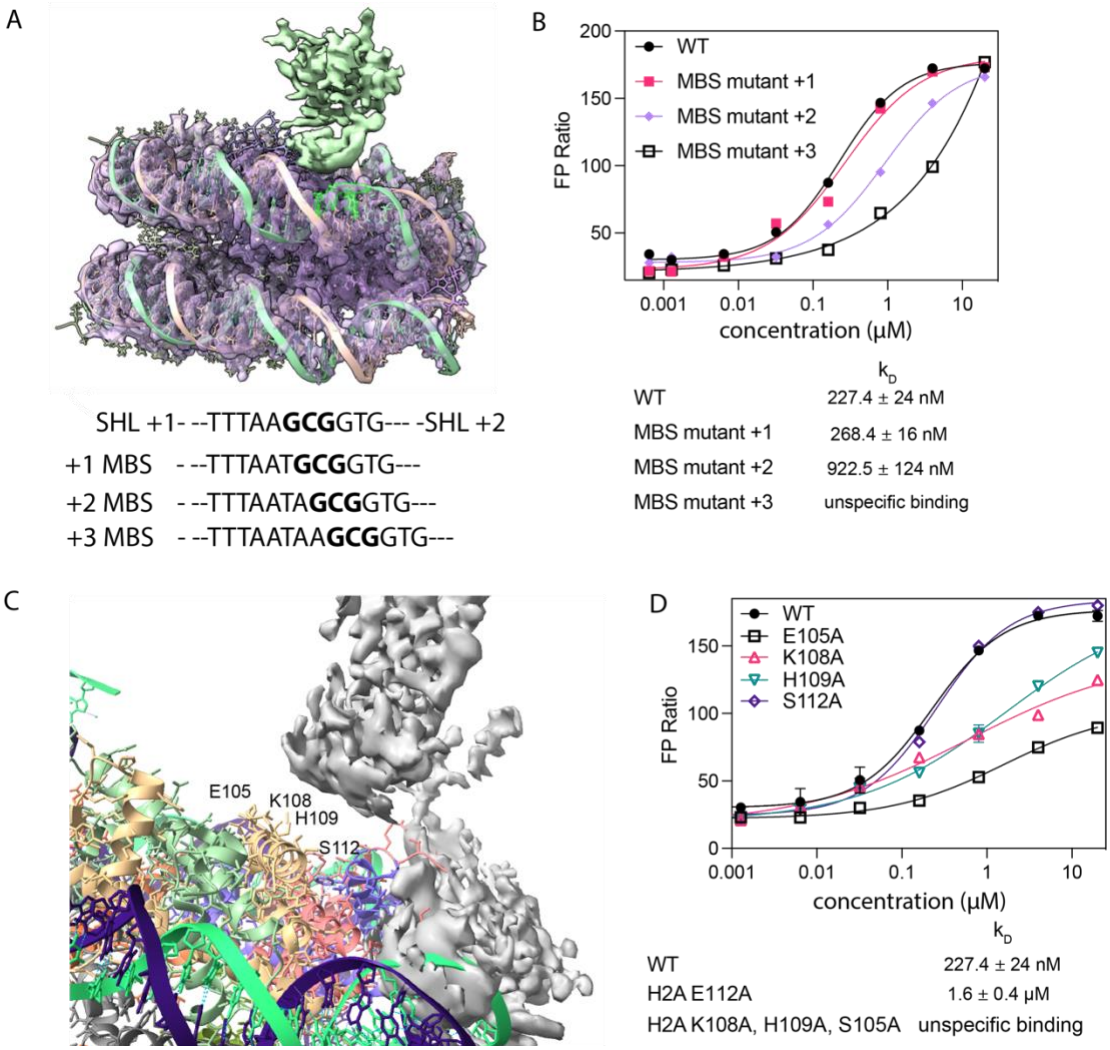

Figure 3.6. B-Myb DBD recognizes the H2A helix to interact with nucleosomes. A. The density for the DBD was extended without the local mask applied. This density is near the H2A-H2B dimer. **B.** FP assay to determine the K_D for the reconstituted H2A-H2B dimer shows an affinity of 3.0 ± 0.4 μM. **C.** Cryo-EM model showing the H2A helix residues near the DBD density. **D.** Histones carrying the H2A mutation were refolded with WT histones to make octamer and refolded with Widom fluorescently labeled Widom 601 DNA to make mutated nucleosomes.

3.2.3 *B-Myb DBD and MuvB compete for the same binding interface in the nucleosome.*

The current understanding of how B-Myb activates cell-cycle-dependent genes is still being determined. Evidence supports the premise that MuvB and B-Myb are needed as a complex for cell-cycle gene activation and mitosis (Sadasivam S. et al. 2012). However, what causes B-Myb to activate mitotic genes that MuvB previously repressed during the G0 to early G1 phases of the cell cycle remains unknown. We hypothesize that B-Myb functions as a de-repressor by relieving the repression caused by MuvB at the late cell-cycle dependent gene promoters. Evidence from our lab supports the premise that MuvB represses late cell-cycle dependent genes by stabilizing the +1 nucleosome at the promoters (Asthana A. et al. 2022). There is also much evidence that B-Myb is recruited to these promoters through MuvB, and this association is essential to activate a subset of late cell-cycle dependent genes (Muller GA. et al. 2012). Thus, our model is that recruitment of B-Myb to the cell-cycle dependent promoters relieves repression caused by MuvB through destabilizing MuvB association with the nucleosome.

We used the electrophoretic mobility shift assay and the FP assay to investigate the effect of B-Myb DBD binding to nucleosomes in the presence of MuvB. We first determined the migration of the MuvB-nucleosome complex in the native PAGE gel by incubating 1 μM MuvB with 20 nM nucleosomes

(**Figure 3.7.A** Lane 3) indicated by *. Then we counter-titrated B-Myb DBD to MuvB-nucleosome complex and examined the super-shifted band changes (**Figure 3.7.A** Lane 4-11). Super shift corresponding to the B-Myb-nucleosome band was determined by incubating 1 μM DBD with 20 nM nucleosomes. We also wanted to determine if B-Myb and MuvB compete to interact with nucleosomes in a FP assay. We first determined the binding affinity of MuvB with nucleosomes (**Figure 3.7.B**). We titrated MuvB to the fluorescent probe of DBD bound to nucleosomes and found that MuvB can no longer interact with nucleosomes (**Figure 3.7.C**). We also found that when we titrated DBD to MuvB-bound nucleosomes, the FP ratio did not change (**Figure 3.7.D**). Here we cannot rule out a possible competition between DBD and MuvB because the unchanged FP ratio is likely due to having an equilibration of a DBD-nucleosome complex forming concurrently upon competing MuvB.

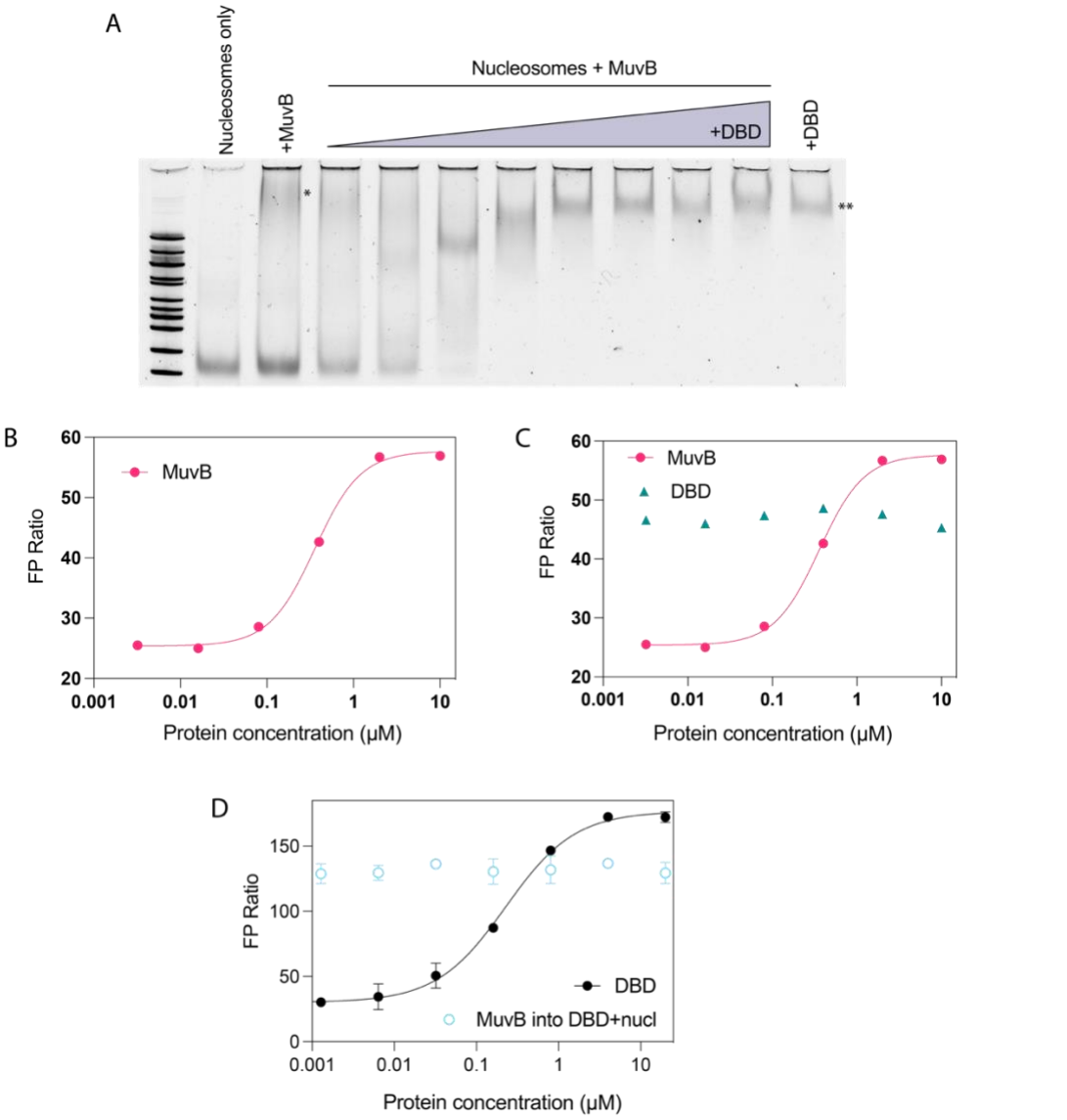

Figure 3.7 B-Myb DBD and MuvB compete for the same binding interface in the nucleosome. A. Lane 2: 20 nM nucleosomes. Lane 3: 1μM MuvB incubated with 20 nM nucleosomes. Lane 4-11: B-Myb DBD (0 μM, 50 nM, 150 nM, 250 nM, 500 nM, 1 μM) counter-titrated to previously incubated 1μM MuvB with 20 nM nucleosomes. Lane 12: 1 μM of B-Myb DBD incubated with 20 nM nucleosomes. **B.** FP assay with MuvB titrated to fluorescein-labeled nucleosomes. MuvB interacts with nucleosomes with an affinity of 358.0 ± 0.2 μM. **C.** DBD was counter-titrated to MuvB-nucleosome fluorescein-labeled complex. **D.** MuvB complex was counter-titrated to the DBD-nucleosome fluorescein-labeled complex.

3.2.4 *DNA binding domain is necessary but not sufficient to activate cell-cycle dependent genes*

To determine whether B-Myb DBD has a biologically relevant role in cell-cycle-dependent gene expression, we used a luciferase reporter assay with a DBD deletion construct in HCT116 cells (**Figure 3.8**). Given the well-established functional role of B-Myb DBD in MBS promoters, we wanted to compare with two known cell-cycle dependent B-Myb targeted promoters Bub1 and Birc5 (Osterloh L. et al. 2007). We found that B-Myb DBD deletion significantly reduced the activation of both cell-cycle dependent, and cell-cycle independent MBS promoters compared to the WT construct. However, Bub1 and Birc5 promoters retained some activity compared to the MBS promoter. Collectively taken, this data shows that B-Myb DBD is necessary contributing to the activity of the cell-cycle dependent promoters.

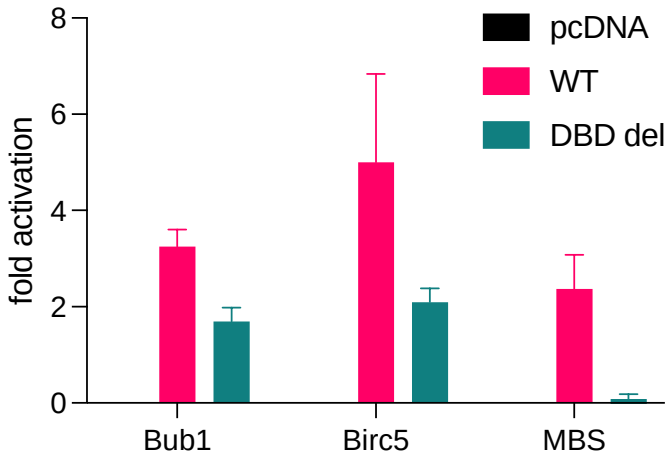

Figure 3.8. Functional comparison of B-Myb WT and DBD deletion mutant on the activity of cell-cycle dependent and independent B-Myb promoters. HCT116 cells were transfected with a luciferase reporter plasmid containing three Myb-binding sites (MBSs) upstream of a minimal promoter and plasmids expressing Flag-tagged wild-type (WT) B-Myb or the DBD deletion mutants. DBD del is the mutant with the entire DNA-binding domain deleted (amino acids 12-182). Mean values ± SD of four biological replicates are given. Expression levels of B-MYB variants in the luciferase assay samples were analyzed by SDS-PAGE/Western blot.

3.2.5 *Functional role of B-Myb DNA binding domain in cells*

Previous literature shows that B-Myb is localized to cell-cycle dependent promoters through the interaction with MuvB Sadasivam S. et al. 2012). Therefore, we wondered if B-Myb could still localize to cell-cycle promoters if the DBD is deleted. To precipitate chromatin bound to B-Myb, we overexpressed strep-tagged B-Myb WT and DBD deletion mutants in HCT116 cells. Chromatin-immunoprecipitation of strep showed decreased binding of B-Myb DBD to the human CCNB2 and Bub1 promoters (**Figure 3.9**). Both DBD and MBD deleted constructs showed substantial loss of binding to both CCNB2 and Bub1 promoters. However, in our assay, we did not see a loss of binding of the MBD mutant at CCNB2 and Bub1 promoters which was seen for CCNB1 promoter in previous studies (Iness A. 2018). However, it is also reported that their MBD mutant stably expressing cells did not show a difference in proliferation compared to WT. Thus, we concluded that DBD is essential to stabilize B-Myb at the cell-cycle dependent promoters by interacting with the most closely positioned nucleosome at the promoter.

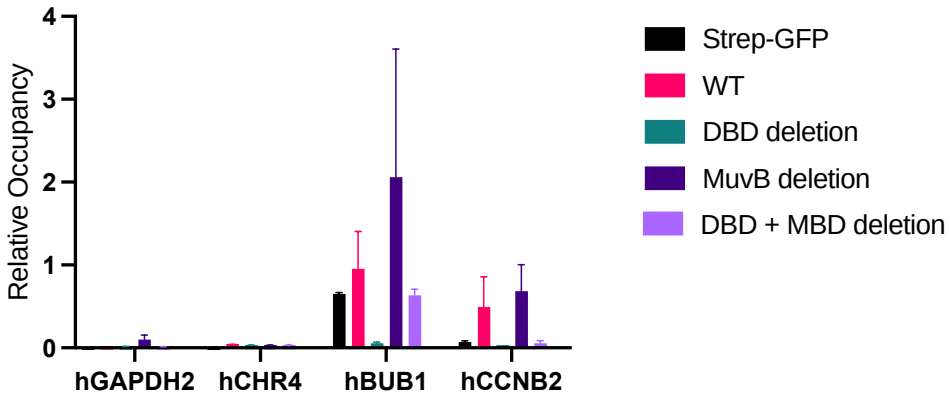

Figure 3.9. Functional comparison of B-Myb WT and DBD deletion mutant on binding to chromatin at the cell-cycle dependent promoters Bub1 and CCNB2. HCT116 cells overexpressed with strep-tagged B-Myb WT, DBD deletion, and DBD+MBD deletion were crosslinked with 1% formaldehyde. Chromatin immunoprecipitated with streptactin resin was digested and extracted to carry out qPCR with Bub1 and CCNB2 primers. Mean values ± SD of three technical replicates of one biological experiment are given.

3.3 Discussion

B-Myb is emerging as an essential biomarker in several cancers. B-Myb's importance in cell proliferation is linked to its interaction with the cell-cycle regulator complex MuvB. MuvB occupies the cell-cycle dependent promoters throughout the cell cycle and recruits B-Myb in the S phase to form an activating complex MMB, which activates genes needed for late cell-cycle dependent genes in mitotic progression. The question in the field has been to understand the mechanism by which B-Myb makes MMB an activating complex. There have been no known hypotheses regarding this mechanism. However, recent structural and biochemical studies have highlighted how MuvB occupies the cell-cycle gene promoters. One study from our lab show that MuvB binds reconstituted nucleosomes in vitro and in cells downstream of several known cell-cycle promoters to repress gene activation in the arrested cells (Asthana A. et al. 2022). Another study focusing on the structure of MuvB bound to a nucleosome shows a possible mechanism of how B-Myb might be converting MuvB to an activating complex (Koliopoulos MG. et al., 2023). In this study, they claim that B-Myb MBD bound to LIN9 and LIN52 of MuvB remodels the nucleosomal DNA, and this is perhaps how B-Myb destabilizes +1 nucleosome to destabilizes the repression caused by MuvB. This may also explain why only MBD of B-Myb in *Drosophila* is sufficient to rescue the B-Myb knockdown phenotype and show loss of

binding to CCNB1 promoter in a chromatin-immunoprecipitation assay (Andrejka L et al. 2011), (Iness A. 2018). Koliopoulos MG. et al. also show that the interaction with nucleosomes mainly occurs through LIN37 and LIN9 interacting DNA and the acidic patch, which is probably why LIN37 negative cells cannot repress gene expression in arrested cells; however, other MuvB proteins retain binding to target promoters (Mages CF. et al. 2017), (Asthana A. et al. 2022).

The mechanism by which B-Myb overcomes MuvB's repression is still unclear because there's no structural model discovered with just MuvB bound to nucleosomes. Koliopoulos MG and collogues show LIN37 binding to the nucleosomal entry DNA as the nucleosome interacting component; however, there is no mechanism unveiled to explain how this interaction activation of gene expression. Similarly, B-Myb MBD with LIN9 and LIN52 are modeled into the MMB density; however, there is no explanation as to why the small helical fragment of MBD is capable of such dramatic structural change in nucleosomal DNA leading to activating gene expression. Our lab previously published the LIN9-LIN52-MBD complex, which Koliopoulos MG and collogues use for their cryo-EM density. However, we have solved the LIN9-LIN52 complex without MBD which we did not see any significant difference compared to the MBD bound structure, which suggests that the MuvB protein complex does not go through a structural change when B-Myb binds to LIN9-

LIN52 through MBD (**Figure 3.10**). However, a previous study shows that in *Drosophila,* B-Myb MBD is sufficient to activate B-Myb-dependent cell-cycle genes (Andrejka L. et al. 2011). Therefore, it could be that in *Drosophila*, the MBD is sufficient; however, when it comes to higher-order species, other domains of B-Myb, like the DBD, might be essential to activate cell-cycle dependent genes when the cell-cycle promoters are chromatinized and repressed by MuvB. Therefore, we hypothesized that B-Myb DBD interacts with nucleosomes to relieve the stabilized +1 nucleosome, thereby changing the promoter architecture to activate gene expression.

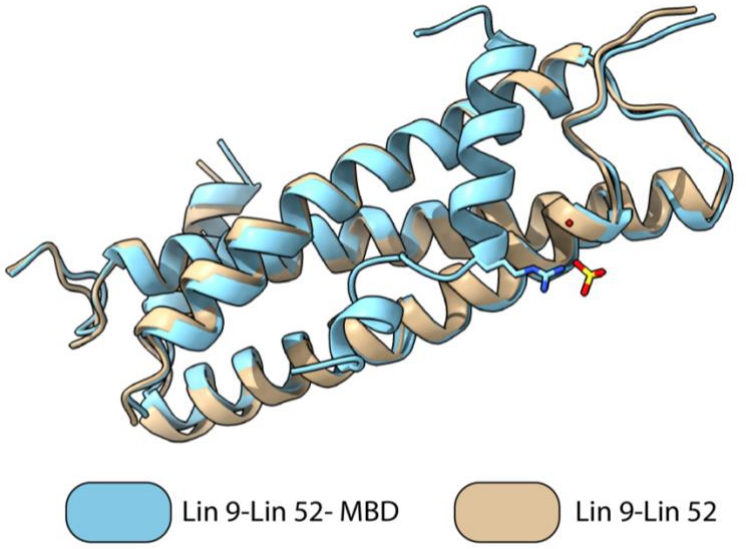

Figure 3.10. MuvB structure is not perturbed upon binding to B-Myb. LIN9-LIN52 forms the binding surface for B-Myb MBD during the S-phase (Guiley KZ. et al. 2018). This domain can interact with MuvB in proliferating cells and rescue the B-Myb knockout phenotype (Iness AN. 2019) (Andrejka L. et al. 2011). However, our crystal structure showed that the LIN9-LIN52 structure does not change when MBD binds (unpublished). Thus, activating the cell-cycle dependent genes when B-Myb is bound to MuvB is not through a conformational change in MuvB.

B-Myb has a highly conserved DNA binding domain with three Myb-like repeats commonly seen in numerous chromatin binding proteins (Boyer LA. et al. 2004). Our results show that B-Myb interacts with nucleosomes both in vitro and in vivo and perhaps modulates activation of cell-cycle dependent genes. The structural and biochemical data suggest that B-Myb DBD interacts with both DNA and the histone core of the nucleosome (**Figure 3.4**). Biochemical assay with mutations in the H2A helix and the DNA suggests that B-Myb interacts with an acidic patch, a partial MBS motif CCGT, and possibly non-specifically with the DNA backbone (**Figure 3.5**). B-Myb DBD has highly conserved acidic and basic pockets, which are known to interact with histone tails and DNA, respectively (Fuglerud BM. et al. 2018). Thus, experiments with DBD mutations are ongoing to determine the amino acid residues essential to interact with the nucleosome. The luciferase assay with a DBD deletion mutant show that DBD is necessary for B-Myb-dependent cell-cycle gene activation (**Figure 3.8**). Initial chromatin-immunoprecipitation assay also shows that B-Myb DBD deletion mutants show loss of binding to cell-cycle dependent gene promoters (**Figure 3.9**). Thus, it is clear that B-Myb DBD is interacting with nucleosomes at the cell-cycle dependent gene promoters. Our B-Myb cryo-EM model show density near the acidic patch of the nucleosome, and mutations in the H2A helix show weakened binding to the DBD and MuvB and B-Myb DBD cannot interact with nucleosomes at the

same time, showing that B-Myb DBD competes with MuvB to interact with nucleosomes. In our previous publication, we showed that B-Myb needs to be phosphorylated for its DBD to interact with DNA, and here we offer that it is valid for nucleosome binding as well (**Figure 3.2.B**) (Wijeratne TU. et al. 2022). Even though B-Myb is expressed in the early S phase, phosphorylation is maximized in the G_2/M phase (Werwein E. et al. 2019). Thus, our model is that when B-Myb is expressed in the early S phase, it is recruited to MuvB through interacting with MBD, and late S phase, when B-Myb gets phosphorylated by CDK2-cyclin A, DBD is released from inhibition and competes with MuvB to interact with nucleosomes (**Figure 3.11**). Our hypothesis is consistent with the model that gene regulation through the transition of heterochromatin to euchromatin is that the repressed genes are occupied by a high concentration of repressor transcription factors compared to activators, and this is overcome by increasing the local concentration of activator transcription factors (Gasser SM. 2001). Further B-Myb DBD knockdown studies in synchronized cells will help to understand how the DBD might be increasing the local concentration of B-Myb to overcome the repression of MuvB and DREAM complex.

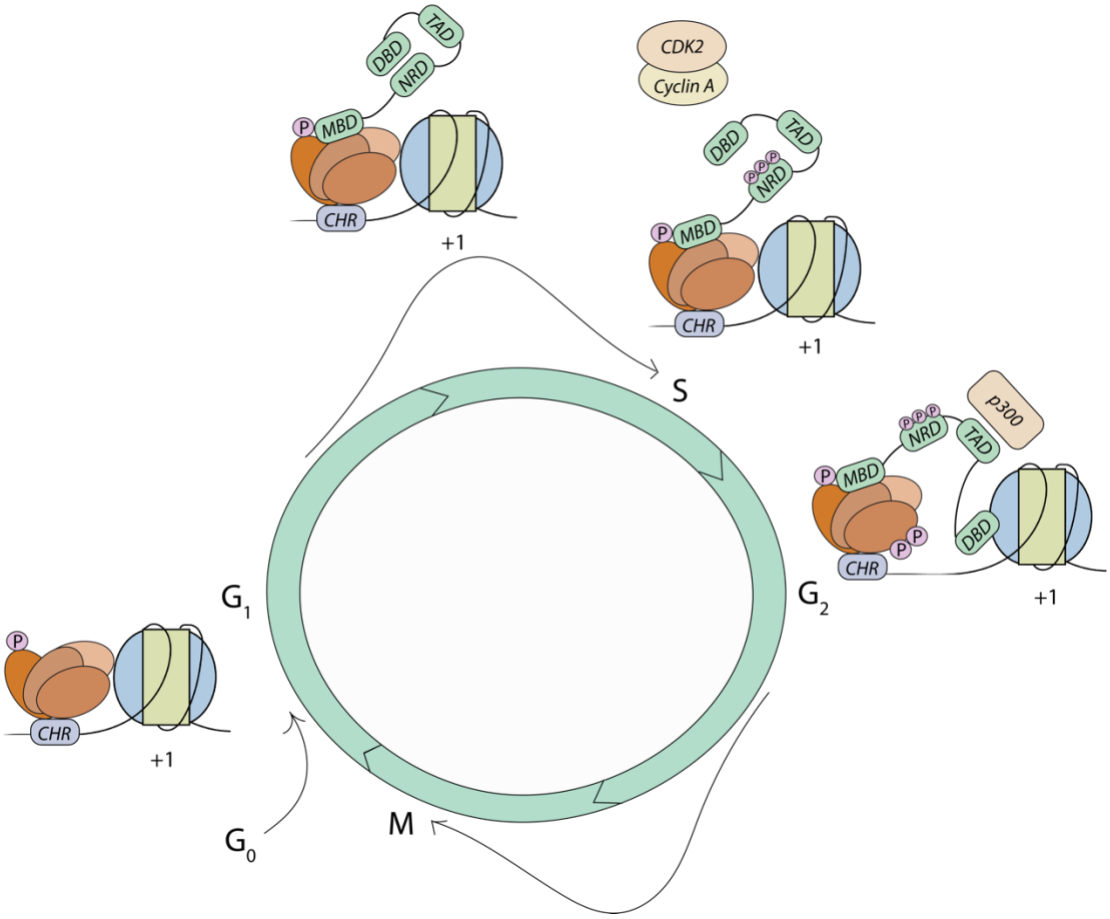

Figure 3.11. Functional model for B-Myb relieving repression caused by MuvB repression at the cell-cycle dependent promoters. During the early S-phase B-Myb gets recruited to cell-cycle dependent promoters through its MBD interacting with MuvB. During the mid-S-phase, B-Myb gets phosphorylated when the autoinhibitory state of DBD is released from NRD. This leads to free DBD, which then interacts with the +1 nucleosome to relieve the interaction of MuvB. Other co-activators like p300 maybe facilitate histone modification and recruitment of transcription machinery to the promoters to activate gene transcription. CHR: cell-cycle homology region.

3.4 Materials and Methods

3.4.1 *Protein expression and purification*

The human B-Myb full-length protein was expressed in Sf9 cells with a cleavable N-terminal Strep-tag using the FastBac expression system. Cells were harvested and lysed in a buffer containing 300 mM NaCl, 50 mM Tris, 1 mM DTT, 10% Glycerol v/v, Sigma Protease Inhibitor (P8340), and 1 mM PMSF (pH 8.0). Protein was purified with StrepTactin Sepharose High-Performance resin (Cytiva) equilibrated in lysis buffer. The lysed cells were clarified by centrifugation at 19,000 rpm for 45 min at 4 °C. The cleared lysate was incubated with resin for 1 h at 4 °C, and the resin was washed with a buffer containing 300 mM NaCl, 50 mM Tris, 1 mM DTT, and 10% glycerol v/v (pH 8.0). The protein was then eluted in 300 mM NaCl, 50 mM Tris, 5 mM desthiobiotin, 10% glycerol v/v, and 1 mM DTT (pH 8.0). Protein was dialyzed into storage buffer (200 mM NaCl, 50 mM Tris, 1 mM BME, and 10% glycerol v/v (pH 8.0)) and stored at −80 °C.

The human B-Myb DBD was expressed in Escherichia coli from an engineered pGEX plasmid with an N-terminal GST tag and a TEV protease cleavage site. Protein was expressed overnight by inducing with 1 mM IPTG at 19 °C. All proteins were lysed in a buffer containing 500 mM NaCl, 40 mm Tris, 5 mM DTT, and 1 mM PMSF (pH 8.0). The lysed cells were clarified by centrifugation at 19,000 rpm for 45 min at 4 °C. Protein lysates were allowed

to bind to equilibrated Glutathione Sepharose resin (Cytiva) for 30 min and washed to remove unspecific proteins. The protein was eluted with a buffer containing 200 mM NaCl, 40 mM Tris, 5 mM DTT, and 10 mM reduced L-Glutathione (pH 8.0). Eluted proteins were further purified using Q-sepharose and cleaved with TEV protease at 4 °C overnight. Proteins were then passed through Glutathione Sepharose resin to remove the free GST and concentrated to run through Superdex-75 (GE Healthcare) into 200 mM NaCl, 25 mM Tris, and 1 mM DTT (pH 8.0).

The *Xenopus laevis* H2A, H2B, H3, and H4 histones were expressed in *Escherichia coli* from a pET vector in pLysS cells. The cells were grown in LB media, induced at OD600 0.60-0.9, and induced with 0.4 mM IPTG. Cells were harvested after 3 hours of incubation at 37 °C. The bacterial pellets were resuspended in Lysis buffer containing 1 M NaCl, 50 mm Tris, 1 mM BME, and 1 mM EDTA (pH 7.5). Resuspended pallets were flash-frozen in liquid nitrogen and stored at -20°C overnight. Cells were lysed using a sonicator and centrifuged at 19,000 rpm for 30 minutes. Pellets containing inclusion bodies were washed with Lysis buffer by mincing with a dounce homogenizer. This step was done 3-4 times with centrifuging at 19,000 rpm for 30 minutes. The pallet was then resuspended in a buffer containing 7 M Guanidine hydrochloride, 20 mM Tris-HCl (pH 7.5), and incubated at 37 °C for 30 mins to extract histones. Undissolved material from the sample was removed by

centrifugation and injected into a Sephacryl S200 column to separate histones from unspecific DNA. Fractions containing histones were dialyzed into a buffer containing 7 M freshly de-ionized urea, 20 mM sodium acetate, 200 mM NaCl, 1 mM EDTA, 5 mM BME, and 10 mM DTT (pH 5.2). The protein was loaded onto a SOURCE S cation exchange column and eluted as a gradient in the same buffer with 1 M NaCl. Fractions containing the histones were dialyzed against the water with 1 mM BME for 72 hours with 3-4 buffer changes. Histones were then run on an SDS-PAGE to check for purity and lyophilized for storage.

Histone octamer was reconstituted by mixing equimolar amounts of histone in a buffer containing 7M guanidine HCl, 20 mM Tris pH 8, and 10 mM BME. The undissolved histones were removed by centrifugation, and the supernatant was dialyzed in a buffer containing 20 mM Tris pH 8, 2 M NaCl, 1 mM EDTA and 10 mM BME for 72 hours with 3-4 buffer changes at 4°C. The Octamer was then eluted from a Superdex 200 (GE Healthcare) column in a buffer containing 20 mM Tris pH 7.5, 2 M NaCl, 1 mM EDTA and 10 mM BME. The octamer was stored at -80°C with 15% glycerol.

3.4.2 *Nucleosome reconstitution*

The nucleosome-core-particle was reconstituted using the Widom 601 positioning sequence. It was amplified by PCR with the forward primer 5’ ATCCCTATACGCGGCCGCCCTGGA-3’ and reverse primer (fluorescein)-5’

ACAGGATGTATATATCTGACACGTG-3'. The DNA was purified by gel-extraction. Following purification, the DNA was resuspended with equimolar amounts of histone octamer in a buffer containing 20 mM Tris pH 7.5, 2 M NaCl, 1 mM EDTA and 10 mM BME. The suspended octamer and DNA mixture was then dialyzed into the same buffer with decreasing NaCl concentration starting from 1 M, 0.75 M, 0.5 M, 0.3 M, 0.2 M, and finally 0.1 M with at least 6 hours of dialysis at 4°C. The nucleosome-core-particle was then eluted from a Superdex 200 (GE Healthcare) and analyzed using 5% native PAGE. Nucleosomes were purified on a monoQ 5/50 ion exchange gradient (GE Healthcare), and nucleosome containing fractions were dialyzed to a buffer containing 20 mM Tris pH 7.5, 0.1 M NaCl, 1 mM EDTA, and 1 mM BME and stored with 15% glycerol at -80°C.

3.4.3 *Cryo-EM sample preparation, plunge freezing, data collection, and data processing.*

B-Myb DBD and nucleosomes were exchanged separately to a buffer containing 20 mM Tris pH 7.5, 0.1 M NaCl, 1 mM EDTA, and 1 mM BME. Nucleosomes and DBD were mixed with a molar excess of DBD at room temperature for 30 minutes (1:3, nucleosome: DBD). The sample was then purified using a Superose 6 3.2/300 column (GE Healthcare) equilibrated in a buffer containing 20 mM Tris pH 7.5, 0.1 M NaCl, 1 mM EDTA, and 1 mM BME. Fractions containing nucleosome-DBD complexes were analyzed by

SDS-PAGE stained with Coomassie. The sample was then concentrated using an Amicon Ultra-0.5mL centrifugal filter (Merck Millipore) and prepared directly for electron microscopy. Three microliters of sample were applied to Quantifoil gold grids (R 1.2/1.3 200-mesh, Quantifoil Micro Tools). Glow discharging was carried out in a PELCO Easy Glow discharge for 7s in an Ar/O_2 environment. Grids were blotted for 3 s at 4°C at 100% humidity in a Vitrobot Mark IV (FEI, Hillsboro, OR, USA) and immediately plunged into liquid ethane.

Data were collected automatically with EPU (Thermo Fisher) on a Cs-corrected (CEOS GmbH, Heidelberg, Germany) Titan Krios (Thermo Fisher) electron microscope at 300 keV. Micrographs were collected using a Gatan K2 summit direct electron detector (Gatan) in counting mode located after a Quantum-LS energy filter (slit width of 20 eV). The acquisition was performed at a nominal magnification of 105,000 × or 130,000 × in EFTEM nanoprobe mode, yielding a pixel size of 1.058 Å. The objective aperture was 100 μm. All datasets were recorded with a dose of 52.3 e-/$Å^{2,}$ and the exposures were fractionated into 40 frames. The targeted defocus values ranged from -0.25 to -2 μm.

All data processing was done using CryoSparc, including 2D and 3D classification, 3D refinement, and CTF refinement (Punjani. A. et al., 2017). 3D map was segmented using UCSF ChimeraX (version 1.13).

3.4.4 *Fluorescence Polarization assay*

Dissociation constants for direct binding between DBD and nucleosomes were determined by titrating increasing amounts of DBD into 20 nM of Cy3-labeled nucleosome. The Widom DNA probe was amplified by the forward primer containing Cy3 dye made by Integrated DNA Technologies and had the following sequence: /5Cy3//iSp9/CTGGAGAATCCCGGTGCCGAGGCC. For DBD + nucleosome assays, DBD and nucleosomes were incubated for 30 min on ice before titrating the labeled MuvB probe in a buffer containing 100 mM NaCl, 20 mM Tris, 1 mM DTT, and 0.1% Tween20 (pH 7.5). FP measurements were acquired on a PerkinElmer EnVision 2103 Multilabel plate reader with excitation at 559 nm and emission at 580 nm. The dissociation constants (K_D) were calculated by fitting millipolarization (mP) values of three technical replicates against concentration using a one-site–binding model in GraphPad Prism 8.

3.4.5 *Electrophoretic mobility shift assay*

B-Myb was serially diluted in a buffer containing 0.5x TBE. 10 nM of nucleosomes were added to each serial dilution and loaded onto a 5% native acrylamide gel. The gel was stained with SYBR Gold (Thermo Fisher Scientific). The gels were scanned using a Typhoon FLA 9500 imager.

3.4.6 *Luciferase reporter assay*

HCT116 colon carcinoma cells were grown in Dulbecco's modified Eagle's medium (Gibco, high glucose, GlutaMAX Supplement, pyruvate) supplemented with 10% fetal bovine serum (Corning, Regular Fetal Bovine Serum) and penicillin/streptomycin (Gibco). Cells were maintained at 37 °C and 5% CO_2.

The 3xMBS luciferase reporter construct was created by inserting a double-stranded oligonucleotide containing three copies of a high-affinity B-Myb–binding site (TAACGGTG) upstream of the herpes simplex thymidine kinase minimal promoter (5-TTATAACGGTCTTAATAACGGTCTTAATAACGGTCTTTTAGCTTCGCATATTAAGGTGACGCGTGTGGCCTCGAACACCGAGCGACCCTGCAGCGACCCGCTTAA-3; MBSs in bold, minimal TK promoter in italics) into the KpnI and NcoI sites of the pGL4.10[luc2] vector (Promega). The ORF of human MYBL2/B-Myb isoform 1 (NM_002466.4) was cloned into pcDNA3.1+ (ThermoFisher Scientific) and fused with an N-terminal Flag tag. Point mutations were introduced following the QuikChange site-directed mutagenesis protocol, and the DBD (amino acids 12-182) was deleted following the NEB Q5 protocol.

Stimulation of the 3xMBS promoter activity was analyzed by luciferase reporter assays with extracts of transfected HCT116 cells. Thirty thousand cells per 48 wells were plated and transfected with 1 µl PEI (Polysciences,

PEI 25K), 75 ng of promoter-reporter plasmids (3xMBS-pGL4.10 or pGl4.10 empty vector), 100 ng of pcDNA3.1 plasmids expressing Flag-B-Myb (WT or mutants), and 25 ng renilla luciferase plasmid (pGL4.70). Cells were lysed 48 h after transfection, and luciferase activity was measured with the Dual-Luciferase Reporter Assay System (Promega) following the manufacturer's recommendations on an EnVision 2105 plate reader (PerkinElmer). Relative promoter activities of the 3xMBS-pGL4.10 reporter after expression of WT or mutant B-Myb were calculated by normalizing to renilla luciferase activity, and the activity of the pGL4.10 empty vector cotransfected with the respective B-MYB constructs.

3.4.7 *Chromatin immunoprecipitation assay*

HCT116 cells were harvested and aliquoted into 10 million cells per tube and cross-linked with 1% paraformaldehyde (Electron Microscopy Sciences). Cross-linking was quenched with 125 mM Glycine (Fisher Scientific). Nuclei were isolated using Buffer A (Cell Signaling) and Buffer B (Cell Signaling. #7007S). Nuclei were MNase-treated, incubated at 37°C for 15 minutes, and direct sonication for 5x 1s to create ~300bp chromatin fragments. Protein-DNA complexes were immunoprecipitated with streptactin magnetic beads (IBA life sciences) overnight at 4°C. Beads were subsequently washed with the following buffer types in order: 6x RIPA (10mM Tris-HCl pH 8.0, 1mM EDTA, 0.1% SDS, 0.1% Sodium Deoxycholate, 0.1%TritonX) supplemented

with 140mM NaCl, 3x RIPA supplemented with 500mM NaCl, 3x LiCl buffer (10mM Tris-HCl pH 8.0, 250mM LiCl, 1mM EDTA, 0.5% Sodium Deoxycholate, 0.5% Triton X), and 3x 10mM Tris-HCl 8.0 (salt-free). Precipitants were eluted twice with 150µl elution buffer (10mM Tris-HCl 8.0, 5mM EDTA, 300mM NaCl, 0.6%SDS) with 30s pulse vortexing and 15min incubation at 37°C. Eluants were treated with RNaseA (Thermo Scientific) for 30 minutes at 37°C, then treated with Proteinase K (Thermo Scientific) for 1 hour at 55°C and reverse cross-linked at 95°C for 20 minutes. DNA was purified using Zymo DNA Clean & Concentrator-5 kits (Zymo Research). qPCR was performed with the GoTaq qPCR Master Mix (Promega) on a Quantstudio 3 Real-Time PCR System (ThermoFisher Scientific).

Chapter 4: Cell-cycle transcription factors E2F1-DP1, E2F4-DP1, and FOXM1 interact with nucleosomes.

4.1 Introduction

In the eukaryotic genome, nucleosomes provide a platform to regulate DNA metabolism by sterically hindering DNA from transcription initiation machinery. In this platform, there are different ways that gene expression can be modulated. Intrinsic structural properties of the DNA, variants of histones in the nucleosome, ATP-dependent chromatin remodeling complexes, and sequence-specific transcription factors are a few examples of nucleosomes being regulated for gene expression (Lorch Y. et al. 1987). Among all these

factors, pioneer transcription factors are emerging as a key player in epigenetic regulation in cell development and differentiation. Pioneer transcription factors are defined as molecular machinery that can distinguish condensed chromatin to interact with the regulatory site in the DNA before transcription machinery gain access (Zaret KS. et al. 2011). Pioneer transcription factors increase the accessibility of secondary transcription machinery to initiate transcription of a particular site in the genome (Iwafuchi-Doi M and Zaret KS. 2014). Thus, pioneer transcription factors have three steps of regulation; they scan the genome to find “naïve” unprogrammed chromatin loci, and they interact with nucleosomes in condensed chromatin without the help of a specific DNA sequence. They recruit chromatin remodelers or transcription initiation complexes to such loci (Zaret KS. et al. 2016).

The first pioneer factors discovered were FoxA and GATA factors which have a wing-helix domain and a zinc finger domain as their DNA binding domains, which are critical players in pluripotency (Bossard P, Zaret KS. 1998), (Gualdi R. et al. 1996) (**Figure 4.1**). Thus, we wondered if transcription factors involved in the cell cycle have the intrinsic ability to interact with nucleosomes. Both E2F and FoxM1 transcription factors are essential in the cell-cycle dependent gene promoters regulating the two waves of gene expressions in the cell cycle. E2F1 plays an activating role during the first

wave of gene expression at early cell-cycle dependent genes during G_1/S phases, and E2F4 plays a repressive function. FOXM1 plays an activating role during the second wave of gene expression during the G_2/M phases (Fischer M. et al., 2022). Thus, it is clear that these two transcription factors are brought to the cell-cycle dependent promoters right before the genes are activated. Therefore, we hypothesized that E2F and FOXM1 proteins might have an intrinsic ability to scan the chromatin and recognize “naïve” unprogrammed chromatin to prime them for activation. We show that transcription factors E2F1-DP1, D2F4-DP1, and FoxM1 show nucleosome binding *in vitro*.

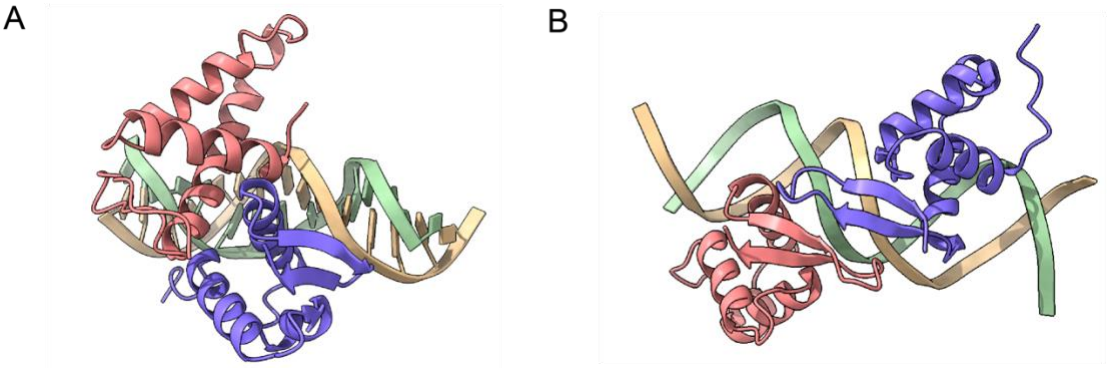

Figure 4.1. Crystal structures of E2F-DP1 complexed with consensus DNA, and FoxM1 complexed with consensus motif. A. E2F-DP1 DNA binding domain complexed with consensus DNA sequence TTTSSCGC (where S is either a G or a C) (PDB ID: 1CF7) (Zheng N. et al. 1999). **B.** FoxM1 DNA binding domain complexed with consensus sequence TAAACA (PDB ID: 7FJ2). Both domains have winged-helix motifs with three alpha-helices and beta sheet (Littler DR. et al. 2010).

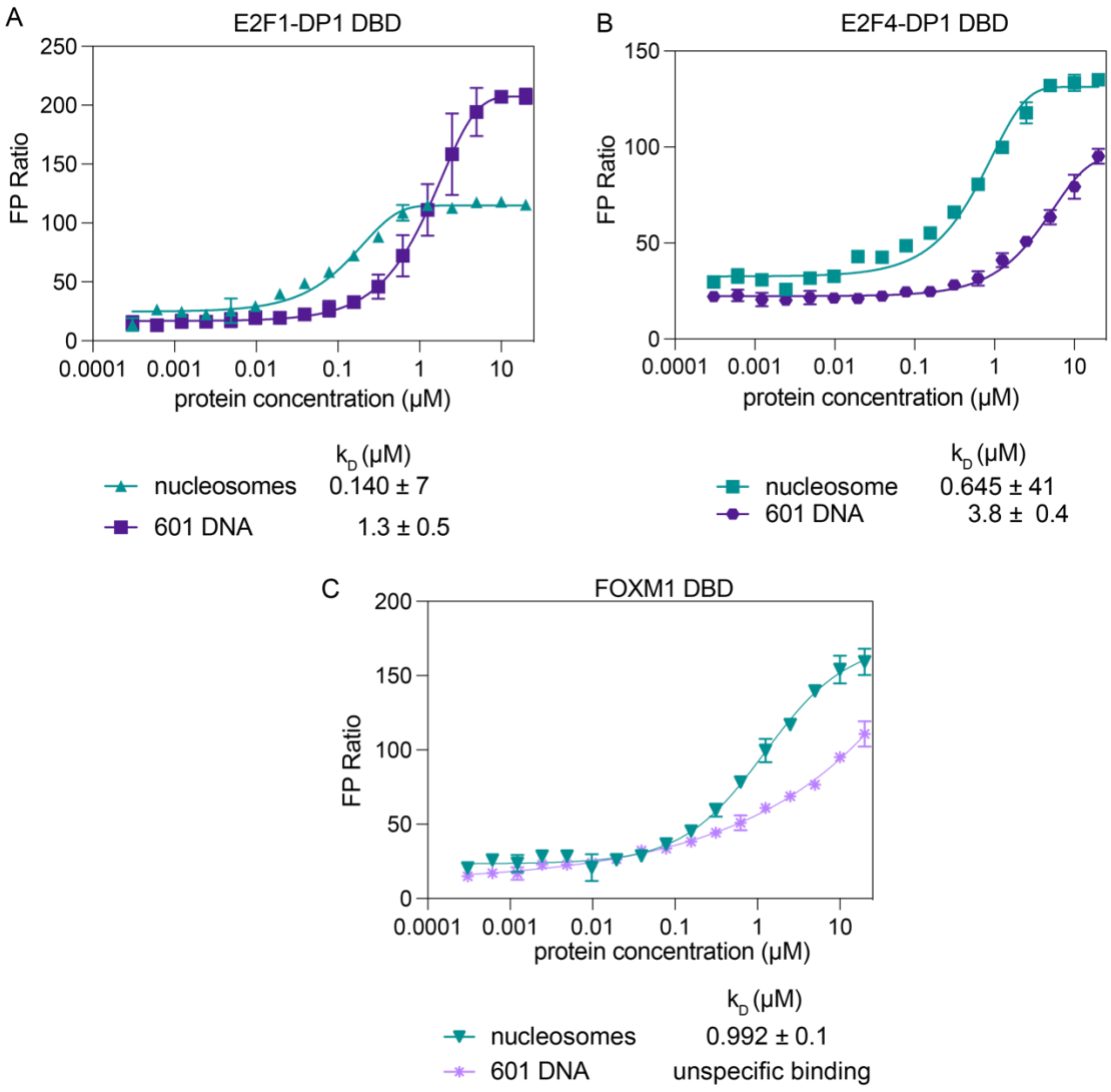

Figure 4.2. The winged-helix domains of E2F1, E2F4, and FoxM1 show a similar binding pattern to nucleosomes tighter than DNA. A, B, C. PF plots for E2F1-DP1, E2F4-DP1, and FoxM1 DBDs binding to Widom 601 nucleosomes with k_D values calculated from the FP assay.

4.2 Results

To determine whether E2F1-DP1, E2F4-DP1, and FOXM1 DNA binding domains can bind nucleosomes, we purified each protein or complex separately in *E. coli* and nucleosomes from *X. laevis* histones as described in Chapter **3**. We used a fluorescence polarization assay to detect binding with nucleosomes refolded with fluorescently labeled Widom 601 DNA. These data indicate that the binding affinity for all three DNA binding domains is higher for nucleosomes than linear DNA (**Figure 5.2**). Altogether, suggesting that wing-helix domains of E2F and FOXM1 can interact with nucleosomes without their consensus sequence. The fact that the binding affinity to linear DNA is less than to nucleosomes suggests that these domains have the intrinsic potential to recognize nucleosomal substrates such as the histone proteins or the bent DNA of the nucleosome.

4.3 Discussion

E2Fs and FOXM1 are essential cell cycle regulators in the G_1/S and G_2/M phases. Even though E2F and FOXM1 have canonical binding motifs, it has been shown that they do not need a consensus motif to localize to their targeted promoters (Rabinovich A. et al. 2018), (Muller GA. et al. 2014), (Sanders DA. et al. 2015). These results contrast the existing model for how transcription factors get recruited to target promoters by directly interacting with high-affinity consensus sequences. It is also now known that

transcription factors get recruited to target promoters by interacting with other proteins already assembled at promoters. However, increasingly it has been observed that proteins containing evolutionary conserved DNA binding domains use protein-protein interactions for functions that diverge from their ancestral function (Nitta KR. et al. 2015). Thus, we hypothesize that such transcription factors use their DNA binding domain for unspecific chromatin interactions. A pioneer transcription factor is defined as a chromatin-binding protein that selectively interacts with nucleosomes that are not accessible to other transcription machinery (Cirillo L. et al. 2002). E2F transcription factors regulate the first wave of cell-cycle dependent genes at the G_1/S phase; these genes are repressed in G_0 or quiescence (Fischer M. et al. 2016). Therefore, we hypothesize that E2F DNA binding domain can target condensed and repressed genes at mitosis to activate them when cells enter the cell cycle at the G_1/S phase. FOXM1 also uses its DNA and MuvB binding domains to localize to cell-cycle dependent genes (Sadasivam S. et al. 2012). E2Fs and FOXM1 also recruit chromatin-modifying enzymes to their target site through protein-protein interactions (Lu Z. et al. 2006), (Marceau AH. et al. 2019). Further studies on high-resolution chromatin architectural changes with mutations on the DNA binding domains will help to understand the mechanism of interacting with nucleosomes and the “pioneering” role in cell-cycle dependent gene regulation.

4.4 Materials and methods

4.4.1 *Protein expression and purification*

The human E2F1, E2F4, DP1, and FOXM1 DBDs were expressed in Escherichia coli from an engineered pGEX plasmid with an N-terminal GST tag and a TEV protease cleavage site. Protein was expressed overnight by inducing with 1 mM IPTG at 19 °C. All proteins were lysed in a buffer containing 500 mM NaCl, 40 mm Tris, 5 mM DTT, and 1 mM PMSF (pH 8.0). The lysed cells were clarified by centrifugation at 19,000 rpm for 45 min at 4 °C. Protein lysates were allowed to bind to equilibrated Glutathione Sepharose resin (Cytiva) for 30 min and washed to remove unspecific proteins. The protein was eluted with a buffer containing 200 mM NaCl, 40 mM Tris, 5 mM DTT, and 10 mM reduced L-Glutathione (pH 8.0). Eluted proteins were further purified using Q-sepharose and cleaved with TEV protease at 4 °C overnight. Proteins were then passed through Glutathione Sepharose resin to remove the free GST and concentrated on running through Superdex-75 (GE Healthcare) into 200 mM NaCl, 25 mM Tris, and 1 mM DTT (pH 8.0). E2F1-DP1 and E2F4-DP1 complexes were made by mixing 1:2 E2F1/4:DP1 molar ratios on ice for 30 minutes and isolating the complex through Superdex-75 (GE Healthcare) into 200 mM NaCl, 25 mM Tris, and 1 mM DTT (pH 8.0).

The *Xenopus laevis* H2A, H2B, H3, and H4 histones were expressed in *Escherichia coli* from a pET vector in pLysS cells. The cells were grown in LB media, induced at OD600 0.60-0.9, and induced with 0.4 mM IPTG. Cells were harvested after 3 hours of incubation at 37 °C. The bacterial pellets were resuspended in Lysis buffer containing 1 M NaCl, 50 mm Tris, 1 mM BME, and 1 mM EDTA (pH 7.5). Resuspended pallets were flash-frozen in liquid nitrogen and stored at -20°C overnight. Cells were lysed using a sonicator and centrifuged at 19,000 rpm for 30 minutes. Pellets containing inclusion bodies were washed with Lysis buffer by mincing with a dounce homogenizer. This step was done 3-4 times with centrifuging at 19,000 rpm for 30 minutes. The pallet was then resuspended in a buffer containing 7 M Guanidine hydrochloride, 20 mM Tris-HCl (pH 7.5), and incubated at 37 °C for 30 mins to extract histones. Undissolved material from the sample was removed by centrifugation and injected into a Sephacryl S200 column to separate histones from unspecific DNA. Fractions containing histones were dialyzed into a buffer containing 7 M freshly de-ionized urea, 20 mM sodium acetate, 200 mM NaCl, 1 mM EDTA, 5 mM BME, and 10 mM DTT (pH 5.2). The protein was loaded onto a SOURCE S cation exchange column and eluted as a gradient in the same buffer with 1 M NaCl. Fractions containing the histones were dialyzed against the water with 1 mM BME for 72 hours with 3-4 buffer

changes. Histones were then run on an SDS-PAGE to check for purity and lyophilized for storage.

Histone octamer was reconstituted by mixing equimolar amounts of histone in a buffer containing 7M guanidine HCl, 20 mM Tris pH 8, and 10 mM BME. The undissolved histones were removed by centrifugation, and the supernatant was dialyzed in a buffer containing 20 mM Tris pH 8, 2 M NaCl, 1 mM EDTA and 10 mM BME for 72 hours with 3-4 buffer changes at 4°C. The Octamer was then eluted from a Superdex 200 (GE Healthcare) column in a buffer containing 20 mM Tris pH 7.5, 2 M NaCl, 1 mM EDTA and 10 mM BME. The octamer was stored at -80°C with 15% glycerol.

4.4.2 *Nucleosome reconstitution*

The nucleosome-core-particle was reconstituted using the Widom 601 positioning sequence. It was amplified by PCR with forward primer 5' ATCCCTATACGCGGCCGCCCTGGA-3' and reverse primer fluorescein-5' ACAGGATGTATATATCTGACACGTG-3'. The DNA was purified by gel-extraction. Following purification, the DNA was resuspended with equimolar amounts of histone octamer in a buffer containing 20 mM Tris pH 7.5, 2 M NaCl, 1 mM EDTA and 10 mM BME. The suspended octamer and DNA mixture was then dialyzed into the same buffer with decreasing NaCl concentration starting from 1 M, 0.75 M, 0.5 M, 0.3 M, 0.2 M, and finally 0.1 M with at least 6 hours of dialysis at 4°C. The nucleosome-core-particle was

then eluted from a Superdex 200 (GE Healthcare) and analyzed using 5% native PAGE. Nucleosomes were purified on a monoQ 5/50 ion exchange gradient (GE Healthcare), and nucleosome containing fractions were dialyzed to a buffer containing 20 mM Tris pH 7.5, 0.1 M NaCl, 1 mM EDTA, and 1 mM BME and stored with 15% glycerol at -80°C.

4.4.3 *Fluorescence Polarization assay*

Dissociation constants for direct binding between E2F1-DP1, E2F4-DP1, FOXM1 DBDs, and nucleosomes were determined by titrating increasing DBD into 20 nM of Cy3-labeled nucleosome. The Widom DNA probe was amplified by the forward primer containing Cy3 dye made by Integrated DNA Technologies and had the following sequence: /5Cy3//iSp9/CTGGAGAATCCCGGTGCCGAGGCC. For DBD + nucleosome assays, DBD and nucleosomes were incubated for 30 min on ice before titrating the labeled MuvB probe in a buffer containing 100 mM NaCl, 20 mM Tris, 1 mM DTT, and 0.1% Tween20 (pH 7.5). FP measurements were acquired on a PerkinElmer EnVision 2103 Multilabel plate reader with excitation at 559 nm and emission at 580 nm. The dissociation constants (k_D) were calculated by fitting millipolarization (mP) values of three technical replicates against concentration using a one-site–binding model in GraphPad Prism 8.

Chapter 5: B-Myb phosphorylation may regulate its binding to p300: TAZ2.

5.1 Introduction

The Myb family of transcription factors is historically known to function through binding to a canonical DNA sequence [T/C]AAC[T/G]G (Biedenkapp H. et al. 1988). The vertebrate Myb family consists of three members, A-Myb, B-Myb, and c-Myb, which are discussed in detail in **Chapters 1** and **2.** All three Myb family members are known to interact with the co-activator p300/CBP through their transactivating domain to activate Myb targeted genes (**Figure 5.1.A**) (Facchinetti V. et al. 1997), (Dai, P. et al. 1996), (Johnson LR. et al. 2002). Additionally, both B-Myb and c-Myb are known to get acetylated by p300 to enhance their activating function (Johnson LR. et al. 2002), (Tomita A. et al. 2000). Genetic screenings have identified a mutation M303V in c-Myb that disrupts p300 binding, leading to defects in hematopoietic stem cell differentiation (Sandberge ML. et al. 2005). C-Myb interacts with p300 through its KIX domain (**Figure 5.1.A**), and this interaction is found to be essential for c-Myb interaction with the Mixed Lineage Leukemia (MLL) protein in pediatric acute leukemia (Goto NK. et al. 2002). Furthermore, the interaction between p300 and c-Myb is important for the induction of acute myeloid leukemia (AML) and also successfully targeted using a small molecule inhibitor (Zuber J. et al. 2011) (Uttarkar S. et al. 2016).

However, in contrast to c-Myb, the B-Myb interaction with p300 is less implicated in oncogenesis. B-Myb interacts with p300 through the TAZ2 domain (Schubert S. et al. 2004), (Oka O. et al. 2012). It has also been shown that CDK2-cyclin A/E mediated phosphorylation is not needed for B-Myb's acetylation by p300; however, phosphorylation is essential for B-Myb dependent gene activation (Johnson LR. et al. 2002)(Schubert S. et al. 2004). Therefore, we wanted to understand how the phosphorylation of B-Myb is linked to p300 binding. This chapter contains a few experiments we carried out to understand the mechanism of B-Myb phosphorylation and p300 TAZ2 binding.

5.2 Results

5.2.1 *The B-Myb transactivation domain interacts with CBP/p300 TAZ2 domain but not with TAZ1 and KIX domains.*

It has previously been shown that the B-Myb transactivation domain (TAD) interacts with TAZ2 of p300 (Schubert S. et al. 2004). We used isothermal titration calorimetry to biochemically characterize this interaction and quantify the affinity (**Figure 5.1.B**). We observed a K_D value of 490 $\pm$ 50 nM and no binding signal to the KIX or TAZ1 domains of p300, similar to what Schubert and colleagues observed (**Figure 5.1.C** and **D**).

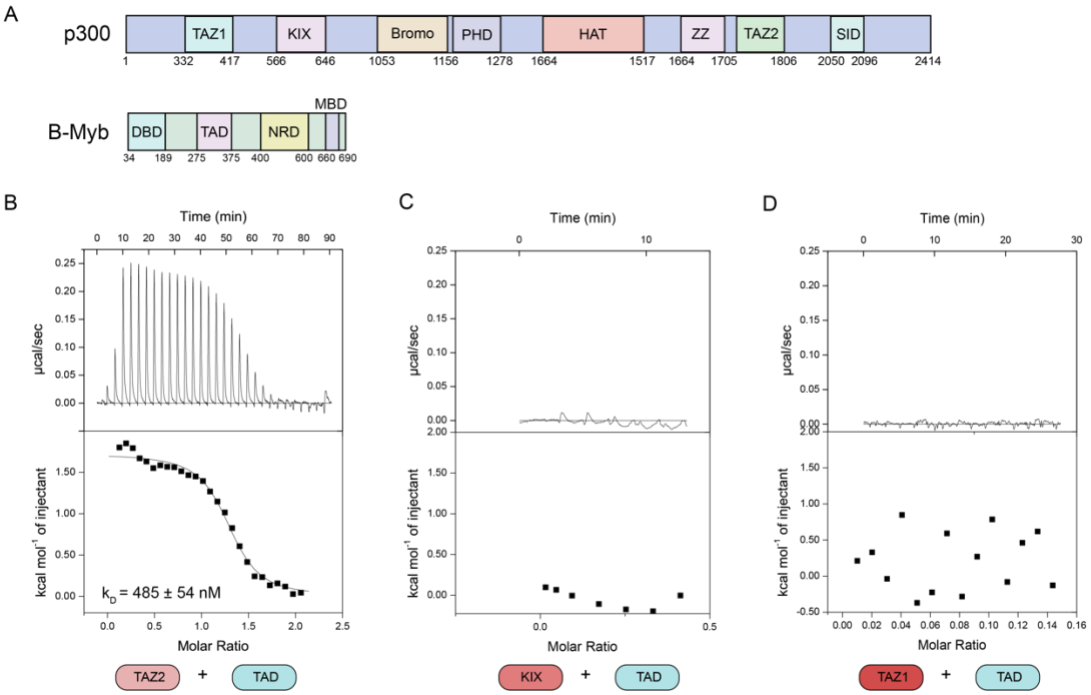

Figure 5.1. Biochemical characterization of B-Myb TAD binding with p300: TAZ2. A. Domain architecture of p300 and B-Myb. **B, C, D.** Isothermal titration calorimetry done by titrating p300 TAZ2, KIX, and TAZ1 to B-Myb TAD.

5.2.2 *Secondary structure propensity of B-Myb transactivation domain and predicted amino acid residues that may be important to interact with TAZ2.*

Structural characterization of B-Myb bound to TAZ2 in previous literature has shown several amino acids of B-Myb TAD that might be important for TAZ2 interaction (Oka O. et al. 2012). We used isothermal titration calorimetry to determine if mutating these residues to alanine will disrupt its binding to TAZ2 (**Figure 5.2.**). We observed only slightly decreased affinity towards NLL when mutated to alanines; (i.e., NLL to AAA); however, when FDL residues were mutated to alanine, affinity decreased to 3.4 μM. The most weakened affinity was seen when VW residues were mutated, i.e., V293A, W294A), which reduced the affinity to 70 μM. Altogether, these experiments show that residues essential for the alpha-helical formation of B-Myb TAD might be necessary to form a stable complex with TAZ2.

5.2.3 *B-Myb competes with p53 transactivation domains AD1 and AD2 to interact with TAZ2 domain.*

The TAZ2 domain of p300 is known to interact with the transactivation domains of many other proteins involved in transcription regulation. The most commonly studied of these proteins to date are the adenovirus E1A oncoprotein and p53 (Ferreon JC. et al. 2009) (Teufel DP. et al. 2007). Given the observation that E1A TAD (STAT1) and p53 TADs (AD1 and AD2) interact with three different

A

FPKREDQEGSPPETSLPYKWVVEAANLLIPAVGSSLSEALDLIESDPDAWCDLSKFDLPEEPSAEDSINNSLVQLQASHQQQVLPPRQPSALVPSVTEYRLDG

275 375

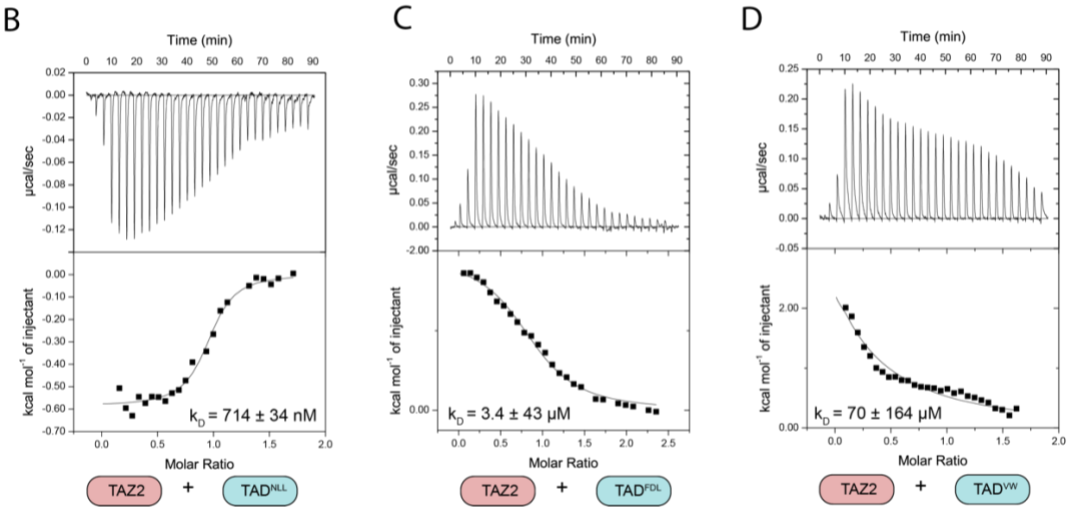

Figure 5.2. B-Myb TAD Mutations based on secondary structure prediction show weakened binding to TAZ2. A. Amino acid sequence of B-Myb TAD. Residues that have a propensity to form an alpha helix are boxed in red. **B. C. D.** Isothermal titration calorimetry assay to determine the binding affinity when these residues are mutated to alanine.

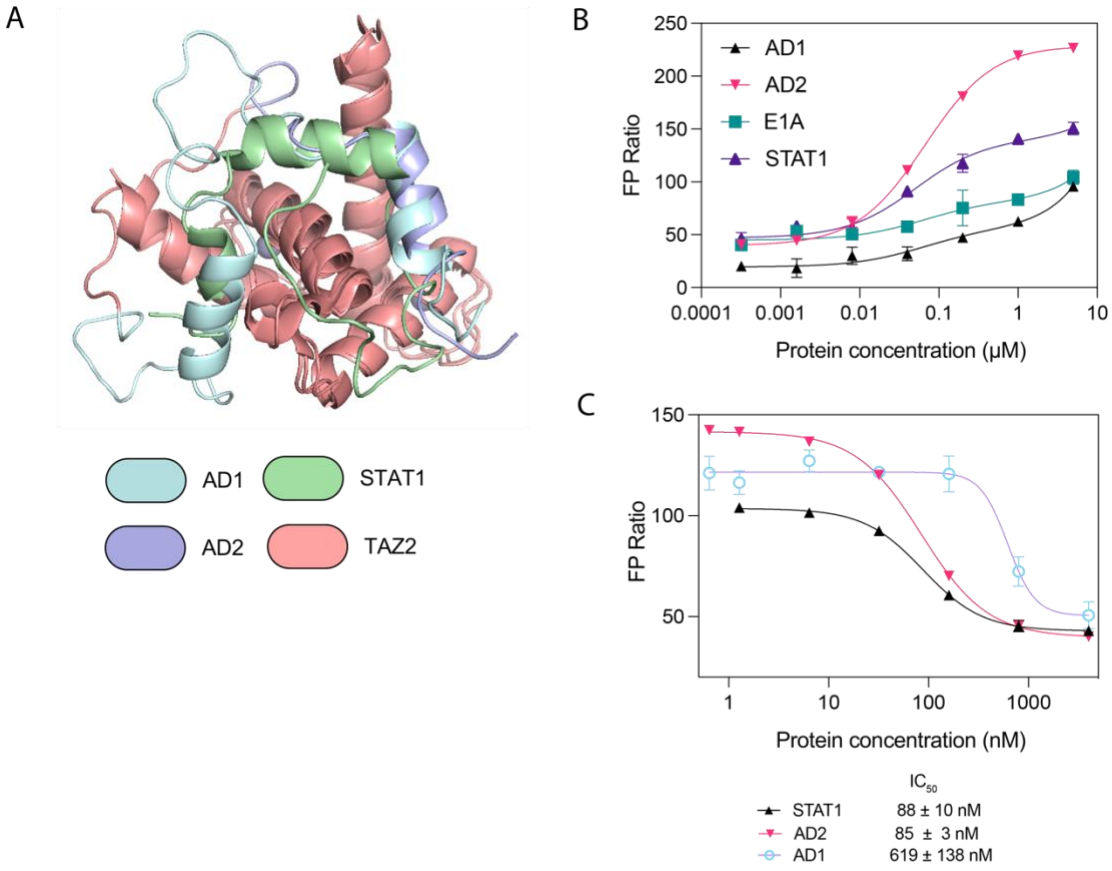

Figure 5.3. B-Myb TAD interacts with the binding surface of STAT1 and AD2 and weakly with AD1. A. Overlay of crystal structures of TAZ2 with AD1-AD2 (light blue), STAT1 (green), and AD2 (purple). **B.** FP assay to determine binding affinities of fluorescently labeled AD1, AD2, and STAT1 with TAZ2. **C.** Competition assay to determine if B-Myb TAD can inhibit AD1, AD2, and STAT1 at 10 nM binding with TAZ2 at 100 nM in the presence of increasing B-Myb TAD concentration.

Interfaces in TAZ2, we wondered to identify which binding interface B-Myb TAD would target (**Figure 5.3.A**). We used fluorescence polarization to test the binding of TAZ2 to fluorescently labeled STAT1, AD1, and AD2 peptides (**Figure 5.3.B**). We observed a KD value for the AD2 peptide of 59 □ 1 nM. The other peptides did not give a saturating signal to fit into a one-site binding model, possibly because the peptides are too small to form a complex that would change the polarization of the fluorophore. However, we observed that all three peptides inhibited binding to TAZ2 by the B-Myb TAD (**Figure 5.3.C**). Thus, it is clear that B-Myb TAD-TAZ2 interaction overlaps with all three TADs but more so with AD2 and STAT1.

5.2.4 *B-Myb phosphorylation by CDK2-cyclin A increases IC_{50} value towards TAZ2-AD1 and TAZ2-AD2 complex*

B-Myb phosphorylation by CDk2-Cyclin A has been well studied, and it has been shown that it is necessary for B-Myb dependent gene activation in both Myb-binding site (MBS) reporter promoters and cell-cycle dependent promoters (Lane S. et al. 1997), (Petrovas C. 2003), (Ziebold U. and Klempnauer KH. 1997) (Sadasivam S. et al. 2012). It has also been shown that acetylation by p300 positively regulates MBS-dependent genes (Schubert S. et al. 2004). Therefore, we wanted to investigate whether phosphorylation is linked to p300 binding. B-Myb gets sequentially phosphorylated by CDK2-Cyclin A and Plk1 (Werwein E. et al. 2019) (**Figure 5.4.A**)

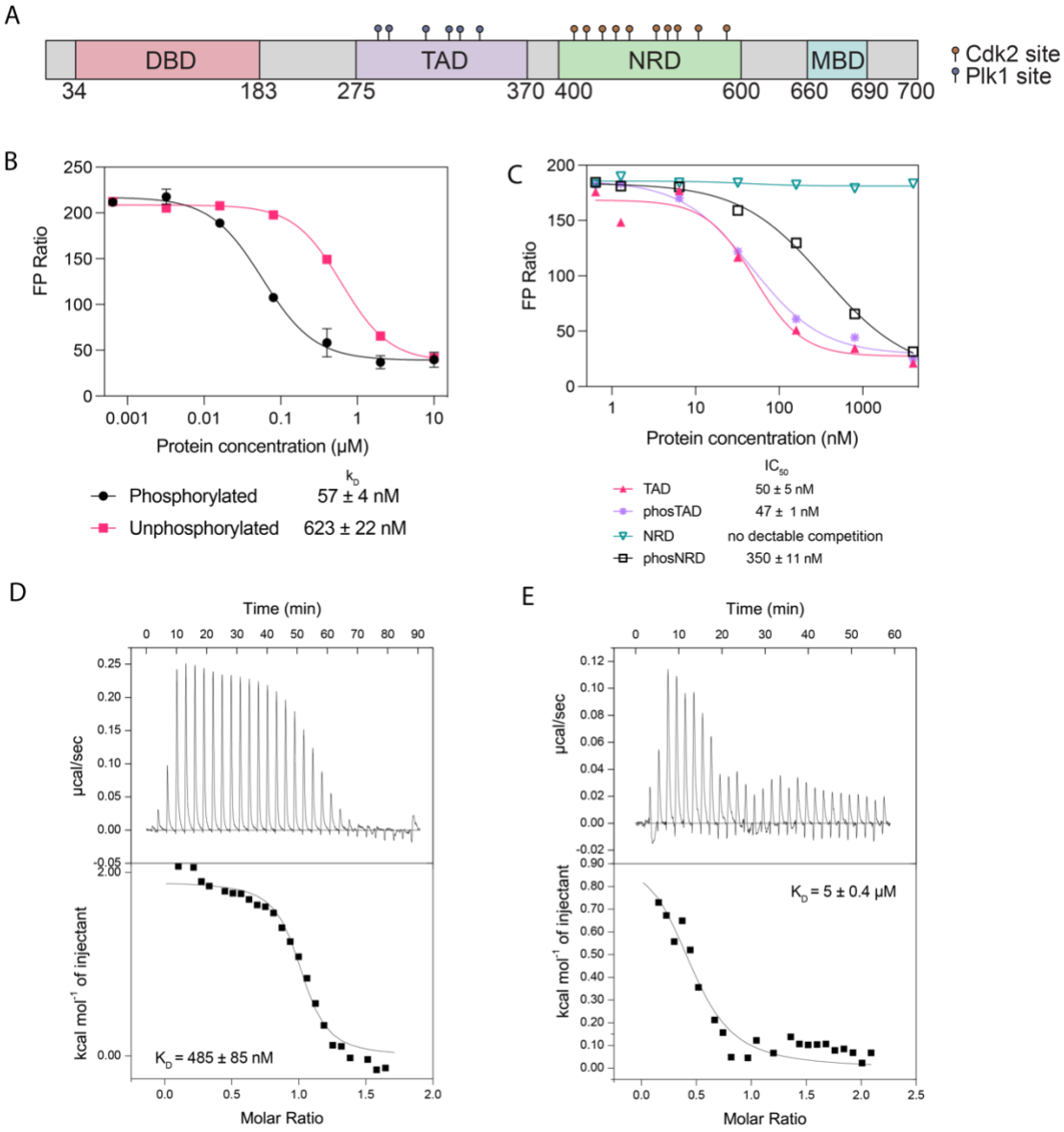

Figure 5.4. B-Myb negative regulatory domain (NRD) when phosphorylated by CDK2-Cyclin A interacts with TAZ2. A. Full-length B-Myb when sequentially phosphorylated with CDK2-Cyclin A and Plk1 can inhibit binding of AD1 to TAZ2 at an IC_{50} value 57 ± 4 nM compared to 623 ± 22 nM. **B.C.** FP competition assay with increasing B-Myb TAD, when phosphorylated with Plk1 and NRD phosphorylated with CDK2-Cyclin A. **D**. TAZ2, titrated into B-Myb TAD phosphorylated by Plk1. **E.** TAZ2 titrated into B-Myb NRD phosphorylated by CDK2-Cyclin A.

To determine whether phosphorylation affects TAZ2 binding, we used the FP competition assay with the AD1 probe (**Figure 5.4.B**). We used the AD1 probe because it has moderate binding affinity, which we assumed would provide an excellent range to monitor stronger or weaker inhibition by phosphorylated TAD. TAZ2 and We found that when B-Myb is phosphorylated by CDK2-Cyclin A and Plk1, the IC_{50} value is much smaller than the unphosphorylated B-Myb, implicating that phosphorylation of B-Myb enhances the affinity towards TAZ2. Then we wanted to investigate whether the TAD or NRD phosphorylation accounts for the increased inhibition. First, we phosphorylated the TAD with Plk1. However, phosTAD did not change the IC_{50} value (**Figure 5.4.C**). However, we used the NRD phosphorylated by CDK2-Cyclin A, which showed some level of detectable inhibition though not as strong as phosphorylated B-Myb TAD (**Figure 5.4.C**). We next tested whether phosTAD and phosNRD could directly interact with TAZ2. Using the isothermal titration calorimetry assay, we observed that, indeed, phosphorylated TAD's affinity to TAZ2 is not significantly different from unphosphorylated TAD, which explains why the inhibition to AD1:TAZ2 complex was not other between unphosphorylated and phosphorylated TAD (**Figure 5.1.B**). However, we observed weak binding between phosphorylated NRD with TAZ2 (**Figure 5.4.E**). This detected interaction is consistent with the observation that it inhibited AD1:TAZ2 in the FP assay (**Figure 5.4.C**).

5.3 Discussion

In this study, we show the biochemical characterization of B-Myb TAD binding to the TAZ2 domain of p300. p300 is a known B-Myb co-activator that interacts with the TAZ2 domain (Johnson LR. et al. 2002). Through B-Myb TAD: TAZ2 chemical shift mapping, it has been identified that the binding surface for B-Myb overlaps with p53 and STAT1 binding sites (Oka O. et al. 2012). Consistent with this data, our findings show that B-Myb TAD binds to the interface targeted by STAT1 and p53 TADs, possibly contacting both AD1 and STAT1 sites, perhaps binding allosterically. We also show that phosphorylation of NRD increases the efficiency with which B-Myb can compete for AD1 peptide from TAZ2, which suggests a possible mechanism by which B-Myb phosphorylation regulates binding to p300 to increase activity at B-Myb targeted promoters. We identified a few amino acid residues that disrupted the association with TAZ2 through an isothermal titration calorimetry assay. We introduced these mutations to HCT116 cells and performed a pull-down assay to determine if we could observe a decrease in binding to p300. However, we could still see the TAD mutants strongly co-precipitating with p300 (unpublished). Thus, more thorough scanning for future mutations in the TAD region will help to understand how B-Myb-p300 interaction regulates B-Myb dependent cell-cycle dependent gene activity.

5.4 Materials and Methods

5.4.1 *Recombinant protein expression and Purification*

The human B-Myb TAD and NRD (B-Myb residues 275-375) were expressed in *E. coli* from an engineered pGEX plasmid with an N-terminal GST tag and a TEV protease cleavage site. Proteins were expressed overnight by inducing with 1 mM IPTG at 19 °C. All proteins were lysed in a buffer containing 200 mM NaCl, 40 mm Tris, 5 mM DTT, and 1 mM PMSF (pH 8.0). The lysed cells were clarified by centrifugation at 19,000 rpm for 45 min at 4 °C. Protein lysates were allowed to bind to equilibrated Glutathione Sepharose resin (Cytiva) for 30 min and washed to remove unspecific proteins. The proteins were eluted with a buffer containing 200 mM NaCl, 40 mM Tris, 5 mM DTT, and 10 mM reduced L-Glutathione (pH 8.0). Eluted proteins were purified using Q-sepharose and cleaved with TEV protease at 4 °C overnight. Proteins were then passed through Glutathione Sepharose resin to remove the free GST and concentrated on running through Superdex-75 (GE Healthcare) into 200 mM NaCl, 25 mM Tris, and 1 mM DTT (pH 8.0). Cdk2-CycA and Plk1 kinase domains were expressed and purified as previously described (Marceau AH. et al. 2019).

To generate phosphorylated protein reagents, kinase reactions were performed similarly to those described (Marceau AH. et al. 2019). B-Myb protein constructs following final purification were incubated with 10 mM ATP, 50 mM MgCl2, and 20% by mass of either Cdk2-CycA, Plk1 kinase domain,

or both Plk1 and Cdk2-CycA, overnight at 4 °C. The kinase reaction was concentrated and run over Superdex-75 (GE Healthcare) to remove kinases and ATP, and phosphorylation of the proteins was confirmed by electrospray mass spectrometry using a Sciex X500B QTOF system.

5.4.2 *Calorimetry*

Dissociation constants (K_D) for DBD and NRD interactions were measured using ITC with a MicroCal VP-ITC system. All proteins were concentrated as needed and dialyzed into a buffer containing 150 mM NaCl, 20 mM Tris, and 1 mM BME (pH 8). TAZ2 (300 μM) was titrated into TAD (30 μM) at 19 °C. The dissociation constant of NRD mutants and phosphorylated NRDs was determined similarly. K_Ds are the average fits from three technical replicates analyzed using the Origin ITC software package, with the SD reported as an error. All the fit stoichiometry (n) values were between 0.6 and 1.

5.4.3 *Fluorescence Polarization assay*

Dissociation constants for direct binding between TAZ2 and STAT1, AD1 and AD2 peptides were determined by titrating increasing amounts of peptides into 20 nM of FAM dye-labeled peptide probes (AD1: PLSQETFSDLWKLLPENNVLSPLPS, AD2: SQAMDDLMLSPDDIEQWFTEDPGPD, STAT1: DPNEEAVSQIFPDSVMLAVQ EGIDLLTFPPA). The peptides were synthesized from genscript. For TAZ2 + peptides assays, TAZ2 and peptides

were incubated for 30 min on ice before titrating the TAD in a buffer containing 150 mM NaCl, 25 mM Tris, 1 mM DTT, and 0.1% Tween20 (pH 8). FP measurements were acquired on a PerkinElmer EnVision 2103 Multilabel plate reader with excitation at 559 nm and emission at 580 nm. The dissociation constants (KD) were calculated by fitting millipolarization (mP) values of three technical replicates against concentration using a one-site–binding model in GraphPad Prism 8.

Chapter 6: Aurora kinase activity is enhanced when auto-phosphorylated and complexed with Bora

6.1 Introduction

Mitosis is the final phase of the cell cycle when the cell goes through the segregation of chromosomes to produce two genetically identical daughter cells (Sazer S. et al. 2014). There is a multitude of protein machinery that participate during mitosis to carefully coordinate the four stages of mitosis: prophase, metaphase, anaphase, and telophase (Yanagida M, 2014). The spindle microtubules and centromeres are two primary mitotic machines that play a crucial role in properly segregating the chromosomes and other cytoplasmic duplicates among the two daughter cells (O'Connell CB and Khodjakov AL. 2007). Mitosis is driven by a wave of protein phosphorylation events by several mitotic kinases, including CDK1-Cyclin B, the Aurora family, the Polo family, and the never-in mitosis gene A (NIMA)–related kinase (NEK)

(Nigg EA. 2001), (Fry AM. et al. 2017). These kinases are often overexpressed in several cancers, including cervical, neuroblastoma, prostate, ovarian, colon, and breast (Javed A. et al., 2023). For example, Aroura A overexpression is linked to uncontrolled centrosome amplification leading to multinucleation and poor execution of cytokinesis (D'Assoro AB. et al. 2016). Therefore, Aurora A kinase is considered an oncoprotein and used as a biomarker for cancer detection (Giet R et al. 2005). Understanding how these kinases are regulated to target cancer therapeutics appropriately is essential.

Several co-activators of Aurora A have been identified to be critical for its activity, including microtubule-binding protein TPX2, the centrosomal protein Cep192, and Bora (Gomez-Ferreria MA. et al. 2007), (Kufer TA. et al. 2002). Out of these co-activators, the Bora activator is vital for the Aurora-mediated activation of Plk1, which activates CDK1 and mitotic entry in cells. Mechanistically, Aurora A increases the accessibility of its activation loop of Plk1 in the presence of Bora and phosphorylates the Threonine 210 in the activation loop (Macůrek L. et al. 2008), (Seki A. et al. 2008). Studies done in C. *elegans* show that Bora also gets activated by phosphorylation of CDK1 and is known to enhance its ability to activate Aurora A mediated Plk1 phosphorylation (Tavernier N. et al. 2015). However, this critical mechanism by which Aurora and Bora interact and how Bora allosterically activates

Aurora A is unknown. Here we show that Aurora A can directly interact with Bora, and the phosphorylation of Bora does not change the affinity.

6.2 Results

6.2.1 *Aurora kinase domain binds to Bora co-activator*

Previous literature has shown that Bora 1-224 is sufficient to activate Plk1 phosphorylation through Aurora A (Thomas Y. et al. 2016). Therefore, we first defined the minimal domain necessary for Bora to form a complex with Aurora A. The most conserved region of Bora is in the N-terminus; therefore, we tested four constructs from amino acid residues 1-124, 41-124, 46-124, and 1-50. We used isothermal titration calorimetry (ITC) to measure binding affinities, and out of the four constructs, amino acids 1-124 and 41-124 showed similar binding affinities of 2.8 and 1.8 μM (**Figure 6.1**). Therefore, we used 1-124 to set crystal trays with Aurora A.

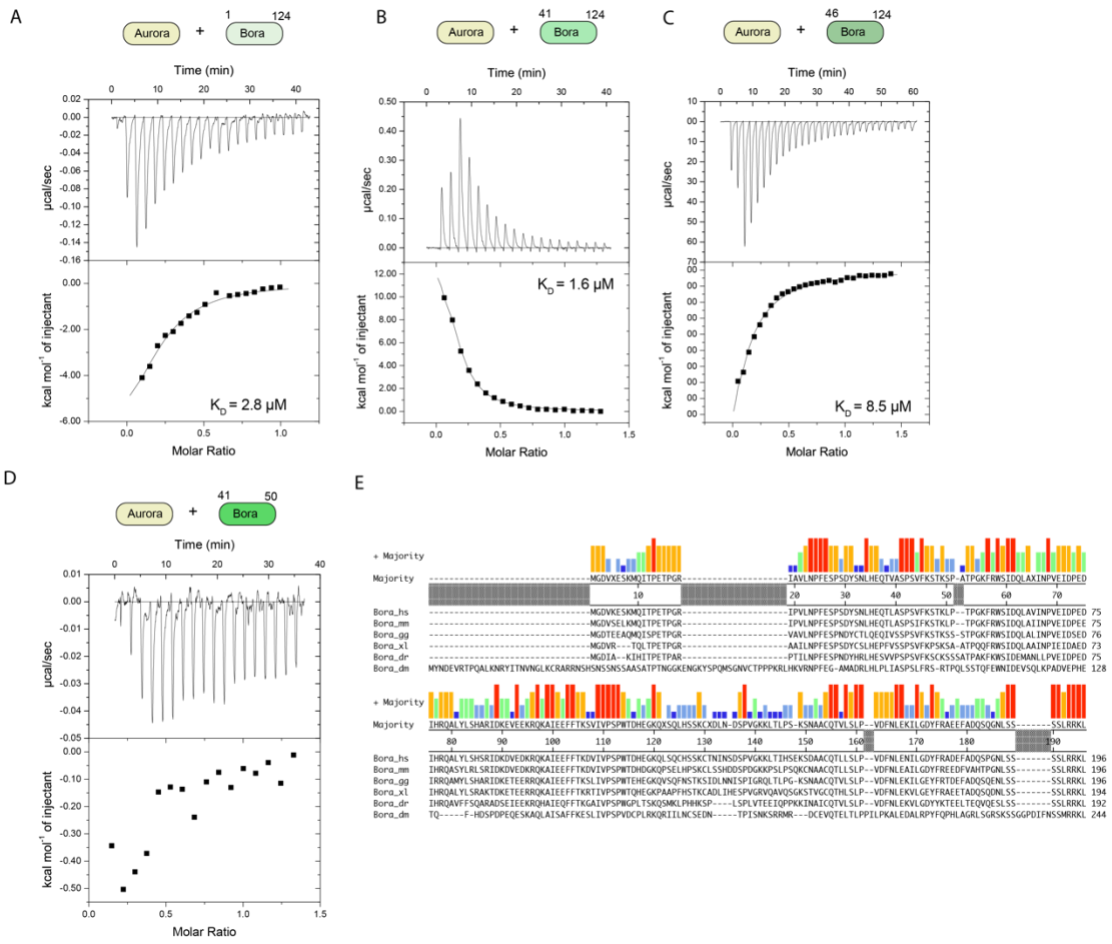

Figure 6.1. Bora amino acids 1-124 directly interact with Aurora A kinase. A.B.C.D. Aurora A crystal construct titrated into Bora constructs as indicated above the graphs (Nowakowski J. et al. 2002)—E. Bora sequence alignment shows conservation across species.

6.2.2 *Initial crystal screening for structure determination*

Initial crystal screens were set up with separately purified Aurora A and Bora 1-124 constructs isolated from gel-filtration chromatography. However, this only led to crystals formed by Aurora A (**Figure 6.2.A**). To increase the likelihood of crystallizing a co-complex, we made a fusion construct with the Bora construct 1-124 fused to the C-terminus of the Aurora A crystal construct. This construct led to needle-shaped crystals, which diffracted to 3.6 Å; however, the model building for Bora was challenging with the resolution (**Figure 6.2.B** and **C**). However, we resolved two Auroa A molecules in the unit cell with density for Bora between the interface of the two Aurora A molecules (**Figure 6.2.D**). More optimization with expanded crystal conditions did not improve the quality of the diffracting crystals.

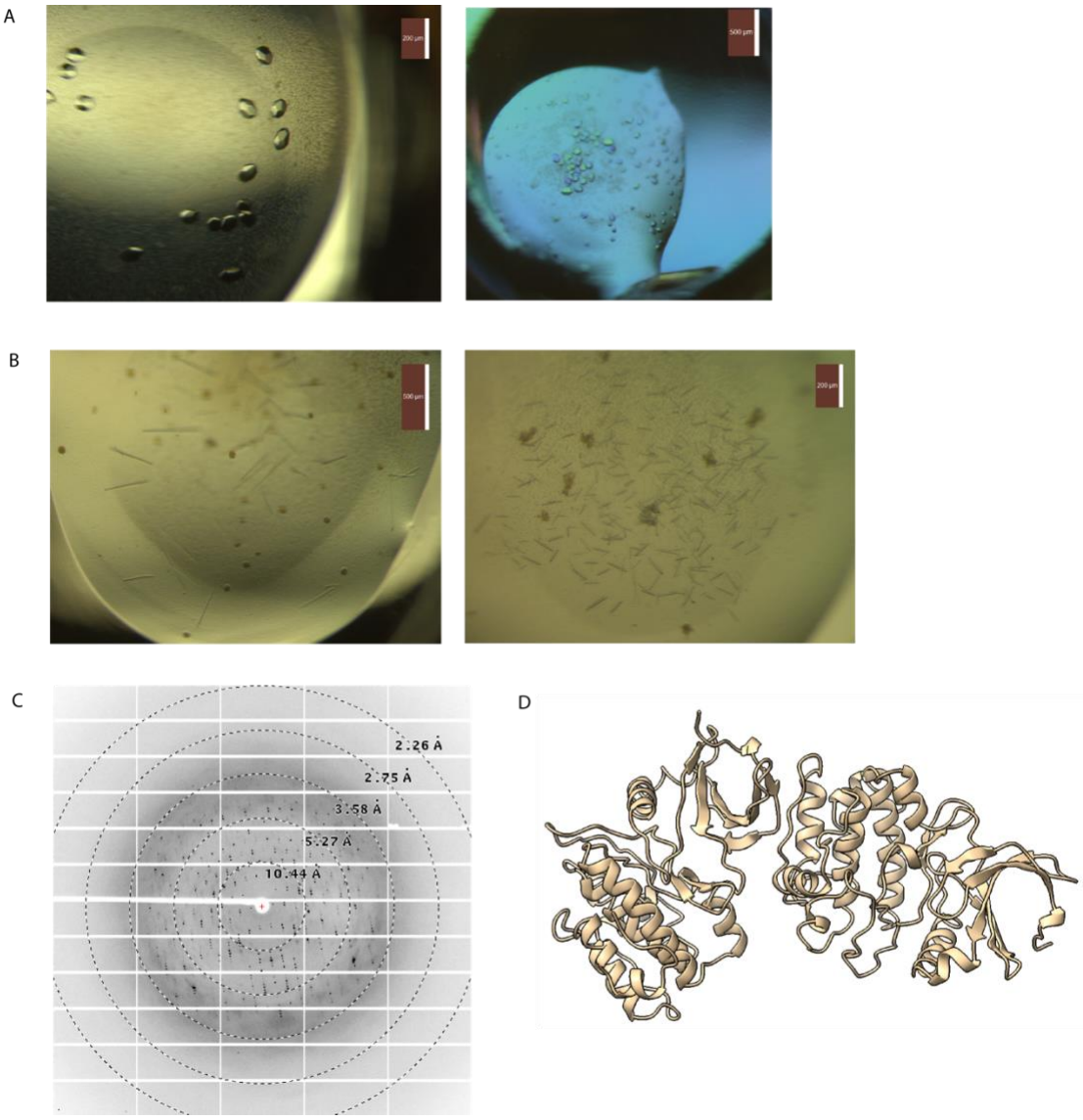

Figure 6.2. Attempts to solve the crystal structure of the Aurora A-Bora complex. A. Crystals trays set with Aurora A and Bora co-eluted from gel-filtration only produced typical Ruger ball-shaped crystals containing Aurora only. **B.** Crystals trays set with Aurora-Bora fusion protein produced needle-like thin crystals. **C.** Diffraction pattern of Aurora-Bora fusion protein crystals. **D.** Molecular replacement showed two Aurora A molecules with unmodeled density corresponding to Bora between the interface of the two Aurora molecules.

6.2.3 *Bora increases the activity of phosphorylated Aurora A towards Plk1 and H3*

It has been well established that phosphorylation of Plk1 by Aurora A requires Bora (Macůrek L. et al. 2008), (Seki A. et al. 2008). Therefore, we wanted to confirm that our construct Bora 1-124 can co-activate Aurora A in an *in vitro* kinase assay (**Figure 6.2.A**). We also wanted to test whether Aurora A autophosphorylation affects its kinase activity. Aurora A gets auto phosphorylated when purified from *E. coli* cells determined through mass spectrometry. Here we tested Aurora A activity towards Plk and H3, in which we saw kinase activity only when Bora is present and increased activity when Aurora A is phosphorylated. Hence, Aurora A can still phosphorylate Plk1 and H3 when in its unphosphorylated form (lanes 3 and 4). It has been known that Bora initially gets phosphorylated by CDK1 to activate Plk1 and then phosphorylated by Plk1 for degradation, the latter we observed in lane 15 (Seki A. Coppinger JA. et al. 2008). Here we also observed that Bora gets phosphorylated by Aurora A (lanes 10 and 11). We also tested whether Bora gets in vitro phosphorylated by CDK2-Cyclin A, which we observed through mass spectrometry but did not change its affinity towards Aurora A by ITC (unpublished). Therefore, further investigation to understand Bora phosphorylation by Aurora A will help to understand if Bora has a second layer of activation through interacting with Aurora A.

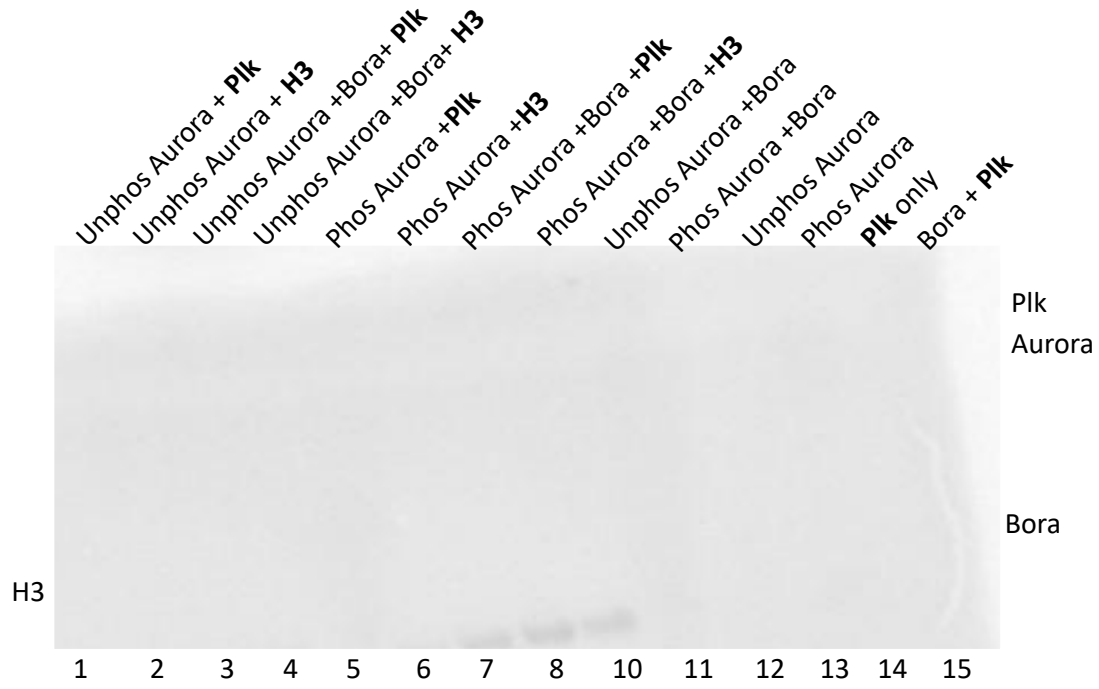

Figure 6.3. Phosphorylated Aurora A enhances kinase activity towards Plk1 in the presence of Bora 1-124. Phosphorylation of the indicated substrates Plk1 and H3 with ^{32}P-ATP.

6.3 Materials and Methods

6.4.1 *Protein expression, purification, in-vitro phosphorylation*

The Aurora A was expressed in *E. coli* BL21 cells with a cleavable N-terminal His tag. Cells were harvested and lysed in a buffer containing 300 mM NaCl, 50 mM Tris, 10 mM Imidazole, 1 mM TCEP, 10% Glycerol v/v, 20 mM $MgCl_2$, Sigma Protease Inhibitor (P8340), and 1 mM PMSF (pH 8.0). Protein was purified with Nickle resin (Cytiva) equilibrated in lysis buffer. The lysed cells were clarified by centrifugation at 19,000 rpm for 45 min at 4 °C. The cleared lysate was incubated with resin for 1 h at 4 °C, and the resin was washed with a buffer containing 300 mM NaCl, 50 mM Tris, 10 mM Imidazole, 1 mM TCEP, 10% glycerol v/v and 20 mM $MgCl_2$ (pH 8.0). The protein was then eluted in 300 mM NaCl, 50 mM Tris, 200 mM Imidazole, 1 mM TCEP, 10% Glycerol v/v, and 20 mM $MgCl_2$ (pH 8.0). Protein was dialyzed into storage buffer (300 mM NaCl, 50 mM Tris, 1 mM TCEP, 10% glycerol v/v, and 20 mM $MgCl_2$ (pH 8.0)) and stored at −80 °C.

The Bora constructs were expressed in *E. coli* from an engineered pGEX plasmid with an N-terminal GST tag and a TEV protease cleavage site. Proteins were expressed overnight by inducing with 1 mM IPTG at 19 °C. All proteins were lysed in a buffer containing 200 mM NaCl, 40 mm Tris, 5 mM DTT, and 1 mM PMSF (pH 8.0). The lysed cells were clarified by centrifugation at 19,000 rpm for 45 min at 4 °C. Protein lysates were allowed

to bind to equilibrated Glutathione Sepharose resin (Cytiva) for 30 min and washed to remove unspecific proteins. The proteins were eluted with a buffer containing 200 mM NaCl, 40 mM Tris, 5 mM DTT, and 10 mM reduced L-Glutathione (pH 8.0). Eluted proteins were purified using Q-sepharose and cleaved with TEV protease at 4 °C overnight. Proteins were then passed through Glutathione Sepharose resin to remove the free GST and concentrated on running through Superdex-75 (GE Healthcare) into 200 mM NaCl, 25 mM Tris, and 1 mM DTT (pH 8.0). Cdk2-CycA and Plk1 kinase domains were expressed and purified as previously described (Marceau AH. et al. 2019).

To generate phosphorylated Bora, kinase reactions were performed similarly to those previously described (Marceau AH. et al. 2019). B-Myb protein constructs following final purification were incubated with 10 mM ATP, 50 mM MgCl2, and 20% by mass of either Cdk2-CycA, Plk1 kinase domain, or both Plk1 and Cdk2-CycA, overnight at 4 °C. The kinase reaction was concentrated and run over Superdex-75 (GE Healthcare) to remove kinases and ATP, and phosphorylation of the proteins was confirmed by electrospray mass spectrometry using a Sciex X500B QTOF system.

6.4.2 *Calorimetry*

Dissociation constants (K_D) for Bora constructs and Aurora A interactions were measured using ITC with a MicroCal VP-ITC system. All proteins were

concentrated as needed and dialyzed into a buffer containing 200 mM NaCl, 20 mM Tris, 20 mM $MgCl_2$, and 1 mM TCEP (pH 8). Bora (500 μM) was titrated into Aurora A (50 μM) at 19 °C. K_Ds are the average fits from three technical replicates analyzed using the Origin ITC software package.

6.4.3 *Crystallization, data collection, and structure determination*

Aurora A and Bora construct 1-124 were separately isolated from a Superdex 200 (GE Healthcare) column in a buffer containing 200 mM NaCl, 20 mM Tris, 20 mM $MgCl_2$, and 1 mM TCEP (pH 8). Bora was added in 3-fold molar excess to 18 mg/mL. After incubation on ice for 30 minutes, both complexes were prepared for crystallization by running through a Superdex 200 (GE Healthcare) column in a buffer containing 200 mM NaCl, 20 mM Tris, 20 mM $MgCl_2$ and one mM TCEP (pH 8), and crystallized by sitting-drop vapor diffusion at 19°C. Crystals formed after two weeks in 200 mM ammonium chloride, 100 mm Tris pH 7.0, 4% PEG 2000. Crystals were frozen in the well buffer with 20% ethylene glycol. Aurora-Bora fusion construct was prepared for crystallization by running through a Superdex 200 (GE Healthcare) column in a buffer containing 200 mM NaCl, 20 mM Tris, 20 mM $MgCl_2$, and one mM TCEP (pH 8) and concentrated to 20 mg/mL. It was crystallized by sitting-drop vapor diffusion at 19°C. Crystals formed after 4 weeks in 100 mM Na-HEPES pH 7.0, 1.0 M $(NH4)_2SO4$, and 2% PEG 4000.

Data were collected at the Advanced Photon Source, Argonne National Laboratory at Beamline 23-IDB. Diffraction spots were integrated using MOSFLM (Leslie 2006), and data were merged and scaled using Scala (Bailey 1994). Phases were first solved for the E721-29 complex by molecular replacement using PHASER (Mccoy et al. 2007). The crystal structure of Aurora A (PDB ID: 1MQ4) was used as a search model and molecular substitute.

6.4.4 *Kinase assays*

Aurora A (10 μM) was mixed with either Plk1 and H3 (5 μM) with and without Bora 1-124 construct (10 μM) in a buffer containing 25 mM Tris, 200 mM NaCl, 20 mM $MgCl_2$, 5 mM Sodium orthovanadate, 5 mM TCEP, 250 μM ATP, and 100 μCi of 32P-γ-ATP (pH 8.0). The substrate was diluted into the reaction buffer, and the reaction was initiated by adding ATP. Reactions were quenched after 30 min by adding SDS–PAGE loading buffer. SDS–PAGE gels were imaged with a Typhoon scanner and bands quantified using the ImageJ software package. For each assay,

three replicates were performed.

References

Ganter S. and Lipsick JS. 1999. Myb and oncogenesis. *Advances in cancer research* **76**:21-60.

Lipsick JS. 2010. The C-MYB story--is it definitive? *Proc Natl Acad Sci USA* **107**(40):17067-8.

Lipsick JS. 1996. One billion years of Myb. *Oncogene* **13**(2):223-35.

Westin, E. H. et al. 1982. Differential expression of the amv gene in human hematopoietic cells. *Proc. Natl Acad. Sci. USA* **79**, 2194–2198.

Okada, M. et al. 1982. c-myb gene analysis in T-cell malignancies with del(6q). *Cancer Genet. Cytogenet*. **48**, 229–236.

Torelli, G. et al. 1987. Expression of c-myb protooncogene and other cell cycle-related genes in normal and neoplastic human colonic mucosa. *Cancer Res*. **47**, 5266–5269

Thompson, M. A., Flegg, R., Westin, E. H. & Ramsay, R. G. 1997. Microsatellite deletions in the c-myb transcriptional attenuator region associated with over-expression in colon tumour cell lines. *Oncogene* **14**, 1715–1723

Li, Y. et al. 2016. c-Myb enhances breast cancer invasion and metastasis through the Wnt/beta-Catenin/Axin2 pathway. Cancer Res. **76**, 3364–3375

Mansour, M. R. et al. 2017. Oncogene regulation. An oncogenic super-enhancer formed through somatic mutation of a noncoding intergenic element. *Science* **346**, 1373–1377

Ogata, K. Morikawa S, Nakamura H, Sekikawa A, Inoue T, Kanai H, Sarai A, Ishii S, Nishimura Y. 1992. Solution structure of a DNA-binding unit of Myb: a helix-turn-helix-related motif with conserved tryptophans forming a hydrophobic core. Proc. *Natl Acad. Sci. USA* **89**, 6428–6432.

Carr MD, Wollborn U, McIntosh PB, Frenkiel TA, McCormick JE, Bauer CJ, Klempnauer KH, Feeney J. 1996. Structure of the B-Myb DNA-binding domain in solution and evidence for multiple conformations in the region of repeat-2 involved in DNA binding: implications for sequence-specific DNA binding by Myb proteins. *Eur J Biochem*. **1**;235(3):721-35.

Cicirò Y, Sala A. 2021. MYB oncoproteins: emerging players and potential therapeutic targets in human cancer. *Oncogenesis*. **26**;10(2):19.

Toscani, A. et al. 1997. Arrest of spermatogenesis and defective breast development in mice lacking A-myb. *Nature* **386**, 713–717

Mettus, R. V. et al. 1994. Murine A-myb: evidence for differential splicing and tissue- specific expression. *Oncogene* **9**, 3077–3086.

Qaddoumi, I. et al. 2017. Genetic alterations in uncommon low-grade neuro epithelial tumors: BRAF, FGFR1, and MYB mutations occur at high frequency and align with morphology. *Acta Neuropathol*. **131**, 833–845.

Armstrong, G. T. et al. 2011. Survival and long-term health and cognitive outcomes after low-grade glioma. *Neuro Oncol*. **13**, 223–234

Brayer, K. J., Frerich, C. A., Kang, H. & Ness, S. A. 2016. Recurrent fusions in MYB and MYBL1 define a common, transcription factor-driven oncogenic pathway in salivary gland adenoid cystic carcinoma. *Cancer Discov.* **6**, 176–187.

Iness, A. N. et al. 2019. The cell cycle regulatory DREAM complex is disrupted by high expression of oncogenic B-Myb. *Oncogene* **38**, 1080–1092.

Lam, E. W. & Watson, R. J. 1993. An E2F-binding site mediates cell-cycle regulated repression of mouse B-myb transcription. *EMBO J*. 12, 2705–2713.

Lorvellec, M. et al. 2010. B-Myb is critical for proper DNA duplication during an unperturbed S phase in mouse embryonic stem cells. *Stem Cells* **28**, 1751–1759.

Tanaka, Y., Patestos, N. P., Maekawa, T. & Ishii, S. 1999. B-myb is required for inner cell mass formation at an early stage of development. *J. Biol. Chem*. **274**, 28067–28070

Lloyd AC. 2013. The regulation of cell size. *Cell* **154**(6):1194-205.

Conlon, I.J., Dunn, G.A., Mudge, A.W., and Raff, M.C. 2001. Extracellular control of cell size. *Nat. Cell Biol*. **3**, 918–921.

Matthews HK, Bertoli C, de Bruin RAM. 2022. Cell cycle control in cancer. Nat Rev *Mol Cell Biol*. **23**(1):74-88.

Foley, E. A. & Kapoor, T. M. 2013. Microtubule attachment and spindle assembly checkpoint signaling at the kinetochore. *Nat. Rev. Mol. Cell Biol*.**14**, 25–37.

Müller GA, Wintsche A, Stangner K, Prohaska SJ, Stadler PF, Engeland K. 2014. The CHR site: definition and genome-wide identification of a cell cycle transcriptional element. *Nucleic Acids Res*. **42**(16):10331-50.

Sadasivam S, DeCaprio JA. 2013. The DREAM complex: master coordinator of cell cycle-dependent gene expression. *Nat Rev Cancer*. 2013 **13**(8):585-95.

Ganter B, Fu S, Lipsick JS. 1998. D-type cyclins repress transcriptional activation by the v-Myb but not the c-Myb DNA-binding domain. *EMBO J*. **17**: 255-268.

Lei W, Liu F, Ness SA. 2005. Positive and negative regulation of c-Myb by cyclin D1, cyclin-dependent kinases, and p27 Kip1. *Blood* **105**(10):3855-61.

Nakata, Y., Shetzline, S., Sakashita, C., Kalota, A., Rallapalli, R., Rudnick, S., Zhang, Y., Emerson, S., Gewirtz, A. 2007. c-Myb contributes to G2/M cell cycle transition in human hematopoietic cells by direct regulation of cyclin B1 expression. *Mol.Cell.Biol*. **27**, 2048–2058.

Guiley KZ, Iness AN, Saini S, Tripathi S, Lipsick JS, Litovchick L, Rubin SM. 2018. Structural mechanism of Myb-MuvB assembly. *Proc Natl Acad Sci USA* **115**(40):10016-10021.

Andrejka L, Wen H, Ashton J, Grant M, Iori K, Wang A, Manak JR, Lipsick JS. 2011. Animal-specific C-terminal domain links myeloblastosis on-coprotein (Myb) to an ancient repressor complex. *Proc. Natl. Acad. Sci. USA* **108**:17438–17443.

Knight AS, Notaridou M, Watson RJ. 2009. A Lin-9 complex is recruited by B-Myb to activate transcription of G2/M genes in undifferentiated embryonal carcinoma cells. *Oncogene* **28**(15):1737-47.

Iness AN, Felthousen J, Ananthapadmanabhan V, Sesay F, Saini S, Guiley KZ, Rubin SM, Dozmorov M, Litovchick L. 2019. The cell cycle regulatory DREAM complex is disrupted by high expression of oncogenic B-Myb. *Oncogene* **38**(7):1080-1092.

Ziebold U, Klempnauer KH. 1997. Linking Myb to the cell cycle: cyclin-dependent phosphorylation and regulation of A-Myb activity. *Oncogene* **15**(9):1011-9.

Musa J, Aynaud MM, Mirabeau O, Delattre O, Grünewald TG. 2017. MYBL2 (B-Myb): a central regulator of cell proliferation, cell survival and differentiation involved in tumorigenesis. *Cell Death Dis*. **22**;8(6):e2895.

Bayley R, Ward C, Garcia P. 2020. MYBL2 amplification in breast cancer: Molecular mechanisms and therapeutic potential. *Biochim Biophys Acta Rev Cancer* **1874**(2):188407.

Qin H, Li Y, Zhang H, Wang F, He H, Bai X, Li S. 2019. Prognostic implications and oncogenic roles of MYBL2 protein expression in esophageal squamous-cell carcinoma. *Onco Targets Ther.* **12**:1917-1927.

Sun C, Li H, Mills RE, Guan Y. 2019. Prognostic model for multiple myeloma progression integrating gene expression and clinical features. *Giga science* **8**(12):giz153.

Calvisi DF, Simile MM, Ladu S, Frau M, Evert M, Tomasi ML, Demartis MI, Daino L, Seddaiu MA, Brozzetti S, Feo F, Pascale RM. 2011. Activation of v-Myb avian myeloblastosis viral oncogene homolog-like2 (MYBL2)-LIN9 complex contributes to human hepatocarcinogenesis and identifies a subset of hepatocellular carcinoma with mutant p53. *Hepatology* **53**(4):1226-36.

Frau M, Ladu S, Calvisi DF, Simile MM, Bonelli P, Daino L, Tomasi ML, Seddaiu MA, Feo F, Pascale RM. 2011. Mybl2 expression is under genetic control and contributes to determine a hepatocellular carcinoma susceptible phenotype. *J Hepatol*. **55**(1):111-9.

Cervellera M, Raschella G, Santilli G, Tanno B, Ventura A, Mancini C, Sevignani C, Calabretta B, Sala A. 2000. Direct transactivation of the anti-apoptotic gene apolipoprotein J (clusterin) by B-MYB. *J Biol Chem*. **275**:21055–21060.

Tanaka Y, Patestos NP, Maekawa T, Ishii S. 1999. B-myb is required for inner cell mass formation at an early stage of development. *J Biol Chem* **274**: 28067–28070.

Vorster PJ, Goetsch P, Wijeratne TU, Guiley KZ, Andrejka L, Tripathi S, Larson BJ, Rubin SM, Strome S, Lipsick JS. 2020. A long lost key opens an ancient lock: Drosophila Myb causes a synthetic multivulval phenotype in nematodes. *Biol Open* **7**;9(5): bio051508.

Yamauchi, T., Ishidao,T., Nomura,T., Shinagawa,T., Tanaka,Y.,Yonemura,S. and Ishii,S. 2008. A B-Myb complex containing clathrin and filamin is required for mitotic spindle function. *EMBO J*., **27**,1852–1862.

Tarasov,K.V., Tarasova,Y.S., Tam,W.L., Riordon,D.R., Elliott,S.T.,Kania,G., Li,J., Yamanaka,S., Crider,D.G., Testa,G.et al. 2008. B-MYB is essential for normal cell cycle progression and chromosomal stability of embryonic stem cells. *PLoS One* **3**, e2478.

Werwein E, Cibis H, Hess D, Klempnauer KH. 2019. Activation of the oncogenic transcription factor B-Myb via multisite phosphorylation and prolyl cis/trans isomerization. *Nucleic Acids Res*. **10**;47(1):103-121.

Marceau AH, Brison CM, Nerli S, Arsenault HE, McShan AC, Chen E, Lee HW, Benanti JA, Sgourakis NG, Rubin SM. 2019. An order-to-disorder structural switch activates the FoxM1 transcription factor. *Elife* **28**;8:e46131.

Ogata, K. et al. 1994. Solution structure of a specific DNA complex of the Myb DNA-binding domain with cooperative recognition helices. *Cell* **79**, 639–648.

Tahirov, T. H. et al. 2001. Crystals of ternary protein–DNA complexes composed of DNA-binding domains of c-Myb or v-Myb, C/EBPαor C/EBPβand tom-1A promoter fragment. *Acta Crystallography* **D57**, 1655–1658.

Rosinski, J. A. and Atchley, W. R. 1998. Molecular evolution of the Myb family of transcription factors: evidence for polyphyletic origin. *J. Mol. Evol*.,**46**, 74–83.

Biedenkapp H, Borgmeyer U, Sippel AE, Klempnauer KH. 1988. Viral myb oncogene encodes a sequence-specific DNA-binding activity. *Nature* **27**;335(6193):835-7.

Ness SA, Marknell A, Graf T. 1989. The v-myb oncogene product binds to and activates the promyelocyte-specific mim-1 gene. *Cell* **22**;59(6):1115-25.

Mizuguchi G, Nakagoshi H, Nagase T, Nomura N, Date T, Ueno Y, Ishii S. 1990. DNA binding activity and transcriptional activator function of the human B-myb protein compared with c-MYB. *J Biol Chem*. **265**(16):9280-4.

Nakagoshi H, Nagase T, Kanei-Ishii C, Ueno Y, Ishii S. 1990. Binding of the c-myb proto-oncogene product to the simian virus 40 enhancer stimulates transcription. *J Biol Chem*. **25**;265(6):3479-83.

Introna M, Golay J, Frampton J, Nakano T, Ness SA, Graf T. 1990. Mutations in v-myb alter the differentiation of myelomonocytic cells transformed by the oncogene. *Cell* **63**(6):1289-97.

Oehler T, Arnold H, Biedenkapp H, Klempnauer KH. 1990. Characterization of the v-myb DNA binding domain. *Nucleic Acids Res*. **18**(7):1703-10.

Ebneth A, Schweers O, Thole H, Fagin U, Urbanke C, Maass G, Wolfes H. 1994. Biophysical characterization of the c-Myb DNA-binding domain. *Biochemistry* **33**(48):14586-93.

Gabrielsen, O. S., Sentenac, A. and Fromageot, P. 1991. Specific DNA binding by c-Myb: evidence for a double helix-turn-helix-related motif. *Science* **253**, 1140–1143.

Ording E, Kvåvik W, Bostad A, Gabrielsen OS. 1994. Two functionally distinct half sites in the DNA-recognition sequence of the Myb oncoprotein. *Eur J Biochem*. **222**(1):113-20.

Jamin N, Gabrielsen OS, Gilles N, Lirsac PN, Toma F. 1993. Secondary structure of the DNA-binding domain of the c-Myb oncoprotein in solution. A multidimensional double and triple heteronuclear NMR study. *Eur J Biochem.* **15**;216(1):147-54.

Carr MD, Wollborn U, McIntosh PB, Frenkiel TA, McCormick JE, Bauer CJ, Klempnauer KH, Feeney J. 1996. Structure of the B-Myb DNA-binding domain in solution and evidence for multiple conformations in the region of repeat-2 involved in DNA binding: implications for sequence-specific DNA binding by Myb proteins. *Eur J Biochem*. **235**(3):721-35.

McIntosh PB, Frenkiel TA, Wollborn U, McCormick JE, Klempnauer KH, Feeney J, Carr MD. 1998. Solution structure of the B-Myb DNA-binding domain: a possible role for conformational instability of the protein in DNA binding and control of gene expression. *Biochemistry* **37**(27):9619-29.

Konig P, Giraldo R, Chapman L, Rhodes D. 1996. The crystal structure of the DNA-binding domain of yeast RAP1 in complex with telomeric DNA. *Cell* **85**(1):125-136.

Tanikawa, J., Yasukawa, T., Enari, M., Ogata, K., Nishimura, Y., Ishii, S., and Sarai, A. 1993. Recognition of specific DNA sequences by the c-myb proto-oncogene product: role of three repeat units in the DNA-binding domain. *Proc. Natl. Acad. Sci. USA* **90**, 9320-9324.

Werwein E, Schmedt T, Hoffmann H, Usadel C, Obermann N, Singer JD, Klempnauer KH. 2012. B-Myb promotes S-phase independently of its sequence-specific DNA binding activity and interacts with polymerase delta-interacting protein 1 (Pdip1). *Cell Cycle* **11**(21):4047-58.

Hanaoka S, Nagadoi A, Nishimura Y. 2005. Comparison between TRF2 and TRF1 of their telomeric DNA-bound structures and DNA-binding activities. *Protein Sci* **14**(1):119-130.

Ko ER, Ko D, Chen C, Lipsick JS. 2007. A conserved acidic patch in the Myb domain is required for activation of an endogenous target gene and for chromatin binding. *Mol Cancer* **7**:77.

Dai P, Akimaru H, Tanaka Y, Hou DX, Yasukawa T, Kanei-Ishii C, Takahashi T, Ishii S. 1996. CBP as a transcriptional coactivator of c-Myb. *Genes and Develepment* **10**(5):528-40.

Oelgeschläger M, Janknecht R, Krieg J, Schreek S, Lüscher B. 1996. Interaction of the co-activator CBP with Myb proteins: effects on Myb-specific transactivation and on the cooperativity with NF-M. *EMBO J.* **15**(11):2771-80.

Facchinetti V, Loffarelli L, Schreek S, Oelgeschläger M, Lüscher B, Introna M, Golay J. 1997. Regulatory domains of the A-Myb transcription factor and its interaction with the CBP/p300 adaptor molecules. *Biochem J*. **324** (Pt 3) (Pt 3):729-36.

Fuglerud BM, Ledsaak M, Rogne M, Eskeland R, Gabrielsen OS. 2018. The pioneer factor activity of c-Myb involves recruitment of p300 and induction of histone acetylation followed by acetylation-induced chromatin dissociation. *Epigenetics Chromatin* **11**(1):35.

Pattabiraman DR, McGirr C, Shakhbazov K, Barbier V, Krishnan K, Mukhopadhyay P, Hawthorne P, Trezise A, Ding J, Grimmond SM, Papathanasiou P, Alexander WS, Perkins AC, Levesque JP, Winkler IG, Gonda TJ. 2014. Interaction of c-Myb with p300 is required for the induction of acute myeloid leukemia (AML) by human AML oncogenes. *Blood* **123**(17):2682-90.

Dyson HJ, Wright PE. 2016. Role of Intrinsic Protein Disorder in the Function and Interactions of the Transcriptional Coactivators CREB-binding Protein (CBP) and p300. *J Biol Chem.* **291**(13):6714-22.

Oka O, Waters LC, Strong SL, Dosanjh NS, Veverka V, Muskett FW, Renshaw PS, Klempnauer KH, Carr MD. 2012. Interaction of the transactivation domain of B-Myb with the TAZ2 domain of the coactivator p300: molecular features and properties of the complex. *PLoS One* **7**(12):e52906.

Bergholtz S., Andersen T.O., Andersson K.B., Borrebaek J., Luscher B., Gabrielsen O.S. 2001. The highly conserved DNA-binding domains of A-, B- and c-Myb differ with respect to DNA-binding, phosphorylation and redox properties. *Nucleic Acids Res*. **29**:3546–3556.

Graf T. 1992. Myb: a transcriptional activator linking proliferation and differentiation in hematopoietic cells. *Curr. Opin. Genet. Dev*. **2**:249–255.

Nitta K.R., Jolma A., Yin Y., Morgunova E., Kivioja T., Akhtar J., Hens K, Toivonen J, Deplancke B, Furlong EE, Taipale J. 2015. Conservation of transcription factor binding specificities across 600 million years of bilateria evolution. *Elife* 4.

Oh I.H., Reddy E.P. 1999. The myb gene family in cell growth, differentiation, and apoptosis. *Oncogene* **18**:3017–3033.

Mucenski M.L., McLain K., Kier A.B., Swerdlow S.H., Schreiner C.M., Miller T.A., Pietryga DW, Scott WJ Jr, Potter SS. 1991. A functional c-myb gene is required for normal murine fetal hepatic hematopoiesis. *Cell* **65**:677–689.

Toscani A, Mettus RV, Coupland R, Simpkins H, Litvin J, Orth J, Hatton KS, Reddy EP. 1997. Arrest of spermatogenesis and defective breast development in mice lacking A-myb. *Nature* **386**(6626):713-7.

Sala A. 2005. B-MYB, a transcription factor implicated in regulating cell cycle, apoptosis and cancer. *Eur. J. Cancer* **41**:2479–2484.

Dubendorff J.W., Whittaker L.J., Eltman J.T., Lipsick J.S. 1992. Carboxy-terminal elements of c-Myb negatively regulate transcriptional activation in cis and in trans. *Genes Dev*. **6**:2524–2535.

Lane S., Farlie P., Watson R. 1997. B-Myb function can be markedly enhanced by cyclin A-dependent kinase and protein truncation. *Oncogene* **14**:2445–2453.

Takahashi T., Nakagoshi H., Sarai A., Nomura N., Yamamoto T., Ishii S. 1995. Human A-myb gene encodes a transcriptional activator containing the negative regulatory domains. *FEBS Lett.* 358:89–96.

Gonda T.J., Buckmaster C., Ramsay R.G. 1998. Activation of c-myb by carboxy-terminal truncation: relationship to transformation of murine haemopoietic cells in vitro. *EMBO J*. **8**:1777–1783.

Lipsick J.S., Wang D.M. 1999. Transformation by v-Myb. *Oncogene* **18**:3047–3055.

Sadasivam S., Duan S., DeCaprio J.A. 2012. The MuvB complex sequentially recruits B-Myb and FoxM1 to promote mitotic gene expression. *Genes Dev.* **26**:474–489.

Petrovas C., Jeay S. Lewis R.E., 2003. Sonenshein G.E. B-Myb repressor function is regulated by cyclin A phosphorylation and sequences within the C-terminal domain. *Oncogene* **22**:2011–2020.

Bessa M., Saville M.K., Watson R.J. 2001. Inhibition of cyclin A/Cdk2 phosphorylation impairs B-Myb transactivation function without affecting interactions with DNA or the CBP coactivator. *Oncogene* **20**:3376–3386.

Tashiro S., Takemoto Y., Handa H., Ishii S. 1995. Cell type-specific trans-activation by the B-myb gene product: requirement of the putative cofactor binding to the C-terminal conserved domain. *Oncogene* **10**:1699–1707.

Johnson T.K., Schweppe R.E., 1999. Septer J., Lewis R.E. Phosphorylation of B-Myb regulates its transactivation potential and DNA binding. *J. Biol. Chem*. **274**:36741–36749.

Werwein E., Biyanee A., Klempnauer K.H. 2020. Intramolecular interaction of B-MYB is regulated through Ser-577 phosphorylation. *FEBS Lett.* **594**:4266–4279.

Charrasse S., Carena I., Brondani V., Klempnauer K.H., Ferrari S. 2000. Degradation of B-myb by ubiquitin-mediated proteolysis: involvement of the Cdc34-SCF(p45Skp2) pathway. *Oncogene* **19**:2986–2995.

Bastidas M., Gibbs E.B., Sahu D., Showalter S.A. 2015. A primer for carbon-detected NMR applications to intrinsically disordered proteins in solution. *Concepts Magn. Reson*. *A*. **44**:54–66.

Sala A., Kundu M., Casella I., Engelhard A., Calabretta B., Grasso L., et al. 1997. Activation of human B-MYB by cyclins. *Proc. Natl. Acad. Sci. U. S. A* **94**:532–536.

Saville M.K., Watson R.J. 1998. The cell-cycle regulated transcription factor B-Myb is phosphorylated by cyclin A/Cdk2 at sites that enhance its transactivation properties. *Oncogene* **17**:2679–2689.

Ness S.A., Marknell A., Graf T. 1989. The v-myb oncogene product binds to and activates the promyelocyte-specific mim-1 gene. *Cell* **59**:1115–1125.

Seong H.A., Kim K.T., Ha H. 2003. Enhancement of B-MYB transcriptional activity by ZPR9, a novel zinc finger protein. *J. Biol. Chem*. **278**:9655–9662.

Ansieau S., Kowenz-Leutz E., Dechend R., Leutz A. 1997. B-Myb, a repressed trans-activating protein. *J. Mol. Med. (Berl.)* **75**:815–819.

Bartsch O., Horstmann S., Toprak K., Klempnauer K.H., Ferrari S. 1999. Identification of cyclin A/Cdk2 phosphorylation sites in B-Myb. *Eur. J. Biochem.* **260**:384–391.

Sun X., Dyson H.J., Wright P.E. 2021. A phosphorylation-dependent switch in the disordered p53 transactivation domain regulates DNA binding. *Proc. Natl. Acad. Sci. U. S. A* **118**(1):e2021456118.

Basu U., Mishra N., Farooqui M., Shen J., Johnson L.C., Patel S.S. 2020. The C-terminal tails of the mitochondrial transcription factors Mtf1 and TFB2M are part of an autoinhibitory mechanism that regulates DNA binding. J. *Biol. Chem.* **295**:6823–6830.

Pufall MA, Lee GM, Nelson ML, Kang HS, Velyvis A, Kay LE, McIntosh LP, Graves BJ. 2005. Variable control of Ets-1 DNA binding by multiple phosphates in an unstructured region. *Science* **309**(5731):142-5.

Xhani S, Lee S, Kim HM, Wang S, Esaki S, Ha VLT, Khanezarrin M, Fernandez GL, Albrecht AV, Aramini JM, Germann MW, Poon GMK. 2020. Intrinsic disorder controls two functionally distinct dimers of the master transcription factor PU.1. *Sci Adv*. **21**;6(8)

Xu M., Sheppard K.A., Peng C.Y., Yee A.S., Piwnica-Worms H. 1994. Cyclin A/CDK2 binds directly to E2F-1 and inhibits the DNA-binding activity of E2F-1/DP-1 by phosphorylation. *Mol. Cell. Biol.* **14**:8420–8431.

Fu Z, Malureanu L, Huang J, Wang W, Li H, van Deursen JM, Tindall DJ, Chen J. 2008. Plk1-dependent phosphorylation of FoxM1 regulates a transcriptional programme required for mitotic progression. *Nat Cell Biol*. **10**(9):1076-82.

Rubin S.M. 2013. Deciphering the retinoblastoma protein phosphorylation code. *Trends Biochem. Sci.* **38**:12–19.

Bastidas M., Gibbs E.B., Sahu D., Showalter S.A. 2015. A primer for carbon-detected NMR applications to intrinsically disordered proteins in solution. *Concepts Magn. Reson*. A. **44**:54–66.

Delaglio F., Grzesiek S., Vuister G.W., Zhu G., Pfeifer J., Bax A. 1995. NMRPipe: a multidimensional spectral processing system based on UNIX pipes. *J. Biomol. NMR* **6**:277–293.

Lee W., Tonelli M., Markley J.L. 2015. NMRFAM-SPARKY: enhanced software for biomolecular NMR spectroscopy. *Bioinformatics* **31**:1325–1327.

Kornberg RD. 1974. Chromatin structure: a repeating unit of histones and DNA. *Science* **184**(4139):868-71.

Bram S and Ris H. 1971. On the structure of nucleohistone. *J. Mol. Biol* **55**: 325-336.

Olins A.L. and Olins D.E. Spheroid chromatin units (v bodies). 1974. *Science* **183**: 330-332.

Thomas J.O. and Kornberg R.D. 1975. An octamer of histones in chromatin and free in solution. *Proc. Natl. Acad. Sci. USA.* **72**: 2626-2630.

Lutter L.C, Rhodes D., Brown A.S., Rushton B., Levitt M., Klug A. 1977. Structure of nucleosome core particles of chromatin. *Nature* **269**: 29-36.

Blank, T. A. & Becker, P. B. 1995. Electrostatic mechanism of nucleosome spacing. *J. Mol. Biol*. **252**, 305–313.

Luger K., Mader A.W., Richmond R.K., Sargent D.F., Richmond T.J. 1997. Crystal structure of the nucleosome core particle at 2.8Å resolution. *Nature* **389**: 251-260.

Knezetic JA, Luse DS. 1986. The presence of nucleosomes on a DNA template prevents initiation by RNA polymerase II in vitro. *Cell* **45**(1):95-104.

Kamakaka RT. 2003. Heterochromatin: proteins in flux lead to stable repression. *Curr Biol*. **13**(8):R317-9.

Wang J, Jia ST, Jia S. 2016. New Insights into the Regulation of Heterochromatin. *Trends Genet*. **32**(5):284-294.

Fan, Y., Nikitina T, Zhao J, Fleury TJ, Bhattacharyya R, Bouhassira EE, Stein A, Woodcock CL, Skoultchi AI. 2005. Histone H1 depletion in mammals alters global chromatin structure but causes specific changes in gene regulation. *Cell* **123**, 1199–1212.

Kaplan N, Moore IK, Fondufe-Mittendorf Y, Gossett AJ, Tillo D, Field Y, LeProust EM, Hughes TR, Lieb JD, Widom J, Segal E. 2009. The DNA-encoded nucleosome organization of a eukaryotic genome. *Nature* **458**(7236):362-6.

Zhang, Z. & Pugh, B. F. 2011. High-resolution genome-wide mapping of the primary structure of chromatin. *Cell* **144**, 175–86.

Jansen A, Verstrepen KJ. 2011. Nucleosome positioning in Saccharomyces cerevisiae. *Microbiol Mol Biol Rev*. **75**(2):301-20.

Kubik S, Bruzzone MJ, Jacquet P, Falcone JL, Rougemont J, Shore D. 2015. Nucleosome Stability Distinguishes Two Different Promoter Types at All Protein-Coding Genes in Yeast. *Mol Cell*. **60**(3):422-34.

Zhang Y, Moqtaderi Z, Rattner BP, Euskirchen G, Snyder M, Kadonaga JT, Liu XS, Struhl K. 2009. Intrinsic histone-DNA interactions are not the major determinant of nucleosome positions in vivo. *Nat Struct Mol Biol*. **16**(8):847-52.

Deniz Ö, Flores O, Aldea M, Soler-López M, Orozco M. 2016. Nucleosome architecture throughout the cell cycle. *Sci Rep*. **6**:19729.
Lee W, Tillo D, Bray N, Morse RH, Davis RW, Hughes TR, Nislow C. 2007. A high-resolution atlas of nucleosome occupancy in yeast. *Nat Genet*. 39(10):1235-44.

Liu Y, Chen S, Wang S, Soares F, Fischer M, Meng F, Du Z, Lin C, Meyer C, DeCaprio JA, Brown M, Liu XS, He HH. 2017. Transcriptional landscape of the human cell cycle. *Proc Natl Acad Sci USA* **114**(13):3473-3478.

Asthana A, Ramanan P, Hirschi A, Guiley KZ, Wijeratne TU, Shelansky R, Doody MJ, Narasimhan H, Boeger H, Tripathi S, Müller GA, Rubin SM. 2022. The MuvB complex binds and stabilizes nucleosomes downstream of the transcription start site of cell-cycle dependent genes. *Nat Commun*. **13**(1):526.

Zhang W, Tyl M, Ward R, Sobott F, Maman J, Murthy AS, Watson AA, Fedorov O, Bowman A, Owen-Hughes T, El Mkami H, Murzina NV, Norman DG, Laue ED. 2013. Structural plasticity of histones H3-H4 facilitates their allosteric exchange between RbAp48 and ASF1. *Nat Struct Mol Biol*. **20**(1):29-35.

Koliopoulos MG, Muhammad R, Roumeliotis TI, Beuron F, Choudhary JS, Alfieri C. 2023. Structure of a nucleosome-bound MuvB transcription factor complex reveals DNA remodeling. *Nat Commun*. **14**(1):314.

Lowary PT, Widom J. 1998. New DNA sequence rules for high affinity binding to histone octamer and sequence-directed nucleosome positioning. *J Mol Biol.* **276**(1):19-42.

McGinty, R. K. & Tan, S. 2021. Principles of nucleosome recognition by chromatin factors and 628 enzymes. *Curr Opin Struct Biol.* **71**, 16-26.

Müller GA, Quaas M, Schümann M, Krause E, Padi M, Fischer M, Litovchick L, DeCaprio JA, Engeland K. 2012. The CHR promoter element controls cell cycle-dependent gene transcription and binds the DREAM and MMB complexes. *Nucleic Acids Res*. **40**(4):1561-78.

Osterloh L, von Eyss B, Schmit F, Rein L, Hübner D, Samans B, Hauser S, Gaubatz S. 2007. The human synMuv-like protein LIN-9 is required for transcription of G2/M genes and for entry into mitosis. *EMBO J*. **26**(1):144-57.

Iness AN. 2018. Mechanisms of B-Myb oncogenicity in ovarian cancer. Doctoral Dissertation, *Virginia Commonwealth University. VCU Scholars Compass.*

Boyer LA, Latek RR, Peterson CL. 2004. The SANT domain: a unique histone-tail-binding module? *Nat Rev Mol Cell Biol*. **5**(2):158-63.

Mages, C. F., Wintsche, A., Bernhart, S. H. & Müller, G. A. 2017. The DREAM complex through its subunit LIN37 cooperates with Rb to initiate quiescence. *Elife* **6**, e26876.

Wijeratne TU, Guiley KZ, Lee HW, Müller GA, Rubin SM. 2022. Cyclin-dependent kinase-mediated phosphorylation and the negative regulatory domain of transcription factor B-Myb modulate its DNA binding. *J Biol Chem.* **298**(9):102319.

Gasser, S.M. 2001. Positions of potential: nuclear organization and gene expression. *Cell* **104**, 639-642.

A. Punjani, J. L. Rubinstein, D. J. Fleet, M. A. 2017. Brubaker, cryoSPARC: algorithms for rapid unsupervised cryo-EM structure determination. *Nat Methods* **14**, 290-296.

Lorch, Y., LaPointe, J. W. & Kornberg, R. D. 1987. Nucleosomes inhibit the initiation of transcription but allow chain elongation with the displacement of histones. *Cell* **49**, 203–210.

Zaret KS, Carroll JS. 2011. Pioneer transcription factors: establishing competence for gene expression. *Genes Dev*. **25**(21):2227-41.

Iwafuchi-Doi M, Zaret KS. 2014. Pioneer transcription factors in cell reprogramming. *Genes Dev*. **28**:2679–92.

Zaret KS, Lerner J, Iwafuchi-Doi M. 2016. Chromatin Scanning by Dynamic Binding of Pioneer Factors. Mol Cell. **62**(5):665-7.

Bossard P, Zaret KS. 1998. GATA transcription factors as potentiators of gut endoderm differentiation. *Development* **125**(24):4909-17.

Gualdi R, Bossard P, Zheng M, Hamada Y, Coleman JR, Zaret KS. 1996. Hepatic specification of the gut endoderm in vitro: cell signaling and transcriptional control. *Genes Dev*. **10**(13):1670-82.

Fischer M, Schade AE, Branigan TB, Müller GA, DeCaprio JA. 2022. Coordinating gene expression during the cell cycle. *Trends Biochem Sci*. **47**(12):1009-1022.

Zheng N, Fraenkel E, Pabo CO, Pavletich NP. 1999. Structural basis of DNA recognition by the heterodimeric cell cycle transcription factor E2F-DP. *Genes Dev*. **13**(6):666-74.

Littler DR, Alvarez-Fernández M, Stein A, Hibbert RG, Heidebrecht T, Aloy P, Medema RH, Perrakis A. 2010. Structure of the FoxM1 DNA-recognition domain bound to a promoter sequence. *Nucleic Acids Res*. **38**(13):4527-38.

Rabinovich A, Jin VX, Rabinovich R, Xu X, Farnham PJ. 2018. E2F in vivo binding specificity: comparison of consensus versus nonconsensus binding sites. *Genome Res*. **18**(11):1763-77.

Müller GA, Wintsche A, Stangner K, Prohaska SJ, Stadler PF, Engeland K. 2014. The CHR site: definition and genome-wide identification of a cell cycle transcriptional element. *Nucleic Acids Res*. **42**(16):10331-50.

Sanders DA, Gormally MV, Marsico G, Beraldi D, Tannahill D, Balasubramanian S. 2015. FOXM1 binds directly to non-consensus sequences in the human genome. *Genome Biol*. **16**(1):130.

Nitta KR, Jolma A, Yin Y, Morgunova E, Kivioja T, Akhtar J, Hens K, Toivonen J, Deplancke B, Furlong EE, Taipale J. 2015. Conservation of transcription

factor binding specificities across 600 million years of bilateria evolution. *Elife* **4**:e04837.

Cirillo L, Lin FR, Cuesta I, Jarnik M, Friedman D, Zaret K. 2002. Opening of compacted chromatin by early developmental transcription factors HNF3 (FOXA) and GATA-4. *Mol Cell* **9**:279–289.

Fischer, M, Grossmann P, Padi M, De Caprio JA. 2016. Integration of TP53, DREAM, MMB FOXM1 and RB-E2F target gene analyses identifies cell cycle gene regulatory networks. *Nucleic Acids Res***. 44**, 6070–6086.

Lu Z, Luo RZ, Peng H, Huang M, Nishmoto A, Hunt KK, Helin K, Liao WS, Yu Y. 2006. E2F-HDAC complexes negatively regulate the tumor suppressor gene ARHI in breast cancer. *Oncogene* **25**(2):230-9.

Marceau AH, Brison CM, Nerli S, Arsenault HE, McShan AC, Chen E, Lee HW, Benanti JA, Sgourakis NG, Rubin SM. 2019. An order-to-disorder structural switch activates the FoxM1 transcription factor. *Elife* **8**: e46131.

Facchinetti V, Loffarelli L, Schreek S, Oelgeschläger M, Lüscher B, Introna M, Golay J. 1997. Regulatory domains of the A-Myb transcription factor and its interaction with the CBP/p300 adaptor molecules. *Biochem J*. **324** (Pt 3)(Pt 3):729-36.

Dai, P, Akimaru, H, Tanaka, Y, Hou, D.X, Yasukawa, T, Kanei-Ishii, C, Takahashi, T, Ishii, S. 1996. CBP as a transcriptional coactivator of c-Myb. *Genes Dev*. **10**, 528–540.

Johnson LR, Johnson TK, Desler M, Luster TA, Nowling T, Lewis RE, Rizzino A. 2002. Effects of B-Myb on gene transcription: phosphorylation-dependent activity and acetylation by p300. *JBC* **277**(6):4088-97.

Tomita A, Towatari M, Tsuzuki S, Hayakawa F, Kosugi H, Tamai K, Miyazaki, T, Kinoshita T, Saito H. 2000. c-Myb acetylation at the carboxyl-terminal conserved domain by transcriptional co-activator p300. *Oncogene* **9**, 444–451.

Sandberg ML, Sutton SE, Pletcher MT, Wiltshire T, Tarantino LM, Hogenesch JB, Cooke MP. 2005. c-Myb and p300 regulate hematopoietic stem cell proliferation and differentiation. *Dev. Cell* **8**, 153–166.

Goto NK, Zor T, Martinez-Yamout M, Dyson HJ, Wright PE. 2002. Cooperativity in transcription factor binding to the coactivator CREB-

binding protein (CBP). The mixed lineage leukemia protein (MLL) activation domain binds to an allosteric site on the KIX domain. *JBC* **277**, 43168–43174.

Zuber J, Rappaport AR, Luo W, Wang E, Chen C, Vaseva AV, Shi J, Weissmueller S, Fellmann C, Taylor MJ, Weissenboeck M, Graeber TG, Kogan SC, Vakoc CR, Lowe SW. 2011. An integrated approach to dissecting oncogene addiction implicates a Myb-coordinated self-renewal program as essential for leukemia maintenance. *Genes Dev*. **25**:1628–40.

Uttarkar S, Dassé E, Coulibaly A, Steinmann S, Jakobs A, Schomburg C, Trentmann A, Jose J, Schlenke P, Berdel WE, Schmidt TJ, Müller-Tidow C, Frampton J, Klempnauer KH. 2016. Targeting acute myeloid leukemia with a small molecule inhibitor of the Myb/p300 interaction. *Blood* 127:1173–82.

Schubert S, Horstmann S, Bartusel T, Klempnauer KH. 2004. The cooperation of B-Myb with the coactivator p300 is orchestrated by cyclins A and D1. *Oncogene* **23**(7):1392-404.

Oka O, Waters LC, Strong SL, Dosanjh NS, Veverka V, Muskett FW, Renshaw PS, Klempnauer KH, Carr MD. 2012. Interaction of the transactivation domain of B-Myb with the TAZ2 domain of the coactivator p300: molecular features and properties of the complex. *PLoS One* **7**(12): e52906.

Ferreon JC, Martinez-Yamout MA, Dyson HJ, Wright PE. 2009. Structural basis for subversion of cellular control mechanisms by the adenoviral E1A oncoprotein. *Proc Natl Acad Sci USA* 106(32):13260-5.

Teufel DP, Freund SM, Bycroft M, Fersht AR. 2007. Four domains of p300 each bind tightly to a sequence spanning both transactivation subdomains of p53. *Proc Natl Acad Sci USA* **104**(17):7009-14.

Sazer, S., Lynch, M. & Needleman, D. 2014. Deciphering the evolutionary history of open and closed mitosis. *Curr. Biol.* **24**, R1099–R1103.

Yanagida M. 2014. The role of model organisms in the history of mitosis research. *Cold Spring Harb Perspect Biol*. **6**(9): a015768.

O'Connell CB, Khodjakov AL. 2007. Cooperative mechanisms of mitotic spindle formation. *J Cell Sci*. **120**(Pt 10):1717-22.

Nigg EA. 2001. Mitotic kinases as regulators of cell division and its checkpoints. *Nat Rev Mol Cell Biol*. **2**(1):21-32.

Fry AM, Bayliss R, Roig J. 2017. Mitotic Regulation by NEK Kinase Networks. *Front Cell Dev Biol*. **5**:102.

Javed A, Özduman G, Altun S, Duran D, Yerli D, Özar T, Şimşek F, Sami Korkmaz K. 2023. Mitotic kinase inhibitors as Therapeutic Interventions for Prostate Cancer: Evidence from In vitro Studies. *Endocr. Metab. Immune Disord. Drug Targets*. Epub ahead of print. PMID: 36872354.

D'Assoro AB, Haddad T, Galanis E. 2016. Aurora-A Kinase as a Promising Therapeutic Target in Cancer. *Front Oncol*. **5**:295.

Giet R, Petretti C, Prigent C. 2005. Aurora kinases, aneuploidy and cancer, a coincidence or a real link? *Trends Cell Biol*. **15**(5):241-50.

Gomez-Ferreria MA, Rath U, Buster DW, Chanda SK, Caldwell JS, Rines DR, Sharp DJ. 2007. Human Cep192 is required for mitotic centrosome and spindle assembly. *Curr Biol*. **17**(22):1960-6.

Kufer TA, Silljé HH, Körner R, Gruss OJ, Meraldi P, Nigg EA. 2002. Human TPX2 is required for targeting Aurora-A kinase to the spindle. *J Cell Biol*. **158**:617–23.

Macůrek L, Lindqvist A, Lim D, Lampson MA, Klompmaker R, Freire R, Clouin C, Taylor SS, Yaffe MB, Medema RH. 2008. Polo-like kinase-1 is activated by Aurora A to promote checkpoint recovery. *Nature* **455**(7209):119-23.

Seki A, Coppinger JA, Jang CY, Yates JR, Fang G. 2008. Bora and the kinase Aurora a cooperatively activate the kinase Plk1 and control mitotic entry. *Science* **320**(5883):1655-8.

Tavernier N, Noatynska A, Panbianco C, Martino L, Van Hove L, Schwager F, Léger T, Gotta M, Pintard L. 2015. Cdk1 phosphorylates SPAT-1/Bora to trigger PLK-1 activation and drive mitotic entry in C. elegans embryos. *J Cell Biol*. **208**(6):661-9.

Thomas Y, Cirillo L, Panbianco C, Martino L, Tavernier N, Schwager F, Van Hove L, Joly N, Santamaria A, Pintard L, Gotta M. 2016. Cdk1

phosphorylates SPAT-1/Bora to promote Plk1 activation in C. elegans and human cells. *Cell Rep*. **15**, 510–518.

Nowakowski J, Cronin CN, McRee DE, Knuth MW, Nelson CG, Pavletich NP, Rogers J, Sang BC, Scheibe DN, Swanson RV, Thompson DA. 2002. Structures of the cancer-related Aurora-A, FAK, and EphA2 protein kinases from nano volume crystallography. *Structure* **10**(12):1659-67.

Bayliss R, Sardon T, Vernos I, Conti E. 2003. Structural basis of Aurora-A activation by TPX2 at the mitotic spindle. *Mol Cell*. **12**(4):851-62.

Seki A, Coppinger JA, Du H, Jang CY, Yates JR 3rd, Fang G. 2008. Plk1- and beta-TrCP-dependent degradation of Bora controls mitotic progression. *J Cell Biol.* **181**(1):65-78.

Leslie AG. 2006. The integration of macromolecular diffraction data. *Acta Crystallogr D Biol Crystallogr.* **62**: 48-57.

Bailey S. 1994. The Ccp4 Suite - Programs for Protein Crystallography. *Acta Crystallographica Section D-Biological Crystallography* **50**: 760-763.

Mccoy AJ, Grosse-Kunstleve RW, Adams PD, Winn MD, Storoni LC, Read RJ. 2007. Phaser crystallographic software. *J Appl Crystallogr* **40**: 658-674.